



Norwegian University of
Science and Technology

Production of Silicomanganese from Comilog Ore

Reduction Behavior

Joakim Holtan

Materials Technology

Submission date: June 2016

Supervisor: Merete Tangstad, IMTE

Norwegian University of Science and Technology
Department of Materials Science and Engineering

Declaration

I hereby declare that this work has been carried out independently and in compliance with the examination regulations of the Norwegian University of Science and Technology, NTNU.

A handwritten signature in black ink, reading "Joakim Holtan". The script is cursive and fluid, with the first letters of the first and last names being capitalized and prominent.

Joakim Holtan

Trondheim, June 2016

Preface

This thesis describes an investigation of reduction of manganese ore with quartz and limestone. It is the main project and evaluation basis for the course TMT4905 Materials Technology, Master's Thesis at the Norwegian University of Science and Technology, NTNU. The work was performed at the Department of Materials Science and Engineering and was carried out during the spring semester of 2016 with Professor Merete Tangstad as supervisor.

This work is founded by the research centre SFI Metal Production. The work is a part of the Research Domain 2 (RD2), Primary Metal Production with Professor Merete Tangstad as leader.

I hope that this thesis will bring about more knowledge within this field and inspire to further research and development.

Trondheim, June 2016

Joakim Holtan

Acknowledgment

Firstly, I would like to thank my supervisor, Professor Merete Tangstad, for giving me the opportunity to write this project and for insightful discussions. I am grateful to her for all the knowledge that she shared with me and thereby enabled me to carry out this task.

I am very grateful for SFI Metal Production who support my research. The new research centre managed by NTNU will ensure that the Norwegian metallurgical industry maintains its position as a world-leader within energy-efficient, environmentally friendly and competitive production of materials. I am pleased to be a part of this. SFI Metal Production is managed by the Research Council of Norway's SFI program.

I also want to thank Senior Engineer Morten Raanes for his help with the EPMA, Senior Engineer Jonas Einan Gjøvik for his support with the furnace, and Research Scientist Ingeborg Solheim from SINTEF for her support and help during the experiments with the SINTEF furnace. Ingeborg saved me when the first furnace I used was out of order.

Lastly I would like to thank everybody in the diplomroom at the fourth floor for helpful hints and tips along the way.

J.H.

Summary and Conclusions

The reduction behavior of silicomanganese (SiMn) charges based on Comilog ore was investigated. The charges were heated up to different temperatures by using a thermogravimetric graphite tube furnace. The weight loss during heating was measured and compared with slag and metal compositions for each sample for investigating the reduction for the charges. The aim was to investigate the reduction rates for silicon and manganese in SiMn production, and to find out if limestone added as a flux has positive impact on the degree of reduction for silicon and manganese.

For investigating the slag and metal compositions for the samples it was used SEM (EDS) and EPMA.

It was found that the slag in SiMn charges will foam at high temperature when heating rate of 4.5 °C per minute. The temperature for this foaming was 1600 °C for SiMn charge with limestone and 1650 °C for charge without limestone.

The MnO reduction will start at 1400 °C in SiMn charges, and the reduction of silica will start occur at 1550 °C in SiMn charges. These temperatures was found to be the same for SiMn charges both with and without limestone.

The SiMn charges was found to have a liquid slag phase at 1250 °C according to the binary phase diagram for MnO-SiO₂.

SiMn charge with limestone added as a flux had higher degree of reduction of both manganese and silicon than SiMn charge without limestone.

Summary in Norwegian

Sammendrag og konklusjoner

Reduksjonen av silikomangan-charger basert på Comilog-malm ble undersøkt i dette arbeidet. Chargene (blandinger av råmaterialer) ble varmet opp til forskjellige temperaturer i en termogravimetrisk grafittrør-ovn. Vekttapet under oppvarmingen ble målt og sammenlignet med slag- og metallanalysene fra prøvene for å undersøke reduksjonen for chargene. Målet var å undersøke reduksjonshastigheten for silisium og mangan i SiMn-produksjon, og finne ut om kalk tilsatt chargen har positiv innvirkning på reduksjonsgraden av silisium og mangan.

SEM (EDS) og mikrosonde (EPMA) ble brukt til å finne slag- og metallanalysene.

Det ble funnet at slaggen i SiMn-chargene skummer ved høy temperatur. Skummingen starter ved 1600 °C for charge tilsatt kalk, og ved 1650 °C for charge uten kalk.

MnO-reduksjonen starter ved 1400 °C i SiMn-charger, og reduksjonen av SiO₂ starter ved 1550 °C i disse chargene. Disse temperaturene gjelder for både SiMn-charger med og uten kalk.

I SiMn-chargene ble det funnet flytende slaggfase ved 1250 °C. Dette forteller at systemet er i likevekt på grunn av at det stemmer med det binære fasediagrammet for MnO-SiO₂.

Det ble funnet at charger med tilsatt kalk har høyere reduksjonsgrad enn charger uten kalk. Dette gjelder for både silisium og mangan.

Contents

Preface	iii
Acknowledgment	v
Summary and Conclusions	vii
Summary in Norwegian	ix
1 Introduction	1
1 Manganese	1
2 Manganese Alloys	1
3 Goal of the Project	3
2 Theory	5
1 Overview of Chemical Reactions in FeMn Production	5
1.1 Prereduction	5
1.2 High Temperature Area	8
2 Manganese Ores	9
2.1 Chemical Analyses	9
3 Chemical Composition and its Effect on Properties and Slag Structures	11
4 Thermodynamics	14
5 Kinetics	19
6 Phase Diagrams	22
6.1 MnO-SiO ₂ -Al ₂ O ₃ System	22
6.2 MnO-SiO ₂ -CaO System	23
6.3 CaO-SiO ₂ -Al ₂ O ₃ System	24

7	Reduction of Mn Ores	26
7.1	Size Impact	26
7.2	Melting and Reduction	29
3	Experimental Work	31
1	Raw Materials	31
1.1	Comilog Ore	31
1.2	Coke	32
1.3	Limestone	33
1.4	Weight Loss During Prereduction	33
2	Equipment	33
2.1	Thermogravimetric Furnace	33
2.2	Crucibles	37
3	Experiments	38
4	Procedures	40
4.1	Furnace Operation	40
4.2	Temperature During Experiments	41
4.3	Ending Experiments	42
4.4	Reproducibility	42
4.5	Treatment of Samples	43
5	Mathematical Calculations	44
5.1	Mass Balance	44
6	Analysis Methods	47
6.1	Electron Probe Microanalyser (EPMA)	47
6.2	Energy Dispersive Spectroscopy (EDS)	47
4	Results	51
1	Comilog Ore and Quartz	51
2	Comilog Ore, Quartz and Limestone	62

5 Discussion	79
1 Comilog Ore and Quartz	80
2 Comilog Ore, Quartz and Limestone	84
3 Degree of Reduction and Si Distribution	93
4 Melting Temperature of the Charge	98
5 EDS	99
6 Conclusion	103
7 Further Work	105
Bibliography	107
A Mass Balance	I
B Calculations of charge mixture	III
C Raw Data from EPMA	VII
D Raw Data from EDS	IX
E Data for Comparing EDS and EPMA	XIII
F Risk Assessment and Safe Job Analysis	XVII

Chapter 1

Introduction

In the industry, manganese alloys are produced by pyro-metallurgical techniques such as blast furnaces or electric submerged arc furnaces. In both the furnaces, production is carried out by carbothermic reduction of manganese ores, illustrated in equation 1.1.



This chapter gives a brief introduction of manganese and manganese alloys. The aim of this Master's thesis is discussed in the end of this chapter.

1 Manganese

Manganese is the 12th most abundant element in the earth crust. Table 1.1 shows some key properties of the element manganese.

2 Manganese Alloys

Manganese alloys are mostly used in steelmaking as alloying element, as deoxidizer and as a sulphur stabilizer. Steels usually contain from 0.2 % to 2.0 % manganese. Manganese is the cheapest alloying element among those which enhance mechanical properties like strength and toughness in steels (Olsen et al., 2007).

Table 1.1: Properties of Manganese from Aylward and Findlay (2008).

Symbol	Mn
Atomic number	25
Atomic weight	54.94 g/mol
Density at 298 K	7.43 g/cm ³
Melting Temperature	1244 °C
Boiling Temperature	2095 °C
Specific heat capacity at 298 K	0.48 J/K·g
Thermal conductivity at 298 K	7.8 J/(s·m·K)

There are two families of manganese alloys called ferromanganese (FeMn) and silicomanganese (SiMn). SiMn contains typical 17 % - 30 % Si and 58 % - 68 % Mn. Carbon content at saturation level for the SiMn alloys, about 1.5 % for an alloy with 18 % Si. The content of carbon decrease with increasing content of silicon in the alloy.

The different types of manganese alloys may hence be divided into four major groups:

- High carbon ferromanganese, normally with 78 % Mn and 7.5 % C.
- Refined ferromanganese with carbon content ranging from 1.5 % C down to 0.5 % C.
- Silicomanganese with silicon content normally from 17 % to 20 %, corresponding respectively with carbon contents from approximately 2.0 % down to 1.5 %.
- Low carbon silicomanganese with 26-31 % Si and carbon content from 0.5 % down to 0.05 %.

This way to divide the different alloys is mainly based on the carbon content (Olsen et al., 2007).

A trend towards more use of SiMn is seen at the expense of FeMn. This is primary for economic reasons. Silicomanganese adds less phosphorus, carbon, aluminium and nitrogen to the steel compared to a mixture of standard high carbon ferromanganese (HC FeMn) and ferrosilicon with 75 % Si (FeSi75). Standard quality silicomanganese (SiMn) is used in most silicon and manganese containing steels where the combination of carbon, manganese, silicon and trace elements fits the final steel analysis in an economical way.

The use of low carbon silicomanganese in stainless steels and alloy steels provides a more economical production route, where a combination of manganese and silicon is required in a low carbon steel product.

Slag from ferro-manganese furnaces can be used as raw material in silicomanganese furnaces, because of high MnO content in such slags. (Tangstad, 2013)

A lot of the research within manganese alloys has been on FeMn, not so much on SiMn. The industry has assumed that similar mechanisms are valid for SiMn as for FeMn production. The silicon content in manganese alloys decrease the liquidus temperature and will affect the activities of the other elements.

3 Goal of the Project

For this work the aim is to investigate the mechanisms in silicomanganese production. It is believed that the melting and melting behavior will affect the temperature in the high temperature zone. It is hence important to know and investigate the melting mechanisms. This work will study the melting and mixing behavior of Comilog ore with typical fluxes like limestone and quartz. Is limestone added as a flux favorable in SiMn production? The charge will be heated in a thermogravimetric furnace and the resulting weight loss curves will be studied. The resulting mixture will be studied in the SEM or the EPMA. This work is supported by SFI Metal Production.

To avoid misunderstandings it may be necessary to define some terms used in this report (Tangstad, 1996):

Slag Oxide mixture where the manganese is present as MnO.

Charge Mixture of raw materials feed to the furnace.

Flux Material added to the charge for changing environment, e.g. basicity and activities.

Prereduction zone Part of the furnace where the flux and ore are mainly solid. This is above the electrode tip.

Coke bed Part of the furnace where the ore is melted in a surplus of carbonaceous agent, that is below the electrode tip. It could also be defined as the area in the furnace where the electric current runs.

It may also be necessary to specify that silicon is treated and mentioned as a metal throughout the entire thesis, even if silicon really is a metalloid.

Chapter 2

Theory

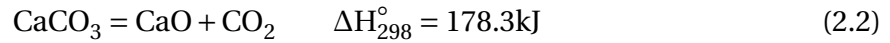
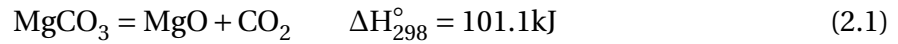
In this chapter earlier investigations and research are presented. First an overview of the chemical reaction in manganese alloy production is shown. Different manganese ores and slag compositions are discussed based on literature in these fields. Later it is presented some data on thermodynamics and kinetics relevant for production of manganese alloys. Phase diagrams for the most relevant slag systems are also presented in this chapter, and lastly it is presented previous literature on reduction of manganese charges.

1 Overview of Chemical Reactions in FeMn Production

1.1 Prereduction

The first step for the charge in the furnace is the prereduction zone. This is before any liquid phase has developed in the raw materials.

The temperature on the top of the charge varies from furnace to furnace, but it is usually between 100 and 600 °C in closed furnaces. Evaporation of water is the first to occur. Then decomposition of carbonates added as flux to the charge will take place, MgCO_3 at about 400 °C and CaCO_3 at about 900 °C. (Tangstad and Olsen, 1995).

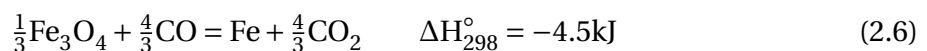


The higher manganese oxides which predominate in manganese ores (MnO_2 , Mn_2O_3 and Mn_3O_4) are relatively unstable and are easily reduced at low temperature in solid state in presence of CO gas. (Tangstad and Olsen, 1995).



Gas reduction of the higher manganese oxides are exothermic reactions, and a considerable amount of heat is produced, thereby preheating the charge materials in the furnace.

Figure 2.1 shows the main reactions in a manganese furnace. As mentioned, in the prereduction zone water evaporate and dolomite and limestone decompose into CO_2 and MgO/CaO . Iron oxides are reduced to metallic iron in the prereduction zone as shown in reaction 2.6. This reaction runs parallel to the reduction of manganese oxides. Complete reduction in solid state to sponge iron is possible.



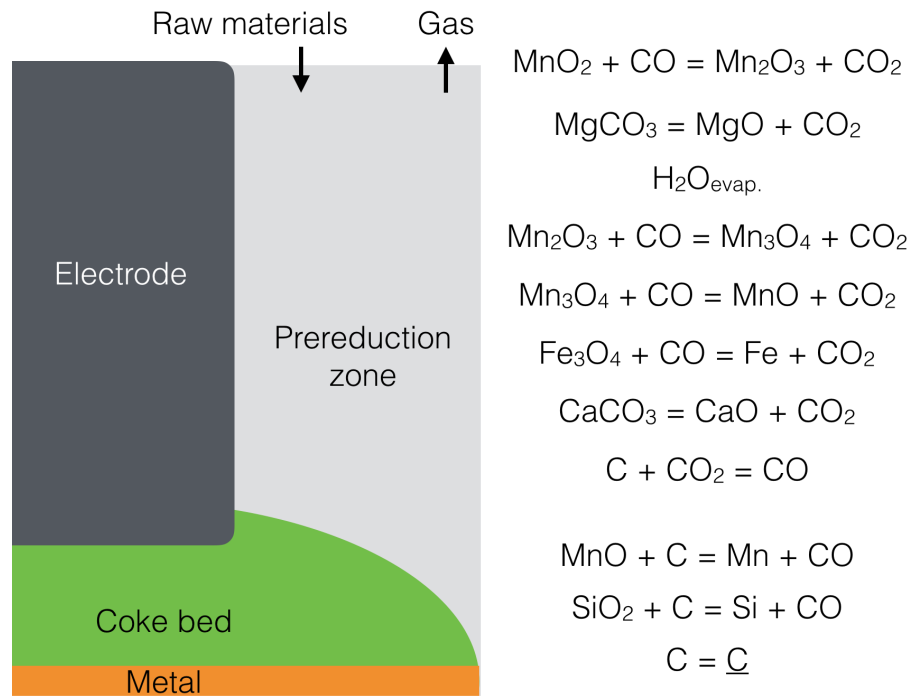
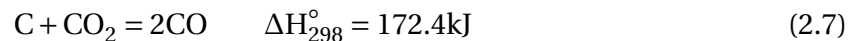


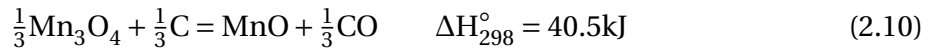
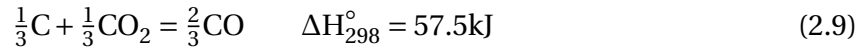
Figure 2.1: Overview of the main reactions in the furnace process. Reactions are not stoichiometric balanced.

When the reactivity of the ore is low, the reduction of Mn_3O_4 occurs at high temperature and the produced CO_2 will react according to the Boudouard reaction shown in reaction 2.7. This will increase the energy and carbon consumption.



Solid Mn_3O_4 converts easily to MnO in presence of CO according to reaction 2.8. The equilibrium CO/CO_2 ratio is $8 \cdot 10^{-5}$ at 1000 °C. The CO gas reduction of Mn_3O_4 is thus a question of kinetics rather than thermodynamics.

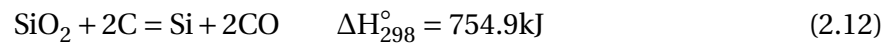
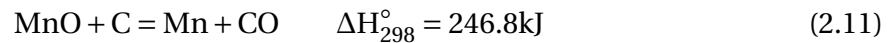
After the temperature has increased to about 1000 °C the reaction on the coke surface is sufficiently rapid to make the ore reduction (reaction 2.8) and the Boudouard reaction (reaction 2.7) to run simultaneously. Thus, CO_2 formed by reaction 2.8 may react with carbon to give the overall reaction 2.10 (Tangstad and Olsen, 1995):



The Boudouard reaction (2.7) is strongly endothermic, and as a result the reduction of Mn_3O_4 as reaction 2.10 is also endothermic.

1.2 High Temperature Area

When the raw materials enters the high temperature area in the furnace, also called the coke bed zone, the ore and the fluxes begins to melt and a partially liquid slag is formed. This slag will flow into a coke layer situated next to and below the electrodes. MnO will be reduced from this slag like shown in reaction 2.11, and SiO_2 will be reduced like shown in 2.12.



It will be formed a $\text{Mn-Fe-Si-C}_{\text{sat}}$ metal. How much of each compound will depend on the slag chemistry and the temperature. Irreducible oxides such as Al_2O_3 , CaO and MgO will stay in the slag phase. MnO and SiO_2 content in the slag is determining by the slag chemistry, temperature and activity of MnO and SiO_2 .

2 Manganese Ores

2.1 Chemical Analyses

Table 2.1 show the typical composition of some major Mn ores. The ores are analyzed at Eramet Norway Sauda and was presented in Tangstad et al. (2004).

Table 2.1: Chemical analyses of manganese ores. Reprinted from Tangstad et al. (2004).

Manganese ore	Mn/Fe	H ₂ O	XH ₂ O	Mn	MnO	MnO ₂	Fe ₂ O ₃	FeO	SiO ₂	Al ₂ O ₃	MgO	CaO	BaO	K ₂ O	P	CO ₂
Comilog MMA	18.5	8.7	5.4	50.5	3.2	76.0	3.9		4.0	5.5	0.3	0.2	0.2	0.70	0.11	0.1
Comilog MMD	9.5	9.0	5.6	44.5	3.3	66.1	6.7		7.7	7.2	0.0	0.1	0.2	0.75	0.09	0.1
Comilog MMR	13.9	9.0	4.9	48.5	2.8	73.4	5.1		5.0	6.1	0.1	0.1	0.3	0.75	0.11	0.1
Comilog MMS	12.0	9.0	6.5	46.5	4.4	68.2	5.5		7.7	7.5	0.0	0.0	0.1	0.75	0.085	0.1
Comilog Sinter	16.7	1.5	0.4	58.5	59.6	19.7		4.5	7.0	6.5	0.0	0.1	0.3	0.75	0.12	0.0
Asman 48	5.1	0.9	0.5	51.3	37.9	34.7	14.3		5.5	0.4	0.7	4.3	0.4	0.0	0.04	0.8
Amapa Sinter	5.1	1.0	0.6	49.1	45.7	18.6		12.5	7.6	7.6	0.5	0.8	0.3	0.3	0.10	0.0
Amapa Miudo 40	3.3	10.0	2.3	41.3	22.4	38.0	18.0		5.9	8.1	0.1	0.3	0.3	0.8	0.11	3.5
Mamatwan	8.2	1.0	0.3	37.8	29.8	23.4	6.6		4.0	0.5	3.5	14.7	0.0	0.0	0.02	17.0
Gloria	7.8	0.4		39.1	31.3	23.6	7.2		5.7	0.3	3.8	12.7	0.1	0.0	0.02	15.4
Groote Eylandt	11.6	2.7		48.8	2.6	73.9	6.0		6.9	4.2	0.1	0.1	0.3	2.0	0.09	0.5
CVRD sinter	11.5	0.6		54.5	52.0	22.5		6.1	5.4	8.7	0.5	1.9	0.3	1.4	0.11	0.2
Wessel 38%	3.2	1.2		42.3	27.8	32.8	18.9		4.9	2.5	1.0	6.0	0.3	0.1	0.04	3.6
Wessel 50%	5.0	0.9		50.2	36.1	35.2	14.5		3.6	0.4	1.0	5.6	0.3	0.1	0.04	2.6

The oxygen content in the ores is an important issue due to the energy consumption in ferromanganese alloy production. This regards to the reduction of higher manganese oxides are exothermic reactions.

Mn content in the ore is also important. Ores with high Mn content, such as Comilog, may give a lower slag/metal ratio which will lower the power consumption.

Mn/Fe ratio in the ore will determine the Mn/Fe ratio in the metal together with the slag basicity. This means that if the ore has a high Mn/Fe ratio, it is a larger degree of freedom in mixing the charge.

Mn/P ratio in the ore will determine the P content in the metal. Steel plants demand low P content, this must be controlled by using low P ores. In respect to low P content the South

Table 2.2: Typical composition of some manganese ores. Reprinted from Tangstad (2013) and one composition from Holtan (2015c).

Deposit	Type	Mn	SiO ₂	Fe	MgO	Al ₂ O ₃	CaO	P
Nikopol (Ukraine)	Oxide	29-43	11-24	1-3	0.8-2	1.4-3.3	4-10	0.15-0.3
	Pyrolusite	47.5	8.6	0.65	0.6	1.6	2	0.2
	Carbonate	22-28	13-16	1.5-3	1.5-2.2	1.7-2.3	7-13	0.3-0.6
Tchiatura (Georgia)	Oxide	30-44	6-17	0.7-4	1-2.5	1.3-2.6	3.8-5.5	0.1-0.4
	Pyrolusite	28	17.6	1.3	1.5	2.9	8.2	0.2
	Carbonate	23-25	16-17	1.3	2.5	2	10	0.15
Comilog (Gabon)	Pyrolusite	46-51	4-8	3-4.7	<0.3	5.5-7.5	<0.2	<0.1
Groote Eylandt (Australia)	Pyrolusite	48.8	7	4.2	0.1	4.2	0.1	0.1
Gloria (South Africa)	Carbonate	39.1	5.7	5	3.8	0.3	12.7	0.02
Mamatwan (South Africa)	Carbonate	37.8	4	4.6	3.5	0.5	14.7	0.02
Zapadny Kamys	Fe-Mn type	17-19	40-42	5-6	1-1.5	5-6.5	1.2-1.7	0.035
Comilog	(Holtan, 2015c)	45.6	6.3	4.4	0.13	6.7	0.28	0.12

African ores are beneficial.

Higher potassium contribute to a higher rate of the Boudouard reaction, that may will increase the energy and carbon consumption.

In Table 2.2 it also is an overview of typical compositions of some manganese ores. This table is from Tangstad (2013) and compare some studies of ore composition. The east european ores are high in phosphorus and low in iron content, and have an intermediate basicity between the South African and the Groote Eylandt/Comilog ores.

3 Chemical Composition and its Effect on Properties and Slag Structures

The slag is a liquid oxide melt and it can be divided in basic and acid oxides. Basicity describe the ratio between acid and basic oxides in the slag. MgO and CaO are the most important basic oxides. SiO₂ and Al₂O₃ are the acid oxides in Mn rich slag. Al₂O₃ may also act as basic oxide in some slags. MnO is basic but it is not used when the basicity ratio is calculated because MnO is reducible. (Brynjulfson, 2013)

MgO and CaO are basic oxides and have similar effect on equilibrium, liquidus composition, viscosity and electrical resistivity. Silica and alumina as both are acid oxides will also have similar effect on slag properties.

Viscosity is a physical property of the slag. The slag structure affect the physical properties, and in this chapter the viscosity is used as an example of how the chemical composition of the slag affect the properties and slag structure. Figure 2.2 show that high amount of acid oxides in the slag makes the slag very viscous. The reason for the high viscosity is that the SiO₂ makes big networks producing anions in manganese silicate slags:



Figure 2.3 shows how the SiO₄⁴⁻ anions may produce long range structures of complex anions. Basic oxides like CaO and MnO will break this network producing cation in slags:



Equation 2.16 is one of the formulas used a lot for calculating the basicity. This formula is mostly used for steel production.

$$LB = \frac{MgO + CaO}{SiO_2} \quad (2.16)$$

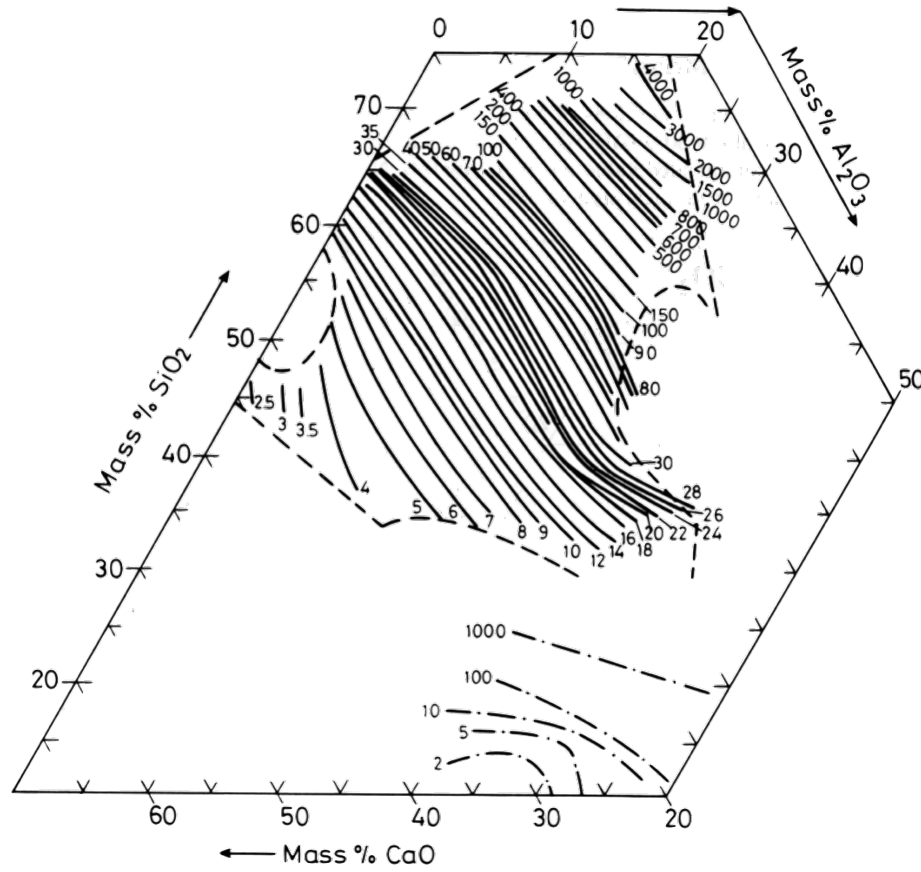


Figure 2.2: Viscosity (poise) in liquid $\text{CaO-SiO}_2\text{-Al}_2\text{O}_3$ slags. (Kvande, 2014).

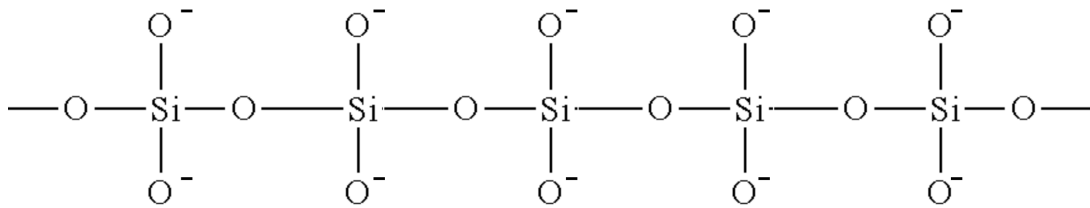


Figure 2.3: Networks of SiO_4^{4-}

For calculating basicity a number named LB2 is typically used for FeMn production:

$$LB2 = \frac{MgO + CaO}{SiO_2 + Al_2O_3} \quad (2.17)$$

For calculation on basicity for SiMn a number named R is used. It is similar to LB2, but silica is not represented in the equation:

$$R = \frac{MgO + CaO}{Al_2O_3} \quad (2.18)$$

Eissa et al. (2004) found that the initial basicity, R ratio (Equation 2.18), of 1.8 gives the maximum recovery for manganese and silicon. This is valid for silicomanganese production and by using dolomite as fluxing material. Adjusting the slag basicity by adding dolomite gives higher metallic yield. Which means it will be higher recoveries of manganese and silicon by adding either limestone or dolomite and limestone together compared with what will be obtained without fluxes added.

4 Thermodynamics

The distribution of Mn and Si between slag and metal is controlled by equilibrium reactions shown under.



The parentheses indicates species in the slag phase and underscore indicates species in the metal phase.

The expected silicon content in the metal can be derived from Equation 2.19.

$$K = \frac{a_{\text{Si}} \cdot p_{\text{CO}}^2}{a_{\text{SiO}_2} \cdot a_{\text{C}}^2} = \frac{\% \text{Si} \cdot \gamma_{\text{Si}}}{\% \text{SiO}_2 \cdot \gamma_{\text{SiO}_2}} \quad (2.24)$$

The partial pressure of CO is assumed to be 1, and the activity of C is assumed to be unit. Then the amount of silicon in the metal at equilibrium can be calculated from Equation 2.25.

$$\% \text{Si} = \frac{K(T) \cdot \% \text{SiO}_2 \cdot \gamma_{\text{SiO}_2}}{\gamma_{\text{Si}}} \quad (2.25)$$

The silicon content in a SiMn alloy is temperature dependent cause K is temperature dependent. The other factors are the activity coefficient of SiO₂ in the slag (γ_{SiO_2}) and the activity coefficient of silicon in the metal (γ_{Si}). The activities of the species are dependent

on the other compounds in the same phase. The activity of a compound is the effective concentration of this compound in the phase.

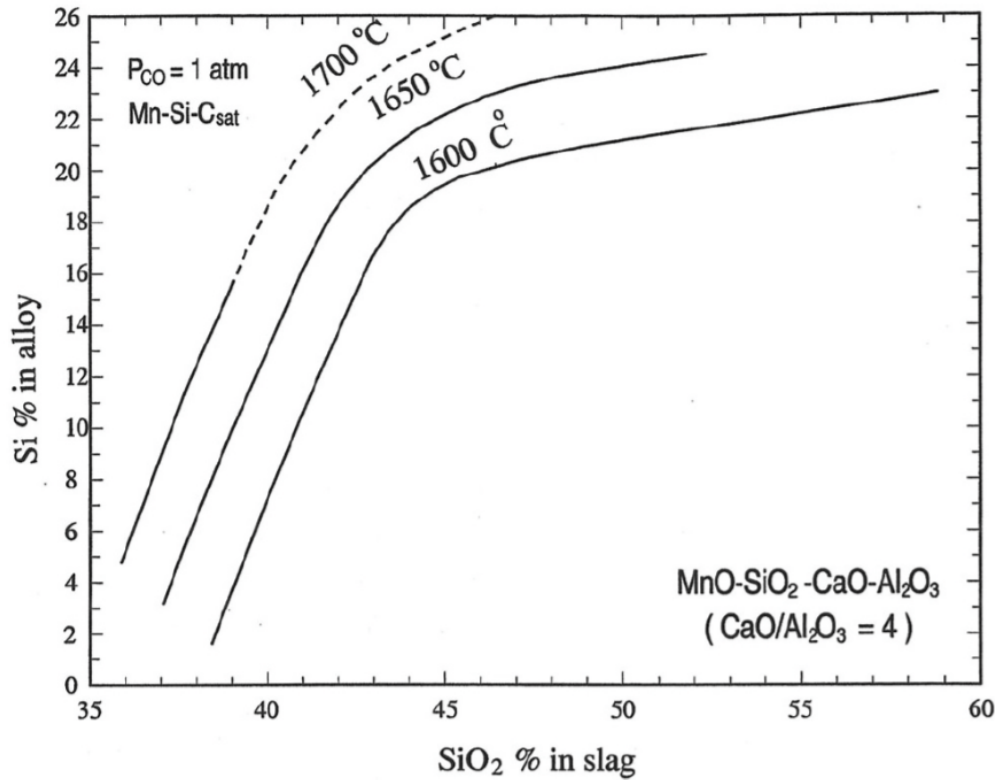


Figure 2.4: The effect of temperature on silicon content in an Mn-Si-C_{sat} alloy at equilibrium with a SiO₂ - CaO - Al₂O₃ - MnO slag with CaO/Al₂O₃ = 4 (Olsen, 2001).

The effect of temperature on silicon content in a Mn-Si-C_{sat} alloy is presented in Figure 2.4. This figure is valid for the Mn-Si-C_{sat} alloy which is in equilibrium with a SiO₂-CaO-MnO-Al₂O₃ slag with R ratio equal 4 (Olsen, 2001). In slags from Comilog charges the R ratio is equal to CaO/Al₂O₃ because of about zero MgO in the slag phase.

The effect of temperature and CO pressure on Si recovery is presented in Figure 2.5. It can clearly be seen from the figure that increased temperature and decreased CO pressure favors high Si recovery. In this figure the activity of silica in the slag is 0.2. This is the normal value for SiO₂ in SiMn slags equilibrated with metal containing 18-20 % Si (Olsen et al., 2007).

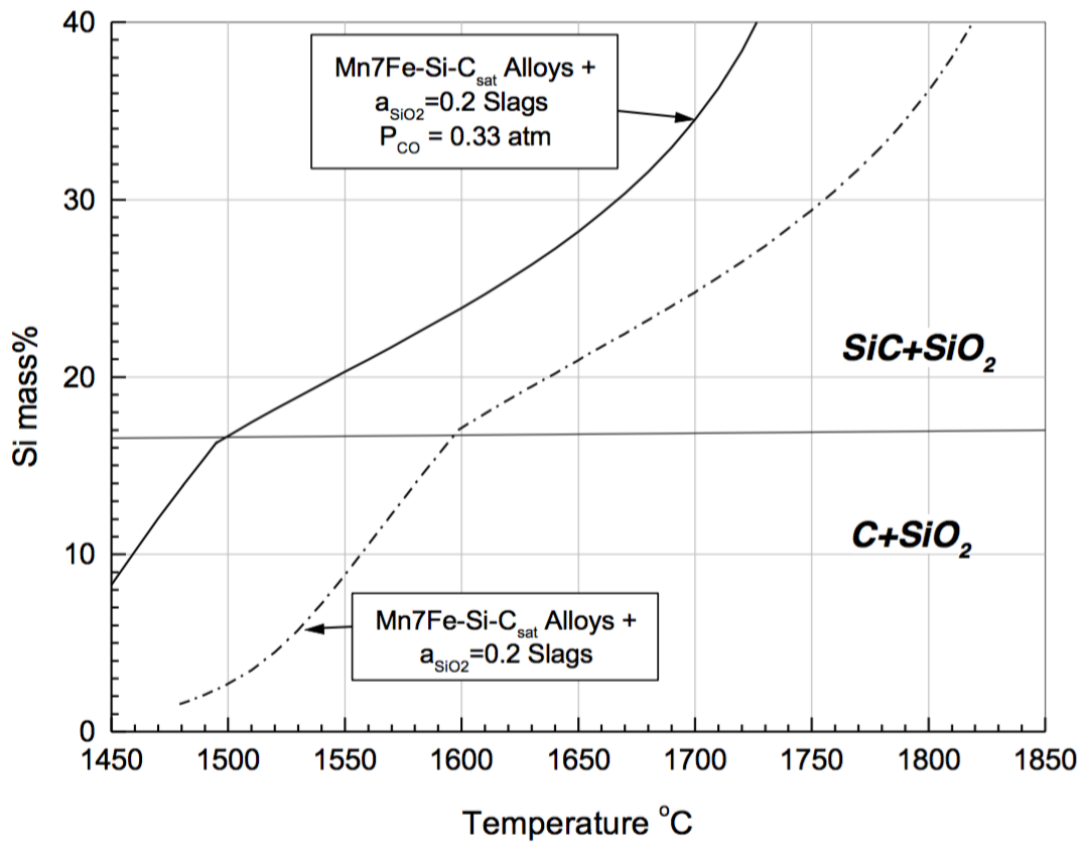


Figure 2.5: Si recovery in Mn-7Fe-Si- C_{sa} alloy as function of temperature at 0.3 atm and 1 atm CO pressure equilibrated with SiO_2 activity of 0.2 in the slag. This graph shows that it is needed between 1600-1650 °C to produce an alloy with 18-20 % Si. (Olsen et al., 2007).

Figure 2.6 show the effect of SiO_2 content and R value in the slag on silicon recovery. This figure is valid for temperature equal 1600 °C and CO pressure equal 1 atm in a Mn-Si- C_{sat} alloy. If R ratio is constant, increased silica content in the slag increase the Si content in the metal. The Si recovery increase fast in the region where C is the stable phase and not so fast in the region where SiC is the stable phase. C is stabil in the range 0-17 % Si in the metal, and with more silicon in the metal SiC is the stabil phase.

Olsen and Tangstad (2004) conclude with that the distribution of Si between the SiMn alloy and the multicomponent $MnO-SiO_2-CaO-Al_2O_3-MgO$ slags is mainly determined by the process temperature, the silica content in the slag and the R ratio.

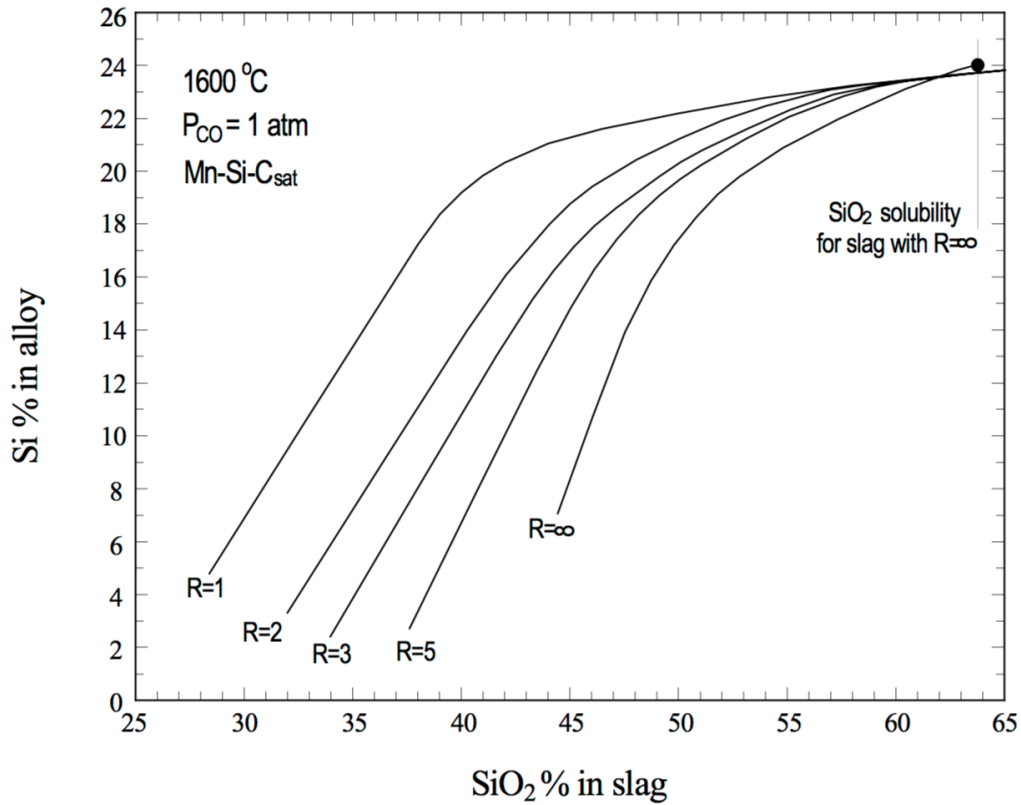


Figure 2.6: Distribution of silicon as function of the R-ratio (Olsen and Tangstad, 2004).

A ternary slag system is shown in Figure 2.7. Curves have constant $a_{\text{MnO}}^2/a_{\text{SiO}_2}$ ratios at 1550 °C, and have been calculated and drawn in the liquid area by Olsen et al. (2007). These curves represent slags which are in equilibrium with the same Mn-Si-C_{sat} alloy, defined by $a_{\text{Mn}}^2/a_{\text{Si}}$ ratio. The silicon contents of each metal alloy in equilibrium with such slags are shown on each curve.

The slag composition becomes unique if one restriction is introduced, for example by fixing the CaO/SiO₂ ratio. Restrictions like this can be shown as straight lines in the ternary diagram. The basicity line in Figure 2.7 represent the ratio:

$$\frac{\text{CaO}}{\text{SiO}_2} = \frac{40}{60} = \frac{2}{3}$$

Fixed basicity and a certain metal composition represent one and only one point in the ternary diagram, and that is at the intersection point of the two lines. It is 5 % Si content which is marked at the basicity line in Figure 2.7. If the silicon content in the metal is 18 %,

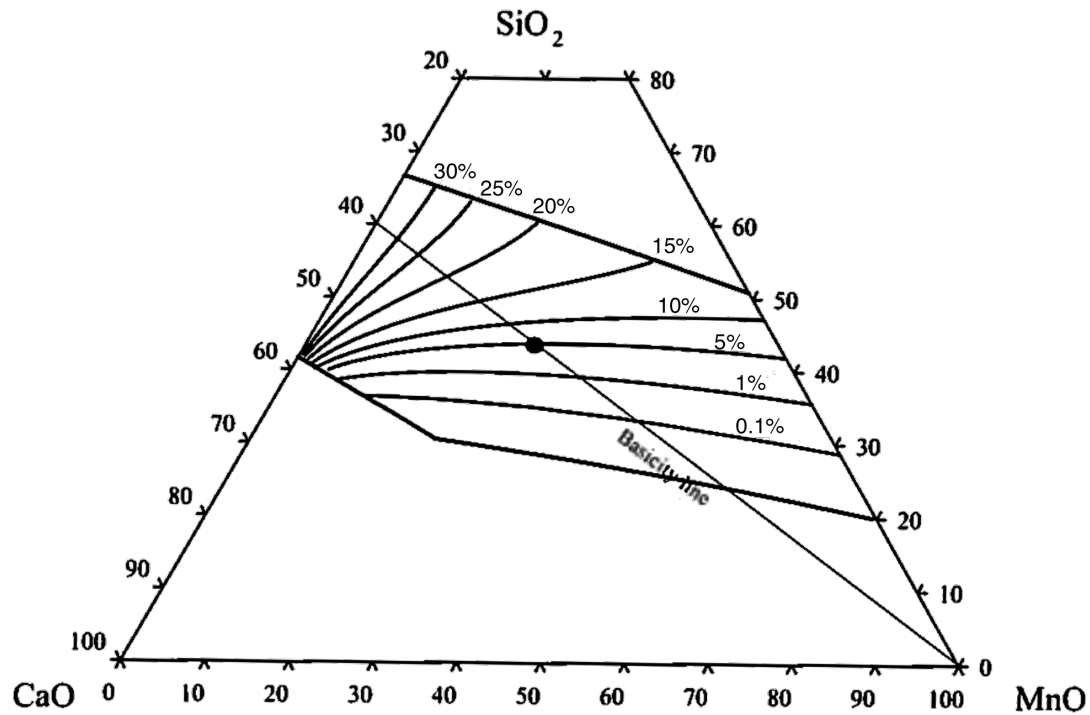


Figure 2.7: Ternary slag diagram for the MnO-SiO₂-CaO system. Calculated constant $a_{\text{MnO}}^2/a_{\text{SiO}_2}$ ratio lines at 1550 °C. Corresponding silicon content of alloys at each curve. Reprinted from Olsen et al. (2007). Slag composition equilibrated with 5% Si metal at given basicity ratio is marked as example.

the MnO content in the slag will be between 10 % and 20 % at this basicity.

Nadir (2015) calculated the equilibrium slag composition as function of temperature. The start composition for this slag can be seen from Figure 2.8. This model is based on these assumptions:

- 100 % of CaO, MgO and Al₂O₃ goes into the slag phase.
- 100 % of iron oxide is reduced to metallic iron at 1200 °C.
- MnO is not reduced until 1200 °C and SiO₂ is not reduced until 1400 °C.
- Only Mn and Si are distributed between the slag and the metal phase.

The results from this model is shown in Figure 2.8. The unreducible oxides show a continues increase in concentration in the slag phase with increased temperature, and that

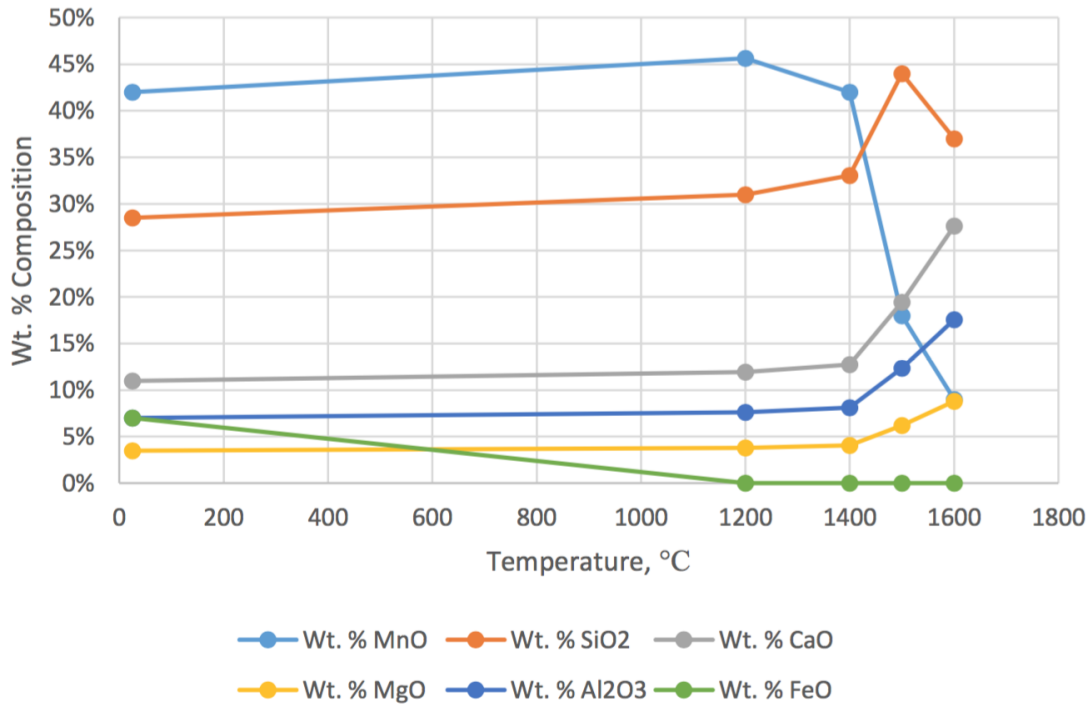


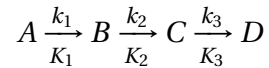
Figure 2.8: Equilibrium slag composition model as function of temperature (Nadir, 2015).

is naturally because of reduction of MnO and SiO₂. From 1200 °C to 1400 °C, only MnO is reduced which can be seen in the figure. Above 1400 °C and until 1500 °C, both MnO and SiO₂ are reduced, however the reduction rate for silica is quite low at these temperatures and hence the MnO content in the slag is observed to constantly decrease and silica content in the slag still increase. Above 1500 °C the reduction rate for SiO₂ also increase which can be seen from the decreasing amount of silica in the slag.

5 Kinetics

From thermodynamics the final, equilibrium state for a reaction may be predicted, but thermodynamic gives no information about the rate at which this equilibrium is reached.

One way to describe the kinetics for a general reaction A-D will be discussed in the following. Look up to the reaction $A \rightarrow D$, where A is the reactants and D is the products (Rosenqvist, 2004).



Here B and C represent the intermediate reaction products. k_1 , k_2 and k_3 represent the forward reaction rates for the three steps, and K_1 , K_2 and K_3 is the equilibrium constants for the different steps in the reaction.

The step with smallest rate constant, k , is the rate determining step.

The rate constants increase with increasing temperature. The Swedish chemist Svante Arrhenius found the relationship between the temperature and the rate constant described in Equation 2.26.

$$k = k_0 \cdot e^{\frac{-E}{RT}} \quad (2.26)$$

R is the gas constant, k_0 is the frequency factor, T is the temperature and E is the activation energy.

Skjervheim (1994) did his Dr.ing. work on the kinetics of reduction of Mn slags in graphite crucibles. The following conclusions were made:

- Substitution of SiO_2 or Al_2O_3 with CaO increases the reduction rate.
- Substitution of SiO_2 by Al_2O_3 did not affect the reduction rate.
- The reduction rate is faster in industrial slag than in synthetic oxide mixtures.
- Iron in the metal phase increases the reduction rate for synthetic slags, but not for industrial slags.
- Sulfur added to the metal increases the reduction rate.
- The source of carbon is important. The average rate of MnO reduction during the slow second stage, was found to be 2.3 times larger per unit area at the slag/graphite interface than at the slag/metal interface. Dijks and Smith (1980) showed that coke and other natural carbon materials gave much higher reduction rate for FeMn slags than

graphite. This probably means that the main part of the reduction in a FeMn furnace will occur at the slag/coke interface.



The strong influence of temperature on the kinetics and the high endothermic behavior of the reactions suggest that the rate limiting step is none other than the chemical reaction from Equation 2.27. The reaction rate can be assumed by the first order equation as given in Equation 2.28 (Ostrovski et al., 2002).

$$R = \frac{-dm_{\text{MnO}}}{dt} = k \cdot A(a_{\text{MnO}} - \frac{P_{\text{CO}} \cdot a_{\text{Mn}}}{K}) \quad (2.28)$$

where k is the chemical reaction rate constant, A is the interfacial area for the chemical reaction, a_{MnO} is the activity in molten slag, P_{CO} is the CO partial pressure in the bulk gas phase, a_{Mn} is the activity of manganese in the metallic phase and K is the equilibrium constant for the reduction reaction.

The driving force for MnO reduction according to Equation 2.28 is the difference between actual MnO activity and the activity of MnO in the slag at equilibrium. The driving force is given in Equation 2.29.

$$a_{\text{MnO}} - \frac{P_{\text{CO}} \cdot a_{\text{Mn}}}{K} = a_{\text{MnO}} - a_{\text{MnO}_{eq}} \quad (2.29)$$

In the two phase region where solid MnO exist MnO will have a high and constant activity. This will result in a fast and constant reduction rate in the two phase area until all solid MnO is reduced. In the liquid slag the reduction rate will continuously decrease due to decrease in the activity of MnO and hence decrease in driving force.

Figure 2.9 illustrate the two stage reduction behavior of MnO. The high and constant reduction rate represent the two phase stage where solid MnO exist, and where the fast drop in reduction rate occur represent the liquidus temperature.

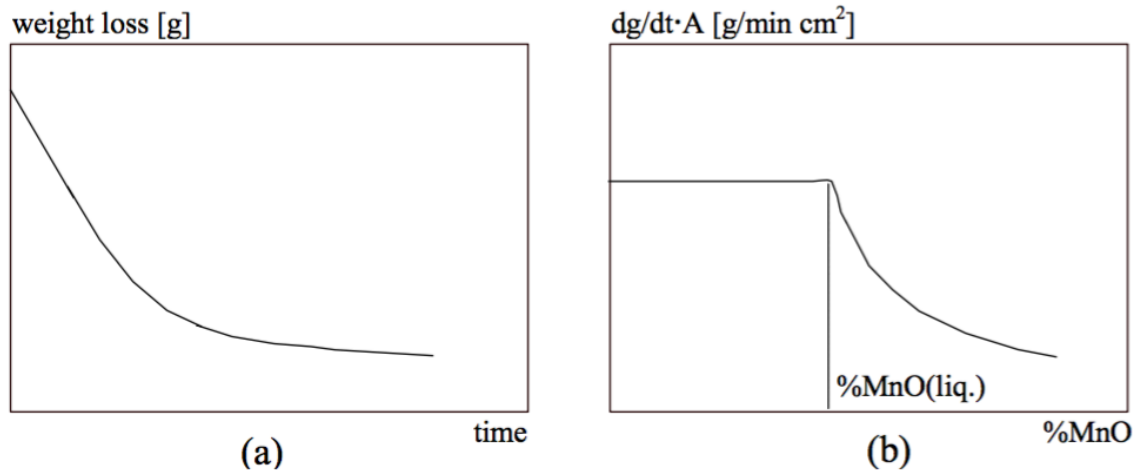


Figure 2.9: The two stage reduction behavior of MnO. (a) weight loss vs. time. (b) Reduction rate vs. % MnO (Olsen et al., 2007).

6 Phase Diagrams

In this chapter ternary phase diagrams for the most relevant slag systems are presented. Phase diagrams are good tools for looking at which phases it should be in the system at different temperatures at equilibrium. It is possible to look at phase diagrams with more than three compounds, but here it is focused on ternary diagrams with three species.

6.1 MnO-SiO₂-Al₂O₃ System

Charges which include Comilog ore, limestone and quartz in typical industrial ratio for SiMn production will typically have composition inside the MnSiO₃ area or the Mn₂SiO₄ area in the phase diagram in Figure 2.10. Which of these primary crystallization areas the total composition will be inside depends on which assumptions that are done. CaO is similar in properties to MnO, so they can be added together in the calculations. With this assumption the total composition will move a bit towards the MnO corner.

The diagram shows that this typical composition is a fully liquid phase above 1300 °C, and may also be fully liquid at as low as 1200 °C depending on the composition.

This total composition is inside the alkemade triangle between Mn-pyroxene, Mn₂SiO₄ and MnSiO₃ or inside the alkemade triangle between silica, MnSiO₃ and Mn-pyroxene. This

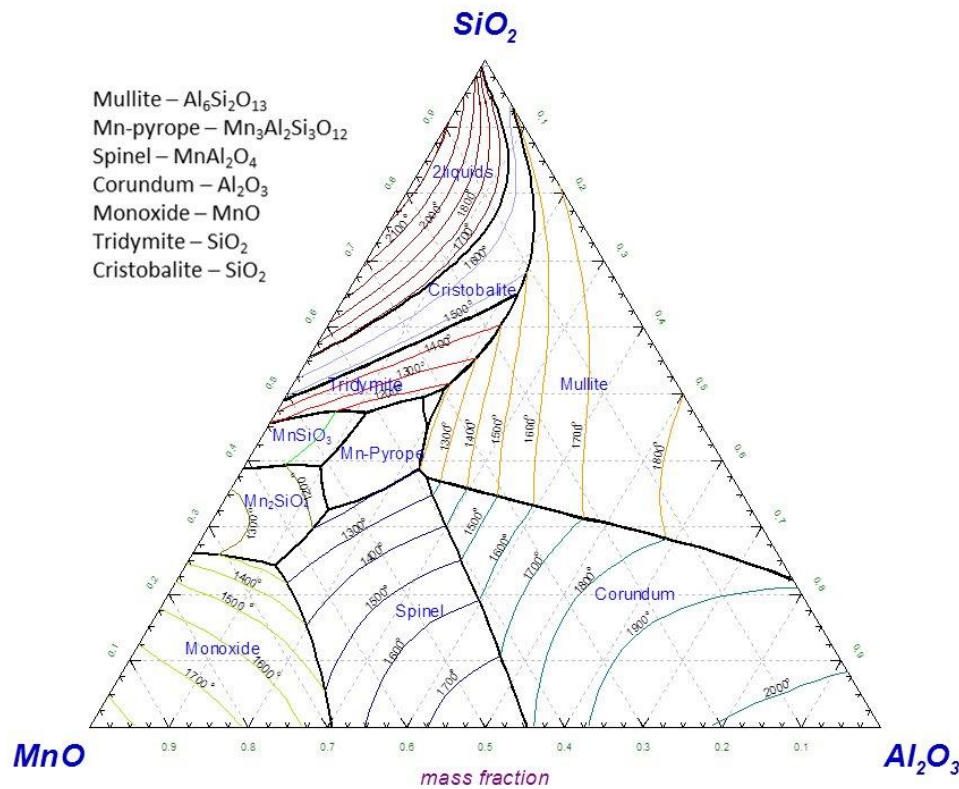


Figure 2.10: Phase diagram for the MnO-SiO₂-Al₂O₃ system. (Tangstad, 2013).

means that the final liquid phase ends up in one of these two eutectic points which both have melting temperature lower than 1200 °C.

6.2 MnO-SiO₂-CaO System

Figure 2.11 shows the phase diagram for the MnO-SiO₂-CaO system. As mentioned earlier CaO and MnO have similar impact to the slag system, and Ca and Mn have great solubility in each other, which is shown with an big area of (Ca,Mn)O phase in the lower part of the phase diagram.

Typical charges for SiMn production have about 40 % silica. That means the total composition of the charge will be inside the 1300 °C isothermal plan and be fully liquid above 1300 °C. The charge may also be liquid at about 1200 °C because of the 1200 °C isotherm in this area in the phase diagram. These temperatures fit good to the temperatures in the MnO, SiO₂, Al₂O₃ phase diagram.

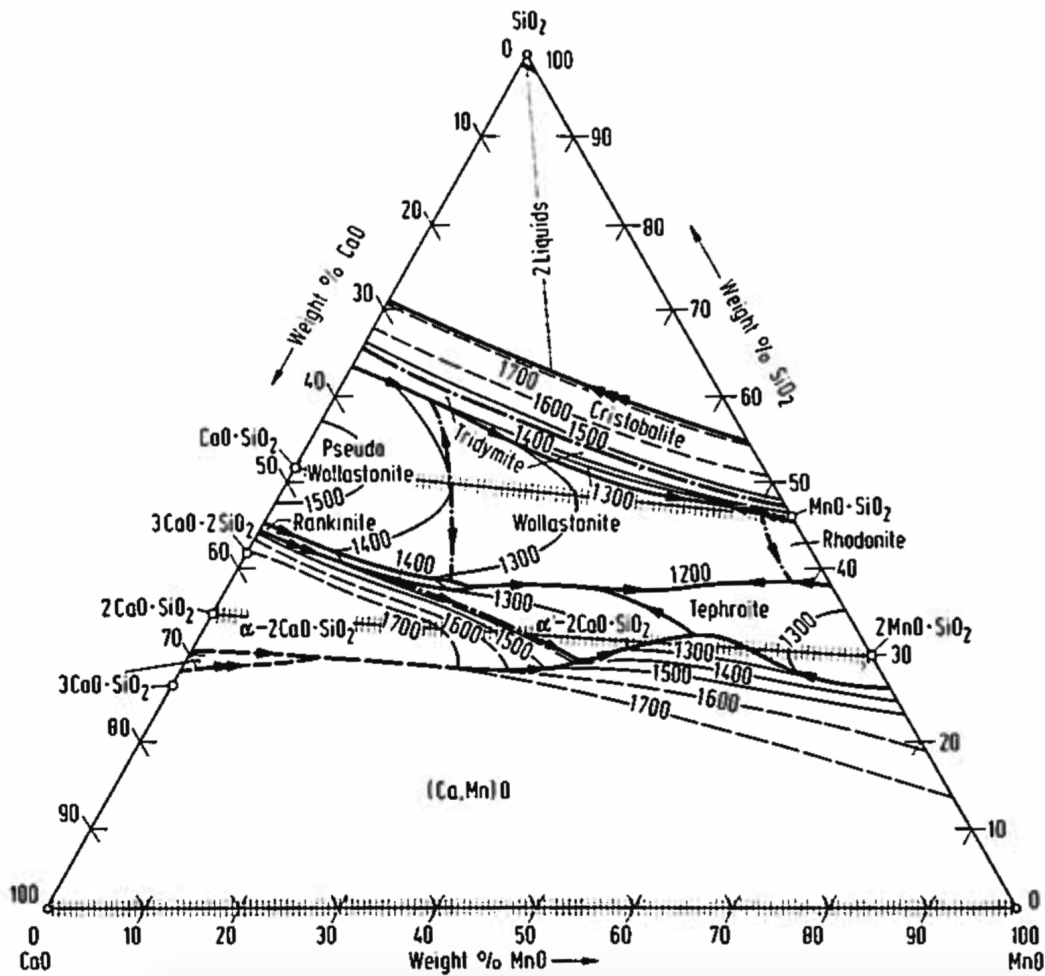


Figure 2.11: Phase diagram for the MnO-SiO₂-CaO system. Reprinted from Allibert et al. (1995).

6.3 CaO-SiO₂-Al₂O₃ System

Phase diagram for the CaO-SiO₂-Al₂O₃ ternary system is shown in Figure 2.12. In this figure it is used A, C and S for the oxides in the ternary system. A means Al₂O₃, C means CaO and S means SiO₂.

Also in this system it is possible to calculate the MnO content together with the CaO, because of the similar effect on the slag. This may also be an OK approximation because the MnO content in the final slag may be quite low, however when it comes to the charge mixture with a high MnO content the approximations are more uncertain.

Slags with 40-60 % silica which are low in alumina have the lowest liquidus temperature

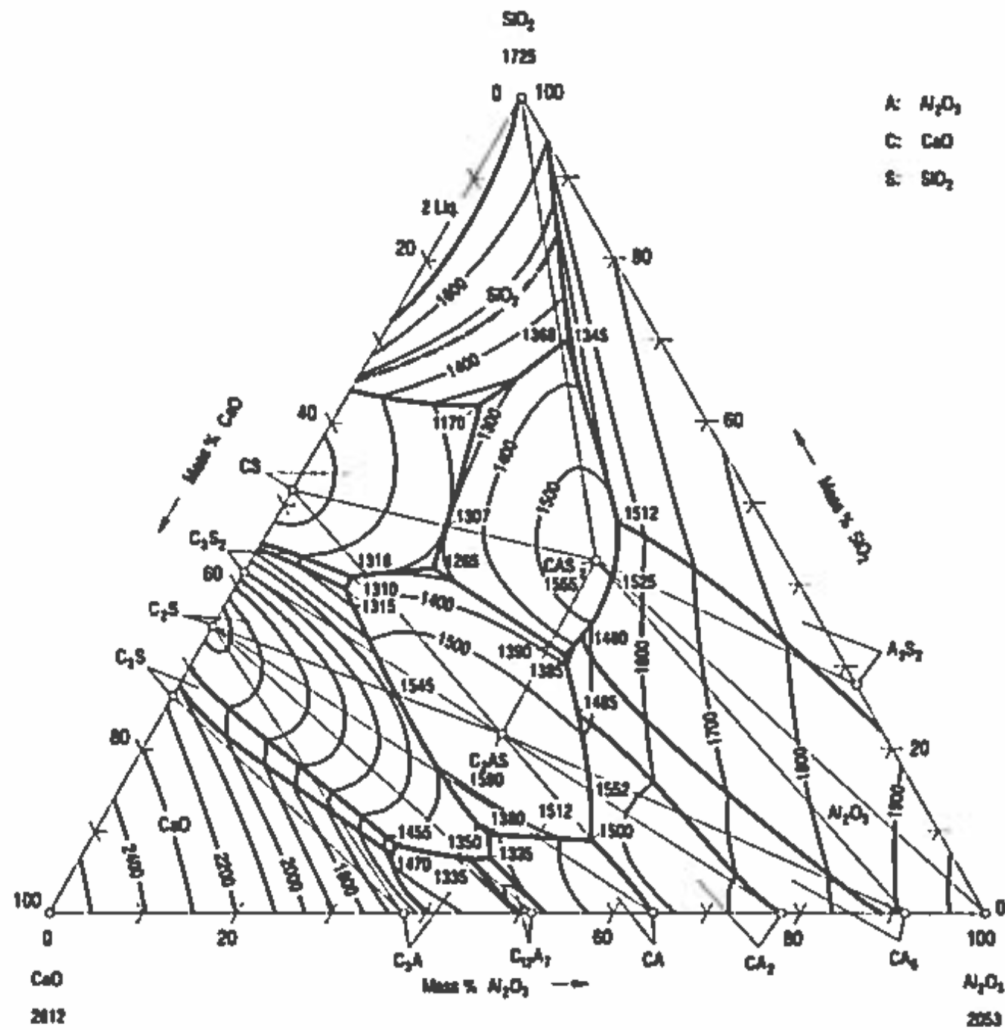


Figure 2.12: Phase diagram for the Al_2O_3 - SiO_2 - CaO system. Reprinted from Allibert et al. (1995).

in this phase diagram.

The calcium silicates have higher melting temperature than the manganese silicates. MnSiO_3 melts at about 1300 °C, and CaSiO_3 melts at higher than 1500 °C. Mn_2SiO_4 melts at about 1350 °C, and Ca_2SiO_4 melts at higher than 2100 °C.

7 Reduction of Mn Ores

7.1 Size Impact

Holtan (2015c) investigated the reduction rate as a function of the size of the raw materials. It was found that the reduction rate depend on the size fractions in FeMn charges with only Comilog ore and coke, and that the reduction rate was independent of size fractions in SiMn charges with quartz. The size fractions that were investigated by Holtan (2015c) was 0.6-1.6 mm and 4.0-6.3 mm. That means that these results are valid within this size fractions.

Figure 2.13 shows that the smallest size fraction of the raw materials is reduced faster than large raw material size fraction for FeMn charges. The blue line represent the 0.6-1.6 mm fraction, and the orange line represent the 4.0-6.3 mm fraction.

Figure 2.14 shows the weight loss curves for SiMn charges with Comilog ore, coke and quartz, with and without limestone added. These curves shows that the reduction rate is similar for charges with small and big size fractions of the raw materials in these charges.

In these figures the first mass loss step is due to reduction of higher manganese oxides to Mn_3O_4 , higher iron oxides to FeO and evaporation of water. This step is the same for all charges, because all weight loss is from the ore. No reactions occur among the different raw materials. The second weight loss step is due to reduction of FeO to metallic iron, and reduction of Mn_3O_4 with CO (g) to MnO. For the experiments with limestone, Figure 2.14b, the weight loss also is due to the decompose of limestone to CaO and CO_2 (Holtan, 2015a).

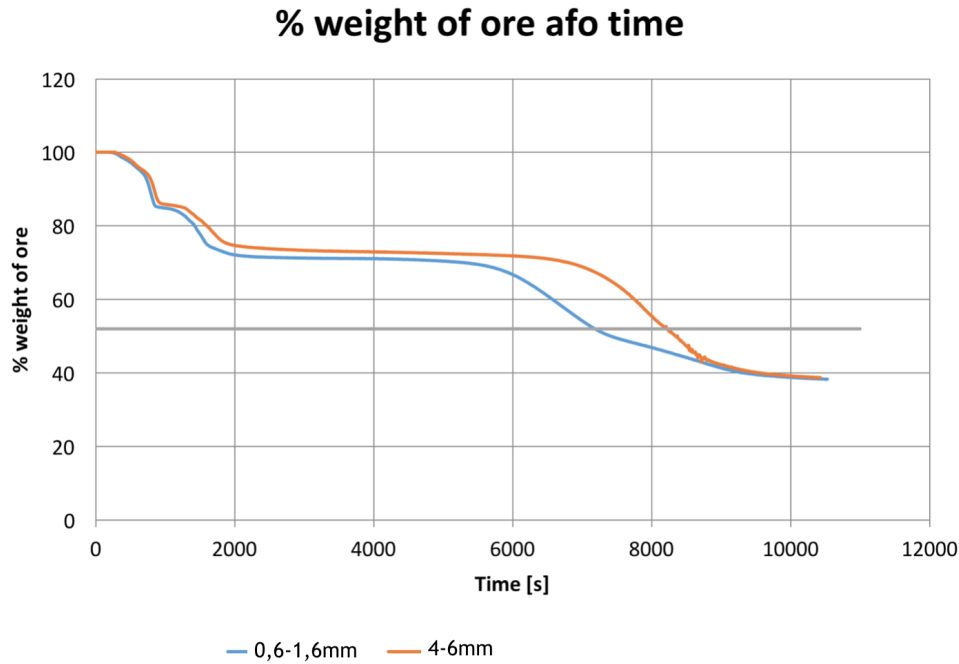


Figure 2.13: Weight loss graphs for comparing size fractions in experiments with Comilog ore and coke, FeMn charge at increasing temperature. Reprinted from Holtan (2015c).

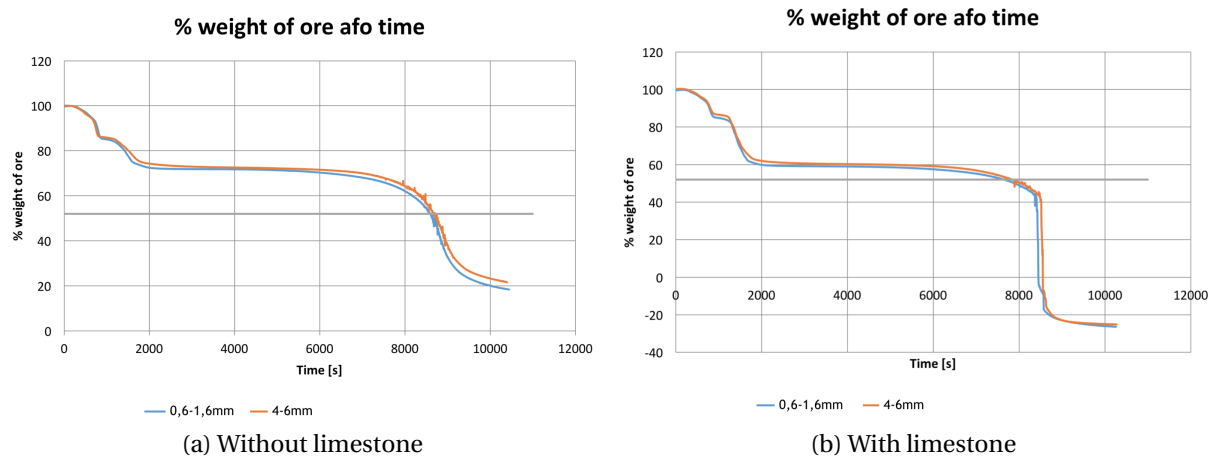


Figure 2.14: Weight loss graphs for comparing size fractions in SiMn charges with Comilog ore and quartz at increasing temperature. Reprinted from Holtan (2015c).

Kim et al. (2016) also investigated the size impact on the reduction rate. In this work it is used the same size fractions as Holtan (2015c). The influence of particle sizes showed different results for FeMn and SiMn charge samples. The mass loss difference between particle sizes was mainly observed with Assmang ore or Comilog ore mixed with only coke,

As.1 and Com.1 in Figure 2.15 respectively. This means that it is difference in reduction rate for the FeMn charge samples. FeMn charge samples with particle size between 0.6-1.6 mm showed earlier mass loss than the samples with particle sizes between 4.0-6.3 mm on the raw materials. In Figure 2.15, curves which are green, are from samples with Assmang ore, and the orange curves are from samples with Comilog ore. Dotted lines represent the small size fraction, and the lines the big size fraction.

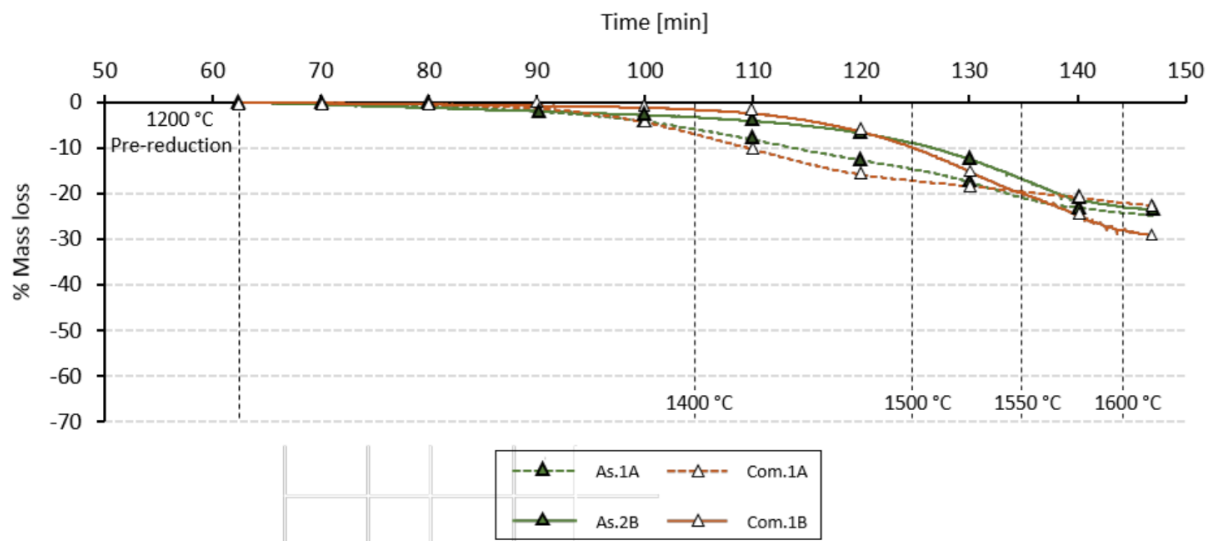


Figure 2.15: Weight loss graphs for comparing size fractions in experiments with manganese ore and coke, FeMn charge at increasing temperature. Reprinted from Kim et al. (2016).

However, when Assmang ore or Comilog ore were mixed with quartz and HC FeMn slag, which is SiMn charge samples, the mass loss difference between the two different size fractions were insignificant compared to FeMn charges during reduction (Kim et al., 2016). Weight loss curves for SiMn charges are shown in Figure 2.16. Dotted lines represent sample with the small size fraction, and lines represent the big size fraction. Light green, As.2 samples, are from experiments with Assmang ore and quartz, dark green, As.3 samples are from experiments with Assmang ore, quartz and HC FeMn slag. The orange curves represent the experiments done with Comilog ore, the light curves with only quartz added, and the dark curves with quartz and limestone added together.

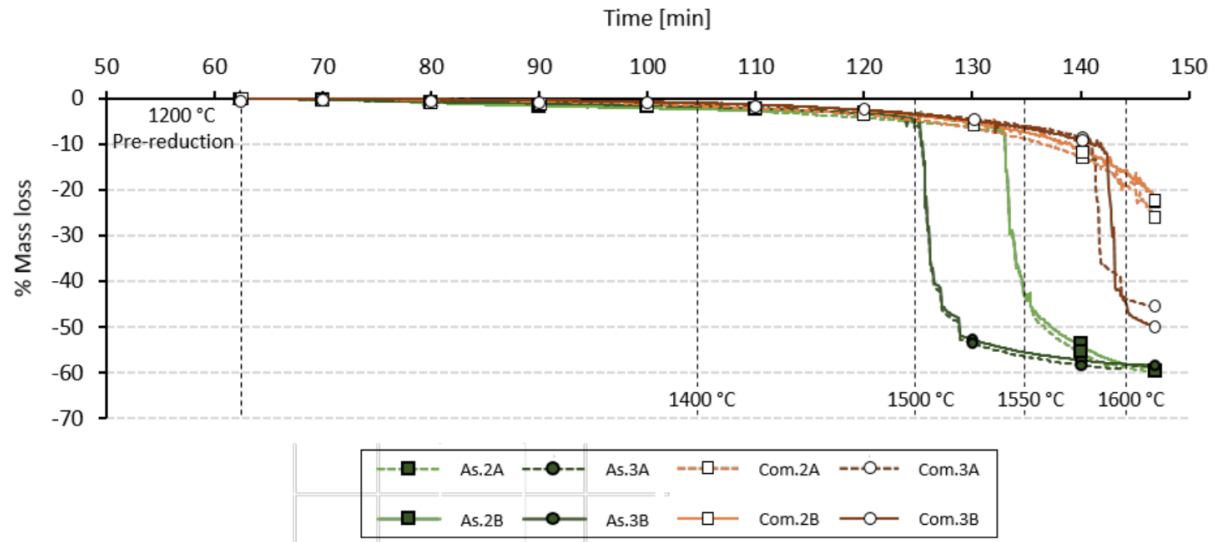


Figure 2.16: Weight loss graphs for comparing size fractions in experiments with SiMn charge at increasing temperature. Reprinted from Kim et al. (2016).

This comparison between FeMn and SiMn charge samples shows that size of raw materials might not be an evaluating variable during the reduction of MnO and SiO₂ for SiMn production. If manganese ore and quartz particles are completely dissolved into a slag phase shortly after prereduction, particle size will no longer be a variable influencing the weight loss and further the reduction of MnO and SiO₂.

7.2 Melting and Reduction

Previous investigations have investigated when the ore will start to behave like a liquid. Gabonese ores, such as Comilog ore, start melting at $1485\text{ °C} \pm 11\text{ °C}$ and are finished melting at $1538\text{ °C} \pm 9\text{ °C}$. The reduction start at $1496\text{ °C} \pm 11\text{ °C}$. These numbers are retrieved from Ringdalen et al. (2010). Assman ore start melting at $1446\text{ °C} \pm 70\text{ °C}$ and are finished melting at $1513\text{ °C} \pm 57\text{ °C}$. The reduction start at $1474\text{ °C} \pm 78\text{ °C}$. From Ringdalen et al. (2010) it seems like Assman ore is reduced at about 20 °C lower temperature than Comilog ore. Kim et al. (2016) also conclude with a lower reduction temperature for Assman ore than for Comilog ore.

Brynjulfsen (2013) found that generally the materials that melt at a low temperature will reduce at a lower temperature than materials that melt at a higher temperature.

Figure 2.17 show models of degree of reduction. This shows that the materials that start to reduce at the lowest temperature, will be 100 % reduced at the lowest temperature.

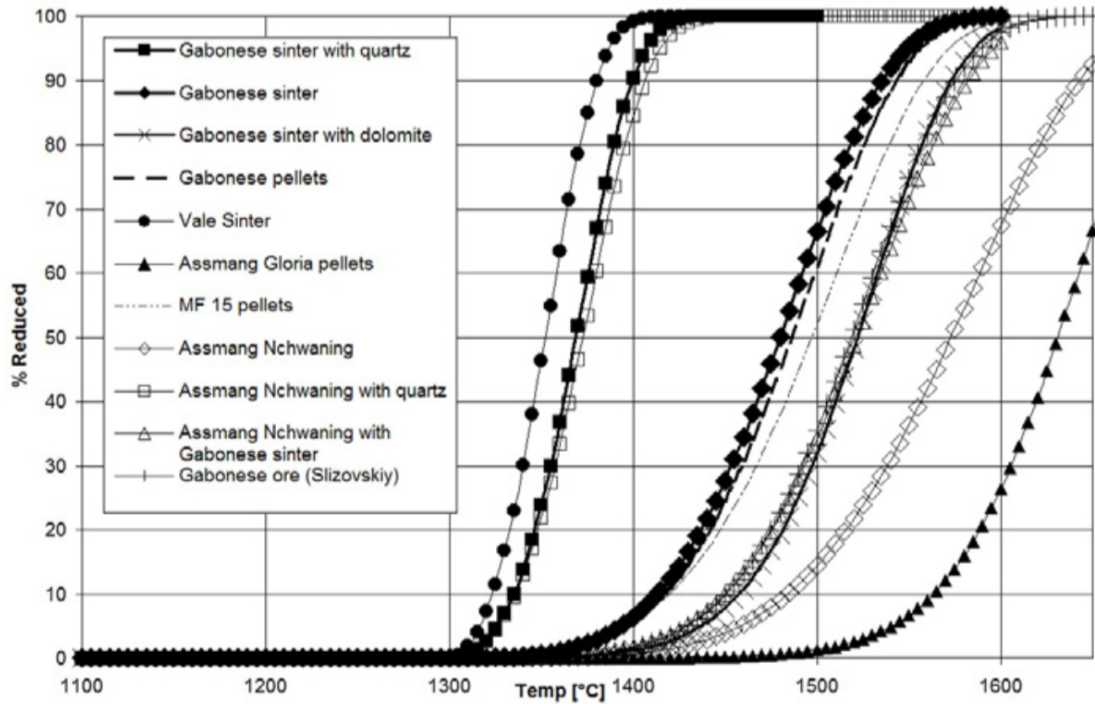


Figure 2.17: Percentage reduced as a function of temperature. Reprinted from Brynjulfsen (2013).

Tangstad (1996) found that charges with same basicity, but with different ores have different reduction rate. Charges with basicity of about 1, Comilog ore is one of the ores that reduces fastest. This is probably caused by the Al_2O_3 to SiO_2 ratio, which is the main difference between the ores. A higher Al_2O_3 to SiO_2 ratio seems to give a higher reduction rate.

Chapter 3

Experimental Work

This chapter contains data of the raw materials used in this work, and the equipment. The execution of the experiments are described in this chapter, and also how the samples and the data from the experiments are treated.

1 Raw Materials

In this work it is used manganese ore, coke, quartz and limestone. The ore used is Comilog ore, and the coke used is Chinese coke. The size of all raw materials were 4.0 mm - 6.3 mm. The raw materials are crushed and then sieved to obtain the right size.

1.1 Comilog Ore

The ore used in the experiments is a Comilog ore analyzed by SINTEF Molab AS and the results are presented in Holtan (2015c). Table 3.1 shows the composition of this ore.

When calculating the weight loss from this ore (shown in Table 3.4) it was assumed 5 % water content, and all Mn content which is not MnO_2 was assumed to be MnO. Iron content was calculated to Fe_2O_3 content. If this is assumed, the total results then became 97 %, so the results was normalized before further calculations.

Table 3.1: Composition of Comilog ore. (Holtan, 2015c).

	%
SiO ₂	6.5
TiO ₂	0.15
P	0.12
S	0.03
Al ₂ O ₃	6.9
Fe ₂ O ₃	6.47
Mn total	46.9
MnO ₂	69.4
MnO	3.91
CaO	0.29
BaO	0.25
MgO	0.13
K ₂ O	0.84
H ₂ O	5.0

1.2 Coke

Table 3.2 shows the composition of the Chinese coke used in this work. SINTEF Molab AS has analyzed the coke and the analyzed results was present in Holtan (2015c).

Table 3.2: Composition of coke. (Holtan, 2015c).

	%
Ash	17.9
Fix C	78.6
Vol	3.5
Ash composition	%
SiO ₂	54.2
TiO ₂	0.97
Al ₂ O ₃	20.8
P ₂ O ₅	0.41
Fe ₂ O ₃	10.1
MnO	3.3
CaO	7.2
MgO	1.8
K ₂ O	0.58
Na ₂ O	0.61

1.3 Limestone

Table 3.3 shows a typical composition of limestone. This is one typical analysis used in this work when calculating weight loss and mass balance.

Table 3.3: Composition of the limestone [wt%] (Tangstad, 2016).

	%
CaO	51.98
SiO ₂	0.96
Al ₂ O ₃	0.26
CO ₂	45.72
MgO	0.96
Total	99.88

1.4 Weight Loss During Prereduction

As shown in Figure 2.1 there are several reactions in the prereduction zone. This reactions causes weight loss. Water evaporate, and some oxygen go off from different oxides.

At 1200 °C it is assumed that:

- All water is evaporated.
- All MnO_x has gone to MnO.
- All FeO_x has gone to metallic Fe.
- All CO₂ has gone off from the carbonates.

The weight loss from the ores in Table 2.1 will then be as shown in Table 3.4.

2 Equipment

2.1 Thermogravimetric Furnace

The furnace used in this work is a thermogravimetric graphite tube furnace. This furnace measures the weight of the sample during the experiment. Setup for the experiments in the

Table 3.4: Calculated weight loss for some manganese ores at 1200 °C.

Ore	Weight loss [%]
Comilog MMA	26.2
Comilog MMD	25.5
Comilog MMR	25.5
Comilog MMS	26.0
Comilog Sinter	5.4
Asman 48	13.7
Amapa Sinter	7.8
Amapa Miudo 40	22.3
Mamatwan	31.0
Gloria	28.0
Groote Eylandt	19.7
CVRD Sinter	6.1
Wessel 38%	18.5
Wessel 50%	15.6
Comilog from Holtan (2015c)	25.7

furnace is shown in Figure 3.1. Detailed setup for the furnace with cooling water tubes, gas flow and scale bar is shown in Figure 3.2.

The software which control the power to the furnace, use the temperature measured by the wall thermocouple which is about 400 °C lower than the temperature measured by the thermocouple inside the furnace when the temperatures are between 1000 °C-1600 °C. The wall thermocouple is a S-type thermocouple, and the one in the bottom is B-type thermocouple. Figure 3.2 shows a detailed drawing of the furnace with scale bar.

Figure 3.3 shows how the temperature inside the furnace varies with height. The temperature on the furnace was set to be constant during the measurement of the temperature gradient. Temperature profile was measured inside furnace without crucible present.

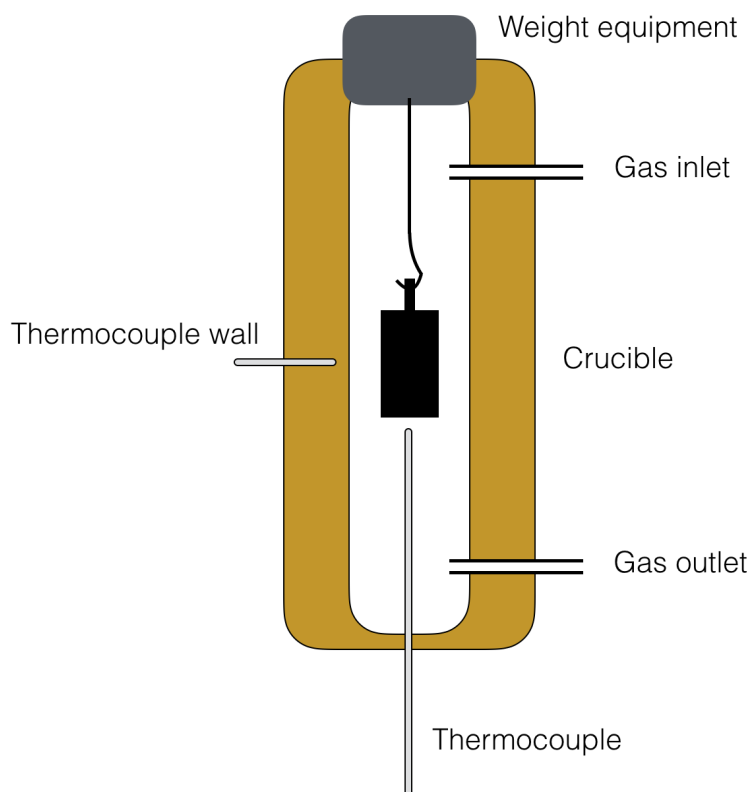


Figure 3.1: Setup of the thermogravimetric furnace (Holtan, 2015b).

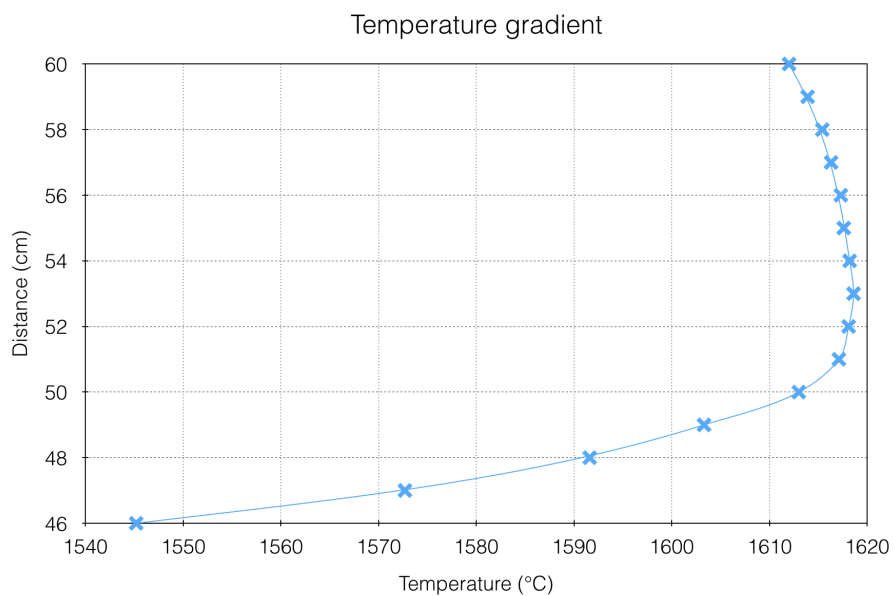


Figure 3.3: Measured temperature gradient inside the furnace.

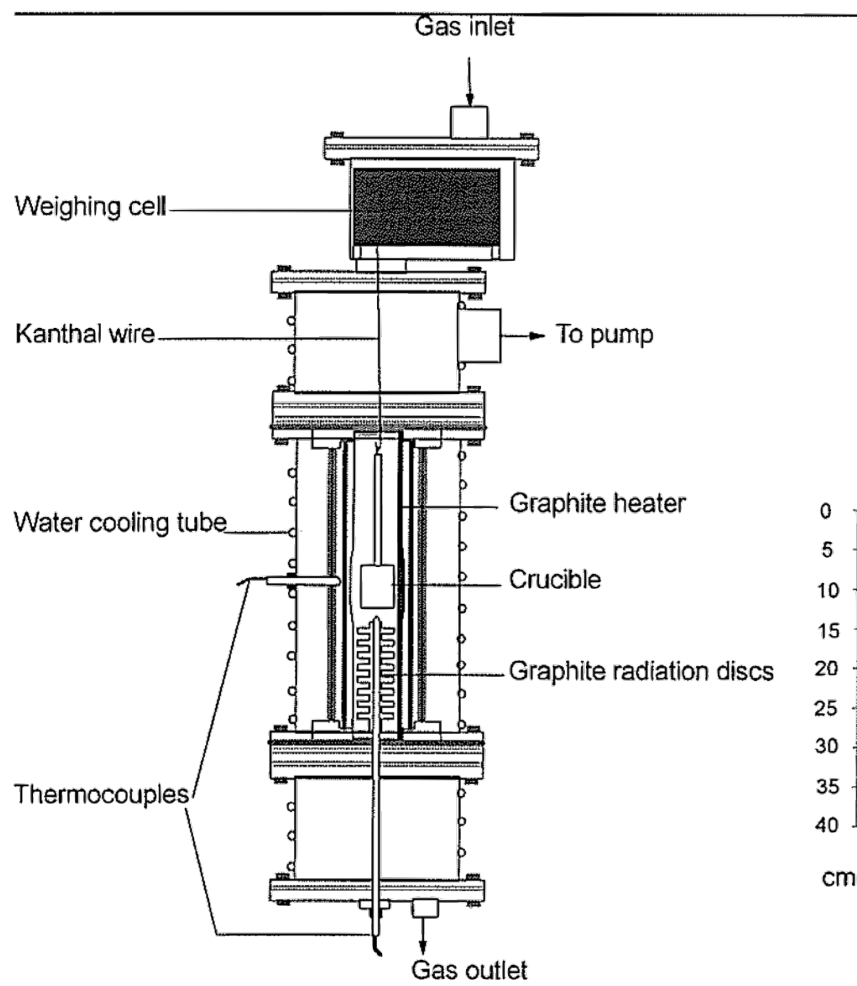


Figure 3.2: Detailed drawing of the graphite tube furnace. Reprinted from Tangstad (1996).

The total height of the crucibles are 10 cm, but the part where the raw materials are, is 7.4 cm. In this experiments the bottom of the crucibles have been placed 50 cm from the bottom of the furnace, due to the temperature gradient. From 50 cm and 10 cm up, it is fairly constant temperature. The temperature varies only about 10 °C. Due to good heat conductivity of carbon, the temperature gradient in the sample will be smaller than shown in Figure 3.3.

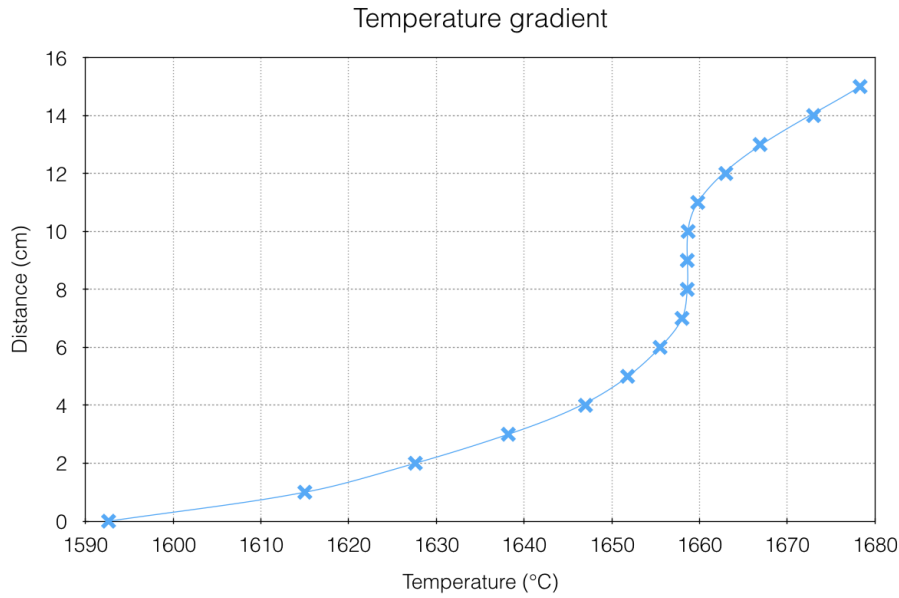


Figure 3.4: Measured temperature gradient inside the SINTEF furnace.

Also SINTEF's thermogravimetric furnace in the SiO lab is used for some of the experiments. The temperature profile inside this furnace was measured the same way as for the first furnace described over. The results from this measurement is shown in Figure 3.4. The crucibles were put into the most stable temperature area in the furnace, that is with the bottom at 6 cm.

2.2 Crucibles

In this work, graphite crucibles are used. Total height of the crucibles plus lid are 10 cm and the diameter is 3.5 cm. The crucible itself is 7.4 cm high, but the suspension of the lid is 2.6 cm. This suspension has a hole so it is easy to place it at the hook inside the furnace. The lid has threads for screwing on the crucible. There are three holes in the lid for the gas to go in or out of the crucible.

The crucibles are tested for weight loss during heating in the thermogravimetric furnace. An empty crucible was heated up to 1600 °C following the temperature profile all the experiments have followed in this work (Figure 3.6), and the weight was measured during heating. The weight of the crucible before heating was 57.16 g, and after heating it

was 57.14 g. The result was no insignificant weight loss in the crucible itself, this is within uncertainty of the weight used to measure the crucible before and after. So the conclusion of this simple experiment is that all weight loss measured in the experiments during this work comes from the raw materials.

3 Experiments

Table 3.5 shows an overview of the experiments done in this work. The charge mixture is calculated to obtain 18 % silicon in the metal phase, and 5 % MnO and 40 % SiO₂ in the slag. Calculations of quartz amount needed in the charge mixture are shown in Appendix B.

Table 3.5: Overview of the experiments done in this work.

Experiment	Max. Temp. [°C]	Comilog Ore [g]	Coke [g]	Quartz [g]	Limestone [g]
L1	1625	17.90	5.83	7.10	5.27
L2	1605	17.95	5.86	7.11	5.29
L3	1350	18.47	5.81	7.11	6.00
L4	1650	5.88	1.95	2.34	1.73
L5	1650	5.94	1.96	2.31	1.80
Q1	1700	23.08	6.86	6.02	0
Q2	1670	7.59	2.29	2.14	0

Table 3.6: Overview of the samples investigated in this work.

Experiment	Max. Temp. [°C]	Comilog Ore [g]	Coke [g]	Quartz [g]	Limestone [g]
1.1	1400	17.92	5.83	7.03	5.27
1.2	1300	18.01	5.90	7.11	5.30
1.3	1250	17.87	5.83	7.04	5.20
2.1	1400	23.05	6.91	6.10	0
2.2	1300	23.06	6.93	6.07	0
2.3	1250	23.16	7.03	6.14	0
6	1600	23.05	7.02	7.11	0
9	1600	17.92	5.83	7.03	5.27

Some of the samples got slag on the lid of the crucible after heating. This was observed for some samples, and for other samples it was observed a rapid mass loss due to slag drop

out of the crucible. This phenomena has to be due to foaming of the slag in the crucible. It was tried to avoid the slag foaming by adding extra coke on the top of the charge in Experiment L5. The red value of the coke mass for this experiment in Table 3.5 indicate that it is added a lot more coke on the top of this charge. The crucible was filled with the charge described in Table 3.5, and then 11.47 g extra coke was added on the top. The crucible become almost completely filled.

In this work it is also investigated some samples from Holtan (2015c) and Holtan (2015a). These samples are present in Table 3.6. Experiments 6 and 9 are from Holtan (2015c) and was hold at 1600 °C for 30 minutes.

Table 3.7: Overview of the weight loss from each experiment.

Experiment	Max. Temp. [°C]	Measured WL [g]	WL furnace [g]	Difference
1.1	1400	7.75	7.75	0
1.2	1300	7.42	7.55	0.13
1.3	1250	7.25	7.25	0
2.1	1400	6.66	6.90	0.24
2.2	1300	6.36	6.31	0.05
2.3	1250	6.27	6.27	0
6	1600	17.97	17.97	0
9	1600	22.34	22.33	0.01
L1	1625	10.69	10.59	0.10
L2	1605	17.73	17.70	0.03
L4	1650	5.30	5.33	0.03
L5	1650	6.30	6.78	0.48
Q1	1700	18.30	18.27	0.03
Q2	1670	6.49	6.58	0.09

Table 3.7 compare the weight loss (WL in the table) measured with a scale before and after the experiments, and the weight loss measured by the weight equipment in the thermogravimetric furnace during the experiments. The difference is relatively small, almost 0 in most of the experiments. Nevertheless it is 7 % difference for experiment L5. The weight loss from the weight equipment in the furnace is the most trustable number because of the uncertainty by using a scale in the lab. The lab scale vary with circulation of air in the room, and the last decimal never fully stabilize. Hence the numbers are very similar and the weight loss measurements are trustable.

4 Procedures

4.1 Furnace Operation

The raw materials are weighed and mixed gently in a weighing boat. Then they are put in the graphite crucible, so the materials are located arbitrarily.

After the crucible is filled with raw materials it is put into the furnace. The crucible hangs in a molybdenum wire and does not touch the graphite walls. The thermocouple is located just under the crucible, about 1 cm to not touch the crucible. See Figure 3.1 for an overview of the setup. Figure 3.5 shows how all apparatuses are put together. The software on the computer measure weight and temperature every five second.

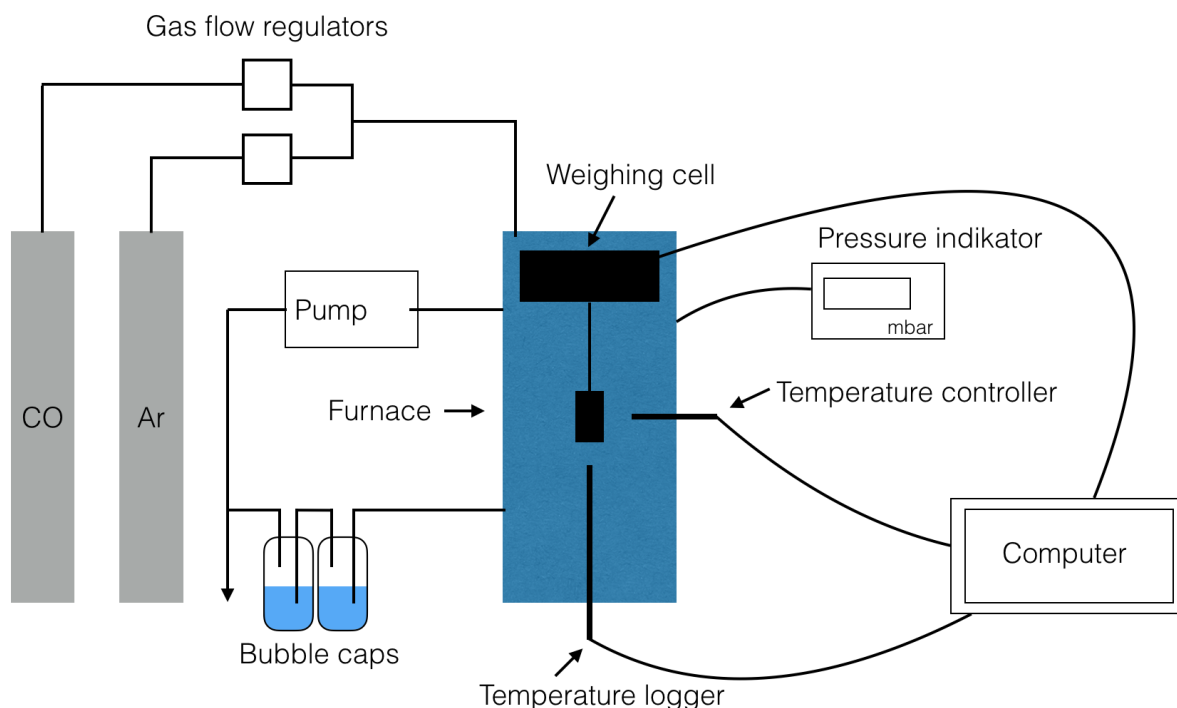


Figure 3.5: The setup for experiments with furnace, gas flow and apparatus.

When the crucible and the thermocouples are located as Figure 3.1 shows, the furnace gas is evacuated until the pressure inside the furnace is less than 4 mbar. Then the furnace is filled with argon gas until pressure reach 700 mbar, and then evacuated again. This is repeated three times, but in the last step argon gas is filled until the pressure is a bit over the atmosphere pressure, about 1050 mbar.

The gas outlet is opened and the gas flow of argon is set to 0.5 l/min. Then the pressure in the furnace is stabilized around 1000 mbar-1020 mbar, according to the pressure in the room.

When the temperature inside the furnace reach 500 °C the gas flow of argon is replaced by gas flow of CO. This flow is also 0.5 l/min. It is used Ar at low temperatures to avoid soothing when CO reacts to C and CO₂.

4.2 Temperature During Experiments

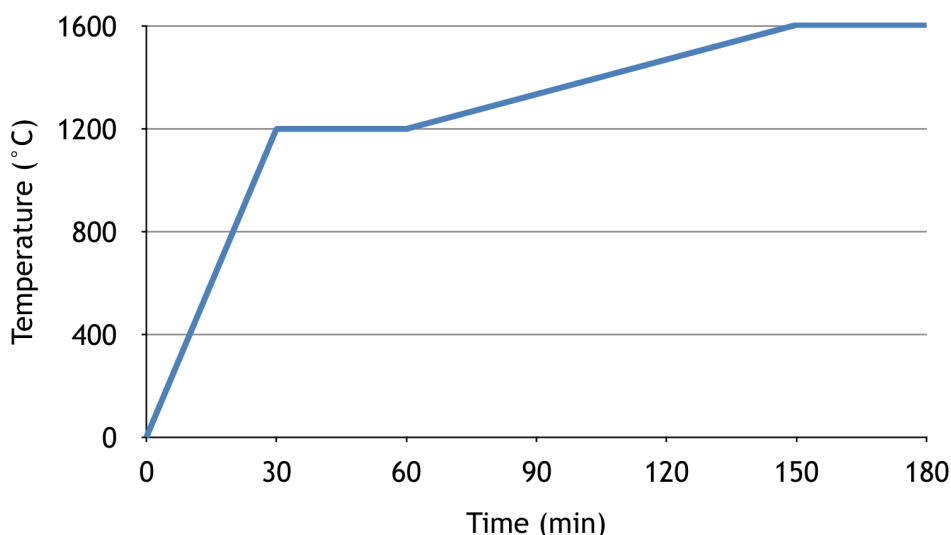


Figure 3.6: Temperature in the furnace during a typical experiment. (Holtan, 2015c).

When the right pressure and atmosphere in the furnace are reached, the power is turned on. The software control the power for getting the right temperature. The controller is in advance set so the temperature in the furnace will follow the graph shown in Figure 3.6. The temperature-time program is retrieved from Holtan (2015c).

It is a fast heating rate up to 1200 °C, and then the temperature is held at 1200 °C for 30 minutes so the prereduction completes. After the temperature is held at 1200 °C for 30 minutes the heating rate is slower, 4.5 °C/min. Slow heating rate is important to obtain the weight change at the right temperatures. This heating rate is chosen to achieve realistic heating rate from the furnaces in the industry. If the raw materials use 1.5 hours from

1200 °C zone to the 1600 °C zone, the heating rate is similar as an industrial furnace.

When the experiments reach the final temperature, the power to the furnace is shut down and the temperature in the furnace decreases.

4.3 Ending Experiments

After the power to the furnace is cut and the temperature decreases, it still is a CO gas flow of 0.5 l/min. When the temperature reach 500 °C-600 °C the gas flow of CO is stopped, and flow of argon is turned on instead. After approximately 1 hour the furnace and the crucible are cold enough to open the furnace and remove the crucible. Before the furnace is opened, it is evacuated and filled with argon again. This is to ensure that all CO is removed.

4.4 Reproducibility

It is important to look at the reproducibility of the experiments. In figure 3.7 the reproducibility is compared for four different experiments with the same charge. All this experiments was with ore, coke, quartz and limestone and followed the same temperature program. The lines are quite similar, that means the reproducibility is good. The biggest difference between the lines are about 0.4 g, hence the reproducibility can be calculated to $0.4 \text{ g} / 8 \text{ g} = 5 \%$. The yellow line marked 9 is from Holtan (2015c).

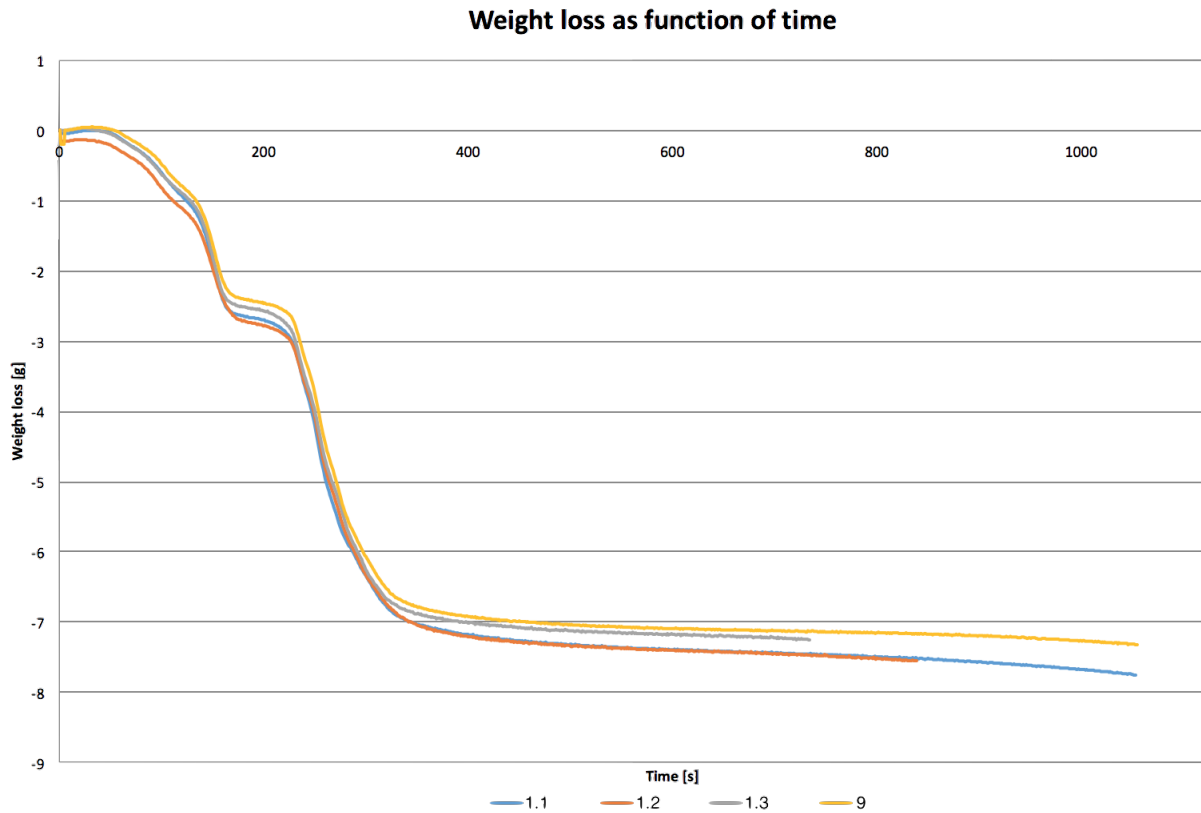


Figure 3.7: Weight loss graphs for four different experiments with the same charge.

4.5 Treatment of Samples

When the crucibles are cold and removed from the furnace, they are filled with epoxy.

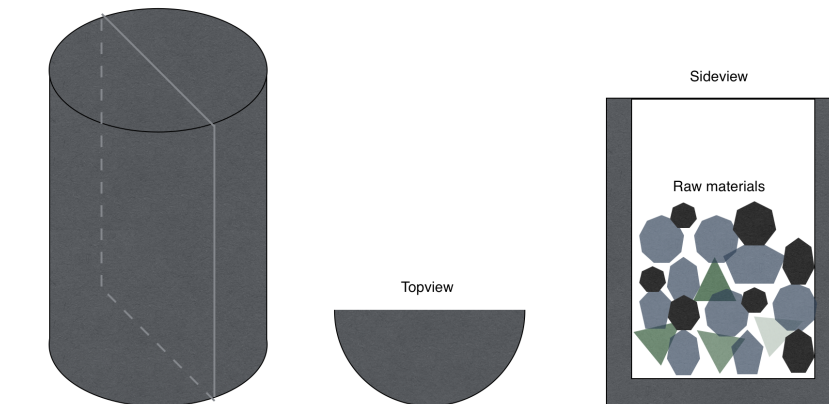


Figure 3.8: A schematic drawing which show how the crucibles are cut.

After the epoxy has cured, the crucibles are cut in two parts. Figure 3.8 show schematically how the crucibles are cut. The line in the drawing to the left in Figure 3.8 show how the crucibles are cut. The drawing in the middle show how it looks like from the bottom after cutting and the drawing to the right show how a typical cross section looks.

The cross section of the crucible is prepared for analysis at the SEM or EPMA. First an area of cross section is cut and then this part is grinded with SiC paper. The first paper is coarse (320 paper) and then it is used finer and finer SiC paper. In the last step it is used 4000 paper. After the preparation with SiC paper the samples are polished with diamants on a polishing apparatus. The last step of polishing is with 1 μm diamants.

5 Mathematical Calculations

5.1 Mass Balance

This part of the chapter will describe how the mass balance set up is, and how the weight loss is calculated for both the prereduction and the reduction.

Molmass	70,94	86,94	60	159,7	56	40,3	102	44	12		
Raw materials	MnO	MnO ₂	SiO ₂	Fe ₂ O ₃	CaO	MgO	Al ₂ O ₃	CO ₂	Fix C	Etc	Tot
Comilog	3,91	69,39	6,48	6,47	0,29	0,13	6,89	0,1			98,66
Coke	0,5907		9,7018	1,8079	1,2888	0,3222	3,7232		78,6	3,5	99,5346
Quartz	0,14		98,25				1,26				99,65
Limestone			0,96		51,98	0,96	0,26	45,72			99,88

Figure 3.9: The chemical analysis of the raw materials used in the mass balance.

Figure 3.9 shows a screenshot from the excel sheet used for the mass balance for the experiments. It shows the chemical analysis for each of the raw material used in this work. More from this excel sheet is shown in Appendix, Table A.1.

Equation 3.1 shows how the mass of each chemical component is calculated. The equation is shown for MnO, but it is calculated the same way for the other components as well.

$$m_{MnO} = m_{Ore} \cdot \frac{MnO_{Ore}}{Ore_{tot}} + m_{Coke} \cdot \frac{MnO_{Coke}}{Coke_{tot}} + m_{Qz} \cdot \frac{MnO_{Qz}}{Qz_{tot}} + m_{Lime} \cdot \frac{MnO_{Lime}}{Lime_{tot}} \quad (3.1)$$

The meanings of the subscripts are explained under. Also shortenings are explained. The subscript has the same meaning for all the raw materials and the compounds.

m_{MnO} MnO added to the experiment [g]. Calculated based on the analysis of the raw materials.

m_{Ore} Amount of Comilog ore added to the experiment [g].

MnO_{Ore} Amount of MnO in the Comilog ore [wt%].

Ore_{tot} The total from the analysis of the Comilog ore [wt%]. 98.66 wt% for the ore used in this work. The total for all the raw materials used in this work can be seen in Figure 3.9.

Qz Quartz

Lime Limestone

After the mass is calculated for every component, the mol of each is calculated. It is assumed that all MnO_x goes to MnO, all iron oxides goes to metallic iron, and all CO₂ goes off in the prereduction. Then the weight loss from the prereduction is calculated as shown in Equation 3.2.

$$\text{Weight loss}_{\text{Prered}} = (n_{\text{MnO}_2} \cdot M_{\text{CO}}) + (n_{\text{Fe}_2\text{O}_3} \cdot 3 \cdot M_{\text{CO}}) + m_{\text{CO}_2} \quad (3.2)$$

Prered Prereduction

n mol

M Molar mass [g/mol]

m mass [g]

For calculating the end slag, the amount of unreducible oxides are used. The mass of MnO in the end slag is calculated as shown in Equation 3.3.

$$\text{Mass}_{\text{MnO}} = \frac{m_{\text{CaO}} + m_{\text{Al}_2\text{O}_3} + m_{\text{MgO}}}{100 - \text{wt}\% \text{ MnO} - \text{wt}\% \text{ SiO}_2} \cdot \text{wt}\% \text{ MnO} \quad (3.3)$$

The amount of SiO_2 in the end slag is calculated equally as MnO, see Equation 3.4

$$\text{Mass}_{\text{SiO}_2} = \frac{m_{\text{CaO}} + m_{\text{Al}_2\text{O}_3} + m_{\text{MgO}}}{100 - \text{wt}\% \text{ MnO} - \text{wt}\% \text{ SiO}_2} \cdot \text{wt}\% \text{ SiO}_2 \quad (3.4)$$

The mass percent of MnO and SiO_2 used in Equations 3.3 and 3.4 are from the slag analysis of each sample.

The mass of the metal is calculated from the difference between the end slag and the primary slag compositions. It is shown for Mn in Equation 3.5. This is calculated equally for silicon as well.

$$\text{Mass}_{\text{Mn}} = (n_{\text{MnO, primary}} - n_{\text{MnO, end}}) \cdot M_{\text{Mn}} \quad (3.5)$$

The weight loss from the reduction is calculated as shown in Equation 3.6.

$$\text{Weight loss}_{\text{Red}} = n_{\text{Mn}} \cdot M_{\text{CO}} + n_{\text{Si}} \cdot 2 \cdot M_{\text{CO}} \quad (3.6)$$

The metal composition is calculated as shown in Equation 3.7. This equation shows the calculation for iron, but it is equally for the other metals as well. The C content is assumed to be 1.5 % if nothing else is mentioned.

$$\text{wt}\% \text{ Fe} = \frac{m_{\text{Fe}}}{m_{\text{Fe}} + m_{\text{Mn}} + m_{\text{Si}}} \cdot (100 - \% \text{ C}) \quad (3.7)$$

6 Analysis Methods

In this chapter the two analysis methods are described. The settings and the parameters for both the EPMA and the SEM are given.

6.1 Electron Probe Microanalyser (EPMA)

Electron probe microanalyzer is used to determine the composition of the different phases in the slag and in the metal. EPMA is a scanning electron microscope (SEM) and take advantage of the x-ray emitted by the sample when it is bombarded with electrons. The samples are grinded with SiC paper and then polished with diamants down to 1 μm . After polishing the samples are coated with carbon due to conductivity, before the measurements in the EPMA.

The samples are observed through backscatter electron image, and the points that are analyzed is picked out based on these images.

Table 3.8: EPMA parameters.

Parameter	Value
Acceleration voltage	15.0 kV
Probe current	8.525 nA
Probe diameter	0 μm

A Jeol JXA-8500F (Field emission) with five wavelength dispersive spectrometer was used in this work. The parameters used in the EPMA are shown in Table 3.8.

6.2 Energy Dispersive Spectroscopy (EDS)

Energy Dispersive Spectroscopy (EDS) on the SEM is used to analyse metal and slag from the samples. The samples are treated the same manner as for the EPMA. The samples are observed by backscatter electrons in the SEM.

The SEM used for this work was a Zeiss Ultra 55 Limited Edition, Field-emission Scanning electron microscope.

Table 3.9: EDS parameters.

Parameter	Value
Acceleration voltage	15.0 kV
Aperture diameter	120 μm
High current mode	yes
Working distance	9-10 mm
Acquisition time	30 seconds

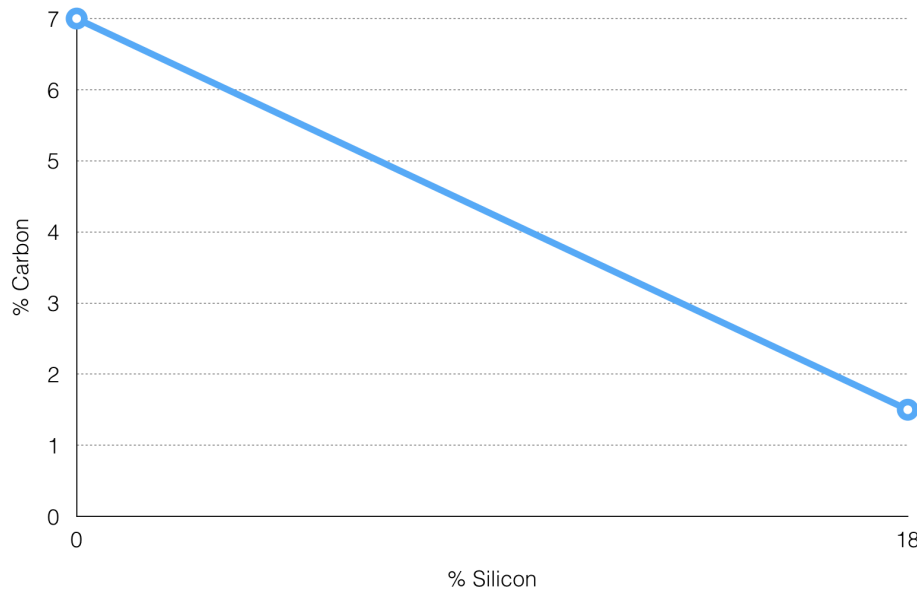


Figure 3.10: Assumed relationship between carbon and silicon content in the metal.

Figure 3.10 shows the assumed relationship between carbon content and silicon content in the metal. The relationship assumed can be expressed by Equation 3.8. The real relationship between the solubility of carbon in the metal and the silicon content is shown in Figure 3.11. This figure is reprinted from Olsen et al. (2007) and is valid for Mn-Si-Fe- C_{sat} metal with a Mn/Fe ratio equal 5.10.

The values from EDS in Table 4.7 are normalized by assume the carbon content based on the analyzed silicon content. Then subtract this number from 100 % and normalize the metals up to the total metal content ($= 100 - C$ content).

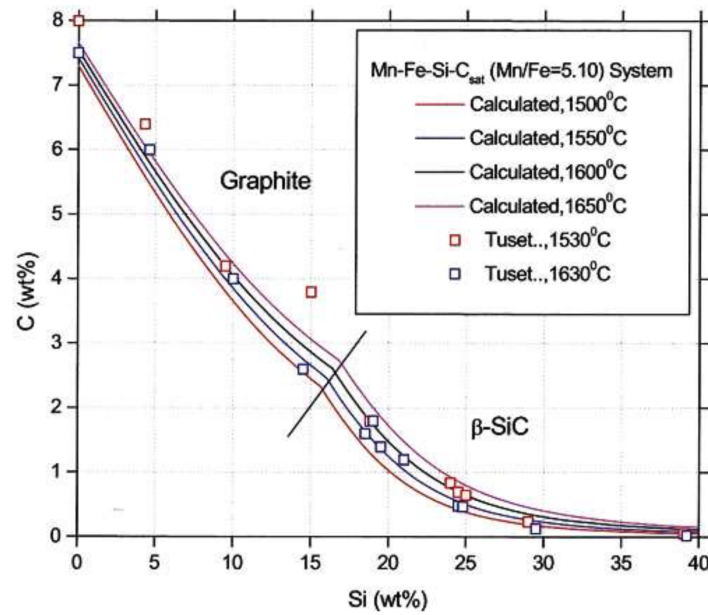


Figure 3.11: Relationship between carbon and silicon content in the metal (Olsen et al., 2007).

$$\%C = \frac{-5.5}{18} \cdot \%Si + 7 \quad (3.8)$$

An example from the Q1 experiment with 13.2 % Si is shown in Equation 3.9.

$$\%C = \frac{-5.5}{18} \cdot 13.2 + 7 = 3.0\%C \quad (3.9)$$

It is assumed 3 % C content in this sample, and the total of Mn, Fe and Si are then 97 %. Hence the content of these elements are normalized up to 97 %. After the normalization, the Si content is increased a bit (up to 14.9 % in this example), and due to the model this will decrease the C content further. This small difference is neglected.

Figure 3.12 shows typical spectra from a metal phase collected by EDS. This example is from Sample Q2.

A typical spectra collected from a slag phase is shown in Figure 3.13.

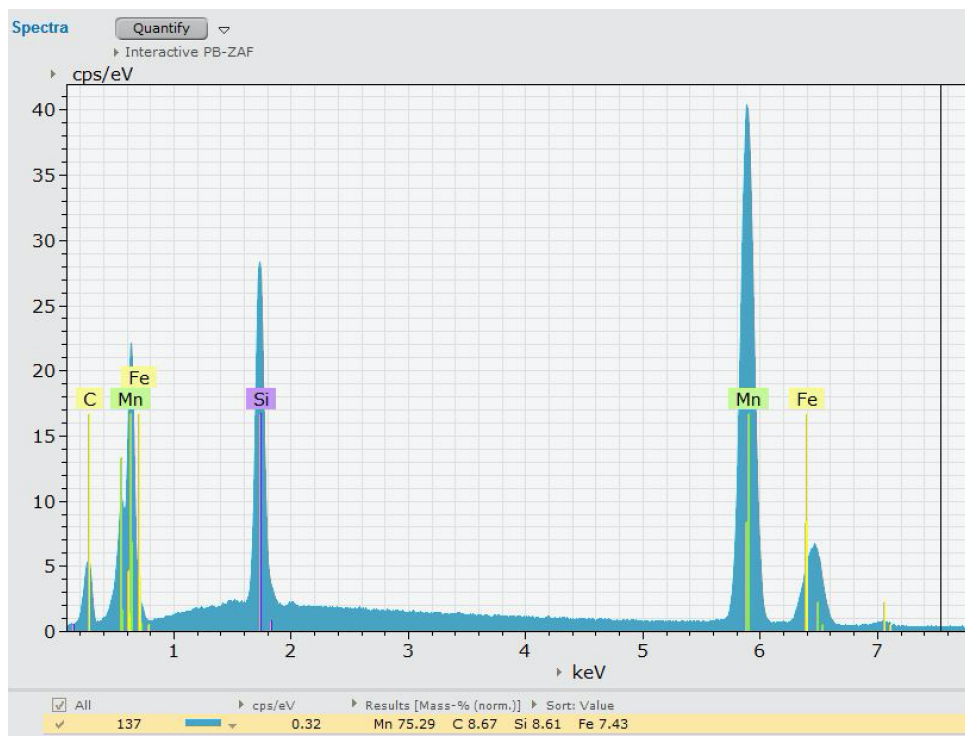


Figure 3.12: Typical EDS spectra for a metal analysis.

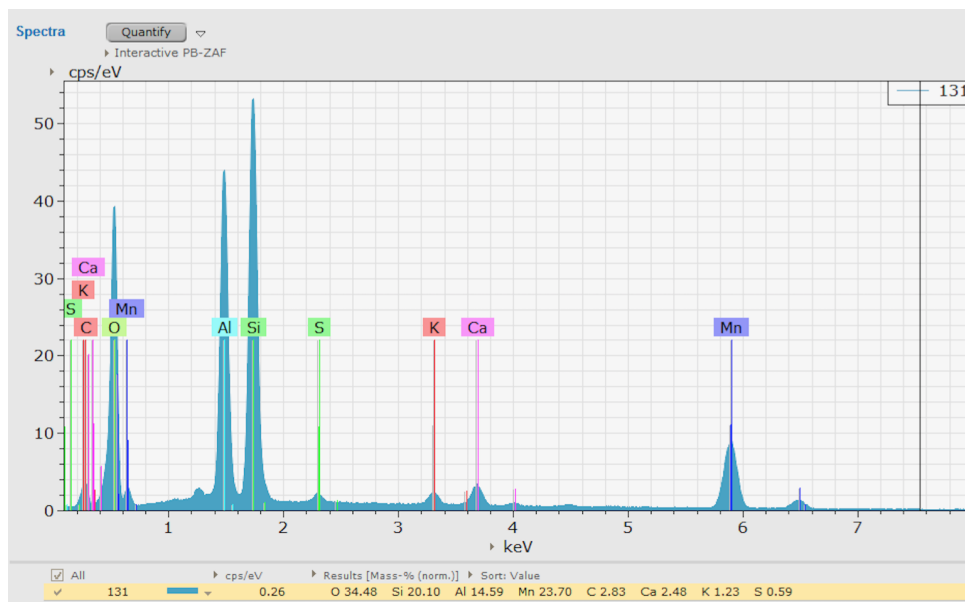


Figure 3.13: Typical EDS spectra for a slag phase analysis.

Chapter 4

Results

In this chapter the results from the experiments are presented. The chapter is divided in two parts, one for the charge with Comilog ore and quartz, and one for the charge with Comilog ore, quartz and limestone.

1 Comilog Ore and Quartz

In the first part of this chapter results from experiments done with Comilog ore and quartz is presented. This is SiMn charge without fluxes added.

Experiment Q1

Experiment Q1 is the first experiment shown in this part. First it is shown some SEM images from the sample which is representative for Q1. It is interesting to see if it is different phases in the slag or if it is one glassy slag phase. The results from the chemical analysis of the slag and the metal are also presented in this chapter. This experiment is stopped at 1700 °C.

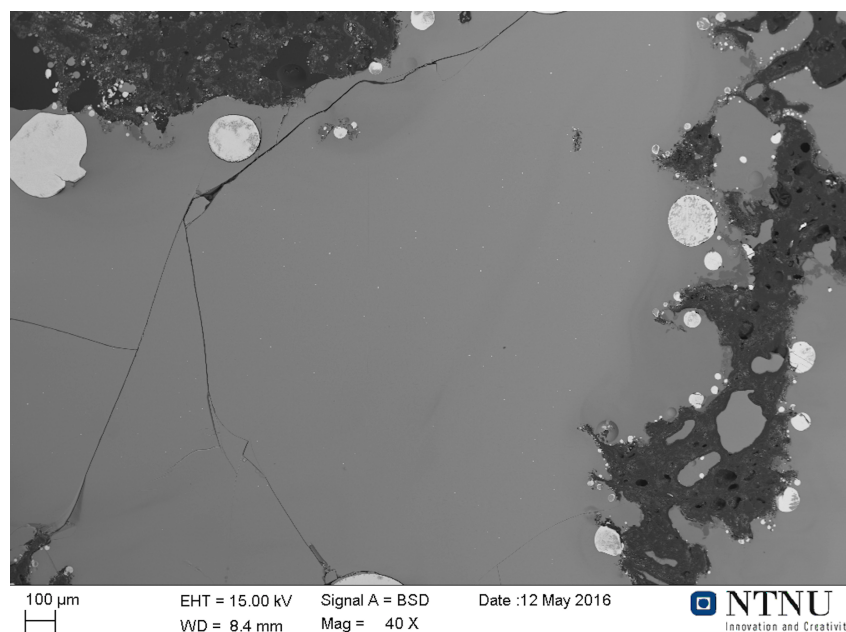


Figure 4.1: SEM (BSD) image from Sample Q1. Glassy slag phase and some metal.

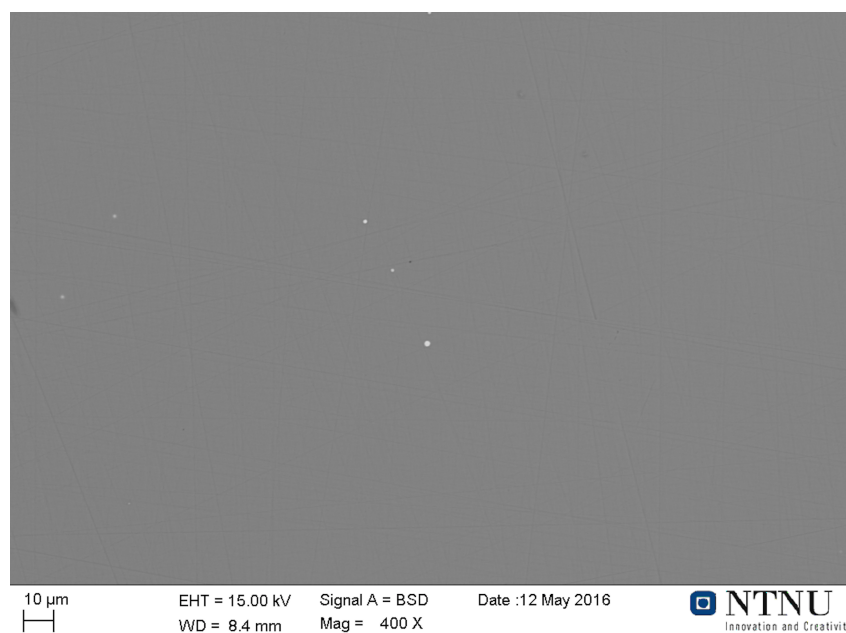


Figure 4.2: SEM (BSD) image of the glassy slag phase in Sample Q1. Black areas are either coke or pores.

Figure 4.1 and 4.2 shows the slag phase from Sample Q1 with different magnification. The slag is a glassy phase and show that we only have one liquid phase. The slag from two different places in the sample is analyzed and presented in Table 4.1. At both this places it

is taken several spot analysis. The standard deviation is calculated based on these analysis. The raw data are attached in Appendix, Table D.2 and D.3.

From Table 4.1 it can be seen that it is two different slags. The $\text{CaO}/\text{Al}_2\text{O}_3$ ratio in both the slags are relatively equal which means the difference is the reduction of the slag. Both the MnO and SiO_2 reduction are much less in Q1*.

The primary slag composition in Table 4.1 is calculated from the raw material mixture as described in Chapter 5. The MnO content has decreased which means that manganese is reduced from the slag phase and is gone into the metal. The silica content has increased a bit from the primary slag, but the amount of slag is much less after the experiment. So it is reduced some silica as well.

Table 4.1: Slag composition analyzed from Sample Q1 [wt%].

	SiO_2	MnO	Al_2O_3	CaO	FeO	MgO	Total
Q1	43.5 ± 2.4	28.7 ± 0.3	23.4 ± 2.0	3.0 ± 0.3	0.0 ± 0.0	0.0 ± 0.0	100
Q1*	47.5 ± 0.4	38.8 ± 0.6	10.9 ± 0.2	1.5 ± 0.1	0.0 ± 0.0	0.0 ± 0.0	100
Primary slag	33.17	58.04	7.94	0.64	0	0.21	100



Figure 4.3: SEM image from Sample Q1. Metal phase.

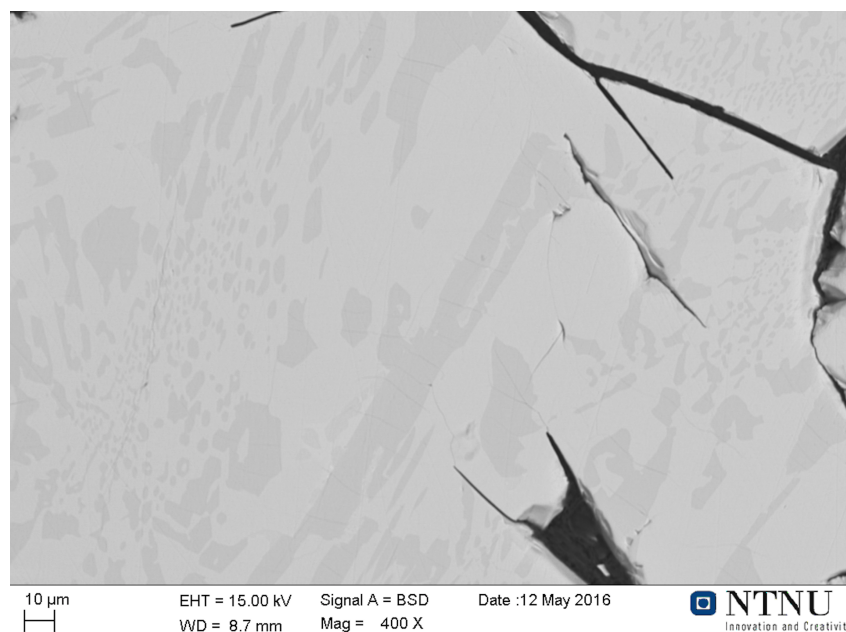


Figure 4.4: SEM image of the metal phase in Sample Q1.

Figure 4.3 and 4.4 shows the metal phase from Sample Q1 with different magnification. The analysis of the metal are presented in Table 4.2 with standard deviation. The table shows that the different metal particles is varying quite a lot in composition, and hence, to use the analysis of the metal as a measure of degree of reduction is not optimal.

Table 4.2: Metal composition analyzed from Sample Q1 [wt%].

	Si	Mn	Fe	Total
Q1	14.9 ± 5.8	74.4 ± 6.5	7.8 ± 0.7	97.0

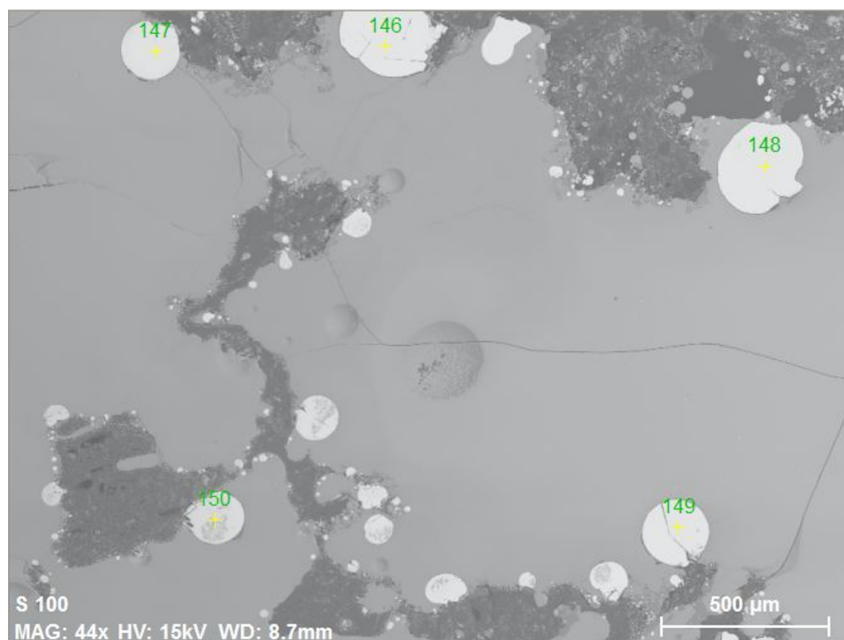


Figure 4.5: SEM image from Sample Q1. Spots where metal analysis are conducted are marked.

Figure 4.5 shows an image of Sample Q1, with slag and some small metal droplets which are analyzed. The composition of each of these metal droplets are shown in Table 4.3. The numbers in this table refers to the image in Figure 4.5. The standard deviation are calculated and the normalized values are also presented in this table. These values are normalized as described in Experimental Work, Chapter 6.2. The deviation is quite big in the metal analyses, which is expected from when the metal droplets was produced. This metal composition must not be mixed up with the composition from Table 4.2. Results presented in Table 4.2 are more trustable because these results are from a much bigger metal droplet in the sample.

Table 4.3: Metal composition analyzed from Sample Q1 [wt%].

	Number	Si	Mn	Fe	Total
Q1	146	18.6	68.48	0	95.5
	147	13.6	68.2	0	89.6
	148	8.9	76.6	0	95.1
	149	11.3	76.3	0	95.8
	150	13.3	73.8	0	95.7
Average:		13.2	72.7	0	94.3
Std. deviation:		3.6	4.1	0	2.7
Normalized:		14.4	79.4	0	96.8

Experiment Q2

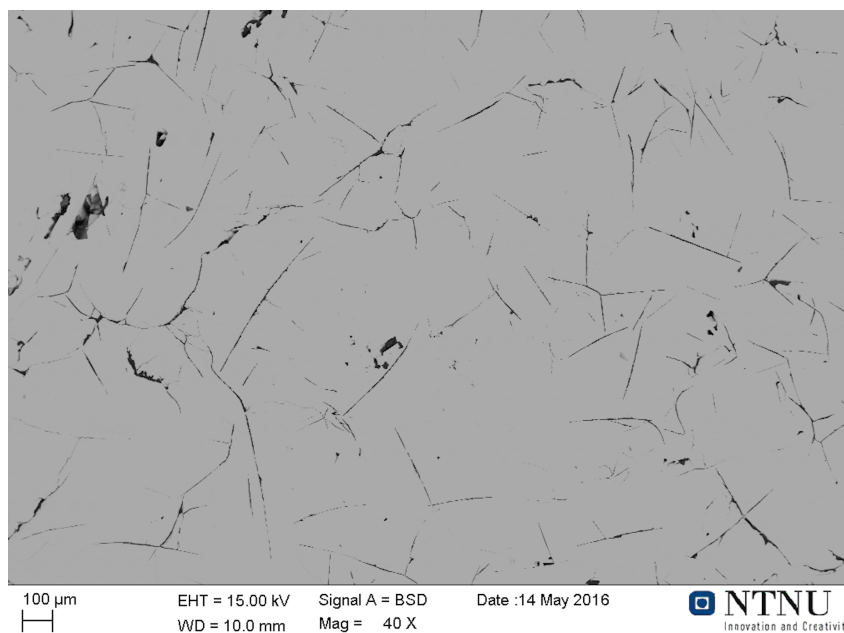


Figure 4.6: SEM image from Sample Q2. Metal phase.

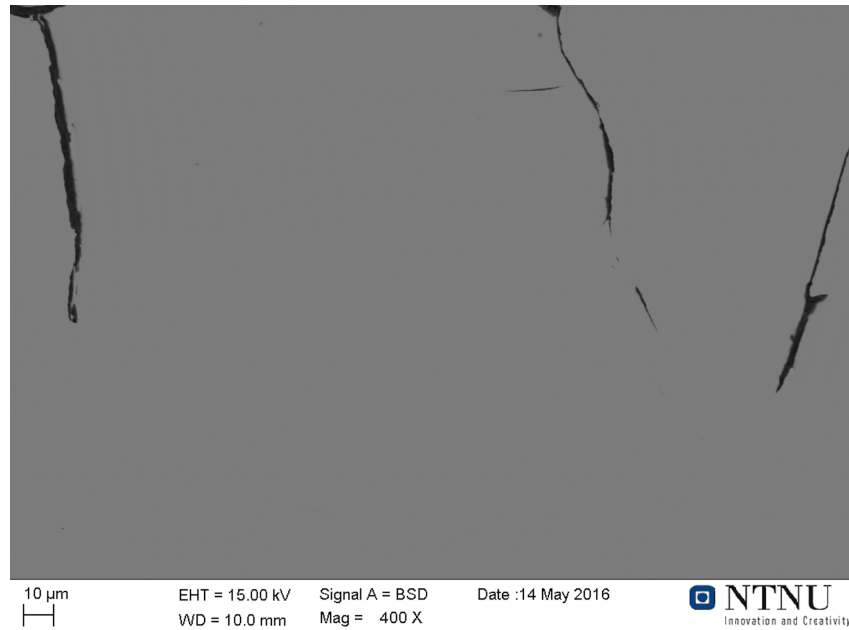


Figure 4.7: SEM image of the metal phase in Sample Q2.

Figure 4.6 and 4.7 shows the metal phase from Sample Q2 with different magnification. This experiment is stopped at 1670 °C. The analysis of the metal are presented in Table 4.4 with standard deviation. These values are normalized as described in Chapter 6.2.

It was not found any slag in Sample Q2.

Table 4.4: Metal composition analysed from Sample Q2 [wt%].

	Si	Mn	Fe	Total
Q1	15.8 ± 5.4	70.6 ± 5.9	10.9 ± 2.1	97.3

Mass Losses and Slag Compositions

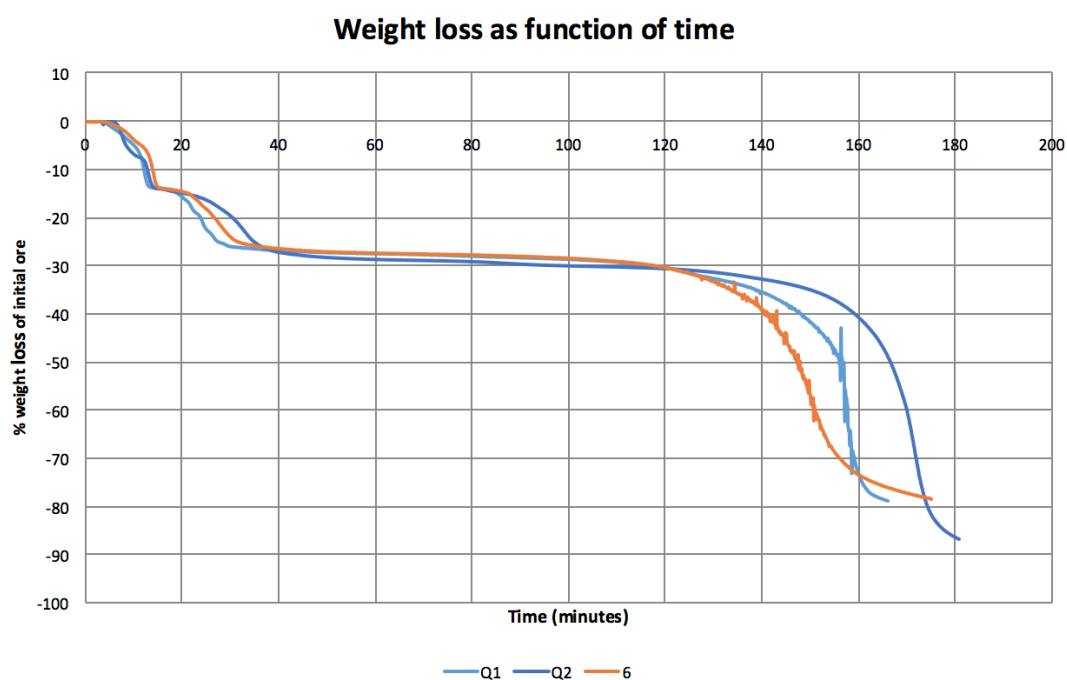


Figure 4.8: Weight loss graphs for experiments at high temperature as function of time.

Figure 4.8 shows the weight loss curves for all experiments with Comilog ore and quartz stopped at higher temperature than 1600 °C. In this figure % weight loss of initial ore mass is plotted as function of time. Figure 4.10 shows the same weight loss curves, but here they are plotted as function of temperature instead of time. Experiment Q2 is done in the SINTEF furnace, and from the Figure 4.10 it can be seen that this furnace has much more stable temperature during heating up to 1200 °C. This can also be seen from Figure 4.9. The temperature time curve from Experiment Q2 is smooth, and the equivalent curves for Experiment Q1 and 6 are not smooth before over 1200 °C. Experiment 6 is retrieved from Holtan (2015c) and this experiment is held at 1600 °C for 30 minutes.

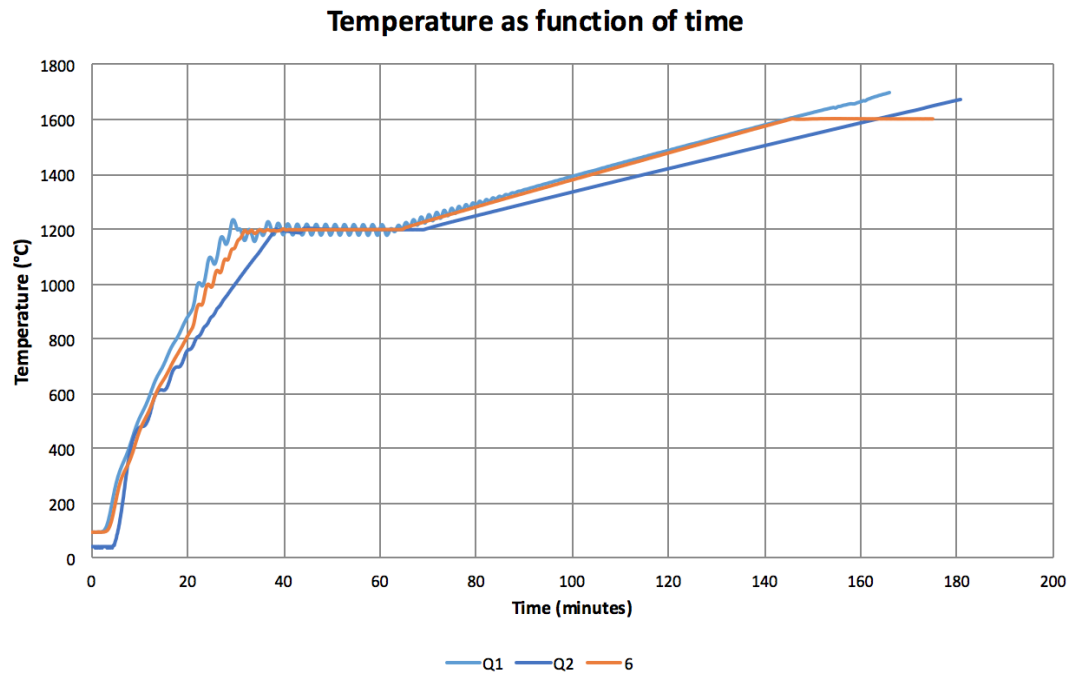


Figure 4.9: Temperature curves as function of time for the experiments stopped at high temperatures.

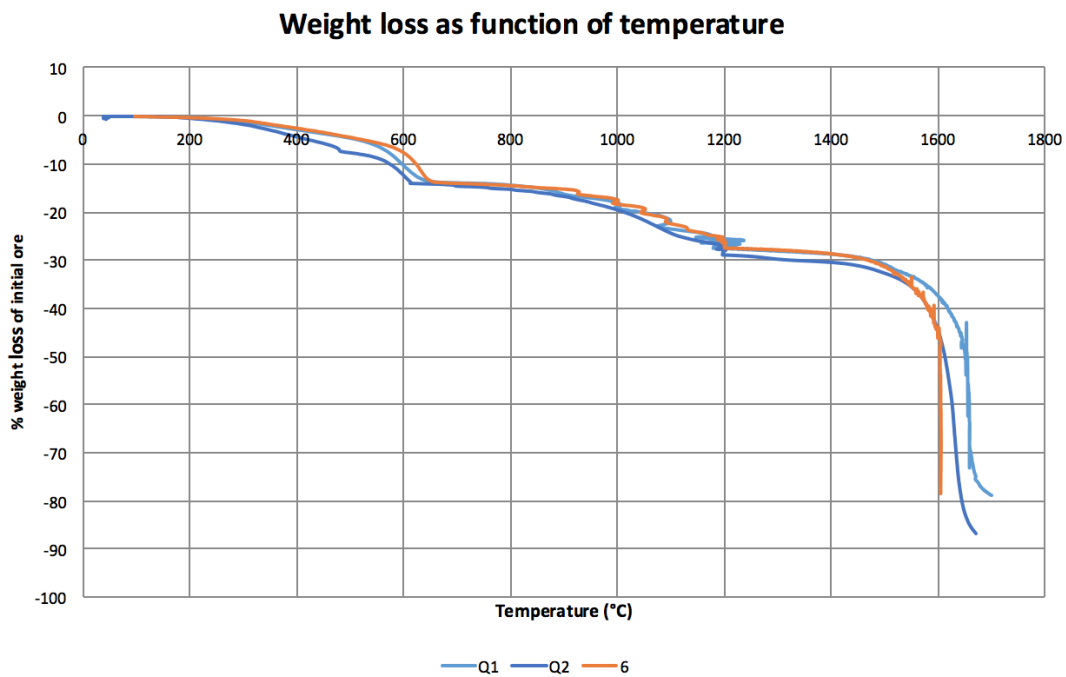


Figure 4.10: Weight loss graphs for experiments at high temperature as function of temperature.

Table 4.5: Slag composition analysed [wt%].

Experiment	Max. Temp. [°C]	SiO ₂	MnO	Al ₂ O ₃	CaO	FeO	MgO	K ₂ O	Total
2.3	1250	45.8	49.8	1.3	0.4	0.3	0	1.5	99.1
2.2	1300	46.1	50.1	0.9	0.1	0.2	0	0	97.4
2.1	1400	35.0	51.3	8.0	0.4	0.1	0	0.7	95.5
6	<i>1600</i>	<i>43.0</i>	<i>12.3</i>	<i>33.0</i>	<i>2.6</i>	<i>0</i>	<i>0</i>	<i>3.0</i>	<i>93.9</i>
Q2	1670			NA					
Q1*	1700	44.8	32.0	19.3	2.5	0	0	1.4	100

Table 4.5 shows an overview of the analysis of the slag from the experiments with Comilog ore and quartz. The experiment marked with * is analyzed with EDS, all others are analyzed by EPMA. Sample Q1 and Q2 is from this work, while the rest is analyzed in this work but was done last fall. Experiment 6 is in italic font because this experiment is held at 1600 °C for 30 minutes. The analysis results from this sample is retrieved from Holtan (2015c).

Table 4.6: Slag composition calculated based on measured wt% MnO and wt% SiO₂ and composition of primary slag of CaO, Al₂O₃ and MgO [wt%].

Experiment	Max. Temp. [°C]	SiO ₂	MnO	Al ₂ O ₃	CaO	MgO	Total
2.3	1250	45.8	49.8	3.97	0.32	0.11	100
2.2	1300	46.1	50.1	3.43	0.28	0.09	100
2.1	1400	35.0	51.3	12.37	1.00	0.34	100
6	1600	43.0	12.3	40.35	3.26	1.09	100
Q2	1670	40	5	49.64	4.01	1.34	100
Q1	1700	44.8	32.0	20.95	1.69	0.57	100

Table 4.6 shows the calculated slag composition for all experiments with Comilog ore and quartz. The values are calculated as described in Chapter 5. The R values for these experiments are 0.11.

Table 4.7 shows the analyzed results from the metal in each sample. The experiments marked with * are analyzed with EDS, all others are analyzed by EPMA. Experiment 6 is in italic font because this experiment is held at 1600 °C for 30 minutes. The analysis results from this sample is retrieved from Holtan (2015c). Experiments marked with * which are analyzed by EDS, are normalized. This is because of EDS gives a high carbon content, about 8-9 %. This is described in Experimental Work, Chapter 6.2.

Table 4.7: Metal composition analyzed [wt%].

Experiment	Max. Temperature [°C]	Si	Mn	Fe	Total
2.3	1250	0.1	97.3	2.6	100
2.2	1300	0.1	78.8	21.1	100
2.1	1400	0	20.7	79.3	100
6	1600	16.7	82.8	0.5	100
Q2*	1670	15.8	70.6	10.9	97.3
Q1*	1700	14.9	74.4	7.8	97.0

Table 4.8: Calculated and measured weight loss from each experiment.

Experiment	Max. Temperature [°C]	Calculated [g]	Measured [g]
2.3	1250		6.27
2.2	1300		6.36
2.1	1400	10.93	6.66
6	1600	17.08	17.97
Q2	1670	5.99*	6.49
Q1	1700	14.25	18.30

In Table 4.8 * mark the experiment where no slag was observed. Hence it is difficult to calculate the theoretical weight loss. For this experiment it is assumed 5 % MnO and 40 % SiO₂ in the slag. Then the number in Table 4.8 is reached.

For experiment 2.2 and 2.3 it is no calculated weight loss in Table 4.8. This is due to the high amount of MnO and SiO₂ in the slag phase. When the theoretical weight loss is calculated, the value is negative. It is obviously impossible. For the same reason it is no calculated metal composition for these two samples in Table 4.9.

Table 4.9: Metal composition calculated from measured slag analysis [wt%].

Experiment	Max. Temperature [°C]	Si	Mn	Fe	Total
2.3	1250				
2.2	1300				
2.1	1400	16.95	65.63	15.92	98.5
6	1600	19.22	71.49	7.78	98.49
Q2	1670	21.21	69.90	7.39	98.5
Q1	1700	15.61	73.25	9.64	98.5

Experiment 2.1 stopped at 1400 °C has about no more weight loss compared with

Experiment 2.2 stopped at 1300 °C. The MnO content in the slag phase is also the same for these experiments, but the silica content has decreased from 46 % to 35 %.

2 Comilog Ore, Quartz and Limestone

In this chapter the results from the experiments done with SiMn charge with added flux are presented. The amount of limestone and quartz is added to obtain a metal with 18 % Si and a slag with 40 % SiO_2 . The flux used in this work is limestone. It is done several experiments at different temperatures and with different amount of raw materials.

Experiment L1

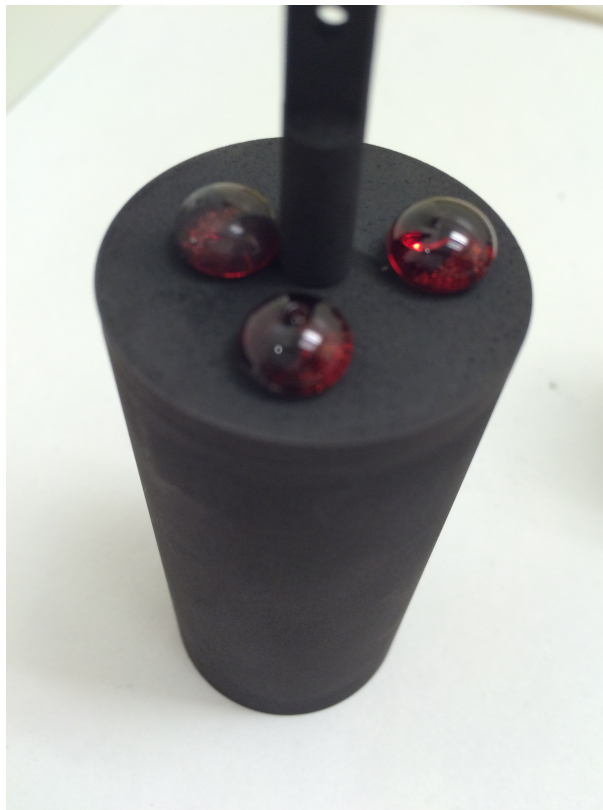


Figure 4.11: Picture of the crucible after Experiment L1. It was found slag on the top of the lid.

After experiment L1 it was found slag on the top of the lid. Figure 4.11 shows a picture of the crucible after the experiment. This experiment was stopped at 1625 °C. In the slag from the top of the lid in this experiment it was found small amount of metal. The slag droplet from the lid and slag and metal from the crucible was prepared for SEM, and these samples are imaged in Figure 4.12.

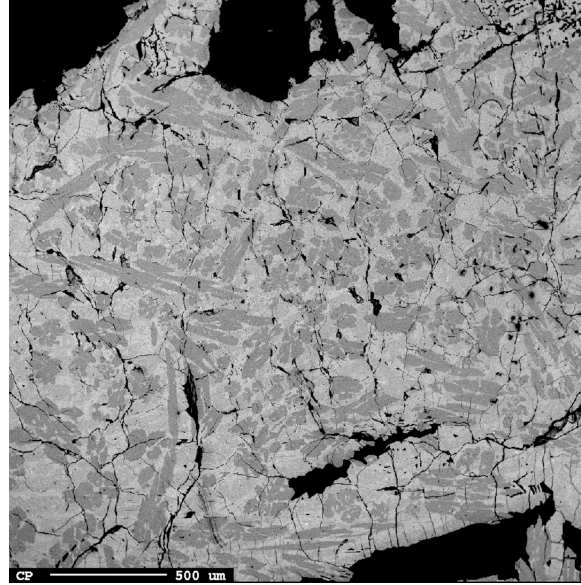


Figure 4.12: The Samples prepared for the EPMA. The slag from the top of the lid is also prepared as shown in this picture.

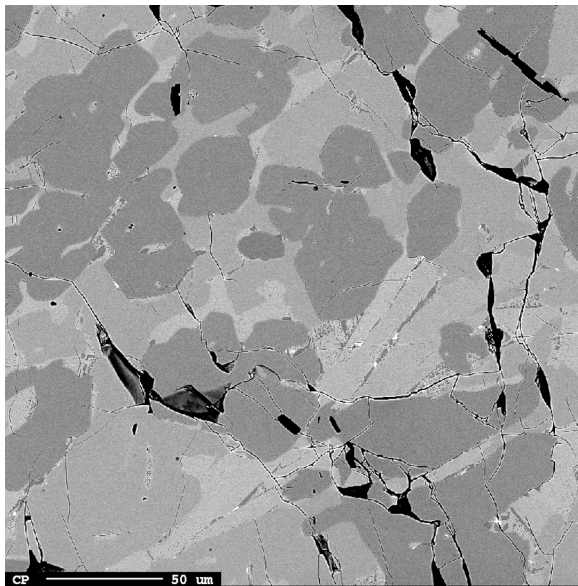
From Figure 4.12 it is clear that the slag phase is glassy. The composition in the slag phase is analyzed and shown in Table 4.10. The standard deviation is also shown in the table. It was taken nine spot analysis in the glassy slag phase from the crucible, and the standard deviation was calculated based on these numbers. From the slag on the lid, it was taken three spot analysis. It can be seen from the table that the slag on the lid and the slag in the crucible is the same.

Table 4.10: Slag composition analyzed [wt%].

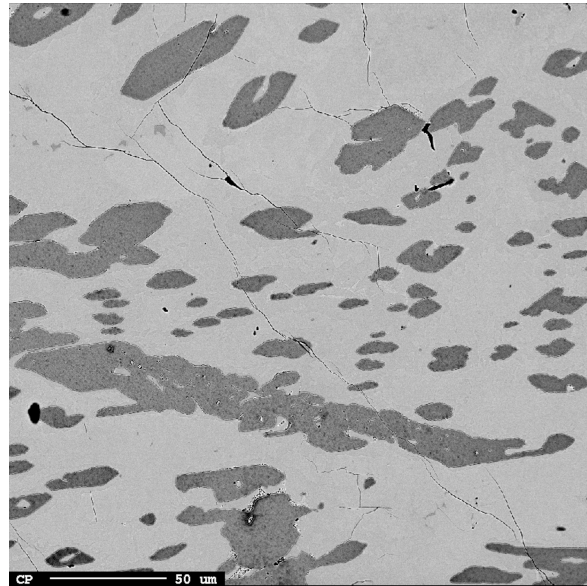
	SiO ₂	MnO	Al ₂ O ₃	CaO	FeO	MgO	Total
Crucible	44.0 ± 1.0	29.4 ± 0.8	6.6 ± 0.1	16.4 ± 0.3	0.1 ± 0.0	0.2 ± 0.0	97.5 ± 0.7
Lid	43.4 ± 0.1	30.0 ± 0.1	6.5 ± 0.0	16.1 ± 0.2	0.1 ± 0.0	0.2 ± 0.0	97.0 ± 0.1



(a) 40x magnification



(b) 400x magnification



(c) 400x magnification

Figure 4.13: SEM Pictures from Sample L1. Pictures (a) and (b) are from the metal phase in the crucible, and Picture (c) is from the metal which was found on the top of the lid after experiment.

Figure 4.13 shows SEM pictures from the metal found in Sample L1. Pictures in Figure 4.13a and 4.13b are from the metal found in the crucible. This metal has several phases, and the analysis of each phase are shown in Table 4.11. The standard deviation is also shown in this table. Picture in Figure 4.13c shows the metal which was found in the slag lump on the lid of the crucible. The analysis of this metal is shown in Table 4.12. Raw data for these analysis are presented in Appendix, Table C.1.

Table 4.11: Metal composition analyzed from L1 [wt%].

Phase	Si	Mn	Fe	Total
Brightest	3.57 ± 0.08	60.83 ± 0.38	30.03 ± 0.52	94.43 ± 0.87
Grey	6.68 ± 0.44	58.85 ± 0.41	28.63 ± 0.10	94.43 ± 0.41
Darkest	0.01 ± 0.01	71.39 ± 0.39	18.08 ± 0.26	89.47 ± 0.20

Table 4.12: Metal composition analyzed from the lid of L1 [wt%].

Phase	Si	Mn	Fe	Total
Brightest	9.77 ± 0.06	85.43 ± 0.17	0.39 ± 0.01	95.58 ± 0.17
Darkest	9.31 ± 0.41	85.91 ± 0.58	0.36 ± 0.02	95.59 ± 0.60

Experiment L2



Figure 4.14: Picture of the crucible after Experiment L2. It was found slag on the top of the lid.

After experiment L2 it was found slag on the top of the lid. Figure 4.14 shows a picture of the crucible after the experiment.

One slag droplet from the lid and slag and metal from the crucible was prepared for SEM, and these samples are imaged in Figure 4.15.

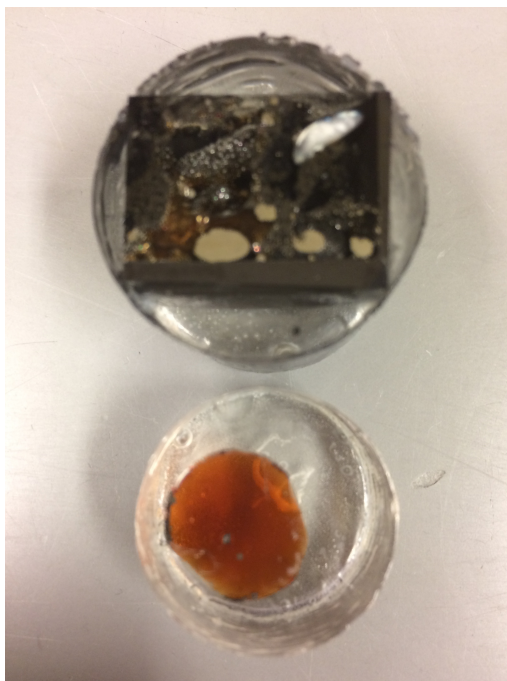


Figure 4.15: The Samples prepared for the EPMA. The slag from the top of the lid is also prepared as shown in this picture.

From Figure 4.15 it is clear that the slag phase is glassy. The composition in the slag phase is analyzed and shown in Table 4.13. It was taken three spot analysis both in the glassy phase from inside the crucible, and from the slag droplet from the lid.

Table 4.13: Slag composition analyzed [wt%].

	SiO ₂	MnO	Al ₂ O ₃	CaO	FeO	MgO	Total
Crucible	47.5 ± 0.3	20.3 ± 0.3	8.5 ± 0.1	17.2 ± 0.0	0.1 ± 0.0	0.2 ± 0.0	97.3 ± 0.6
Lid	45.2 ± 0.2	26.4 ± 0.2	7.4 ± 0.1	17.2 ± 0.0	0.1 ± 0.0	0.2 ± 0.0	97.3 ± 0.2

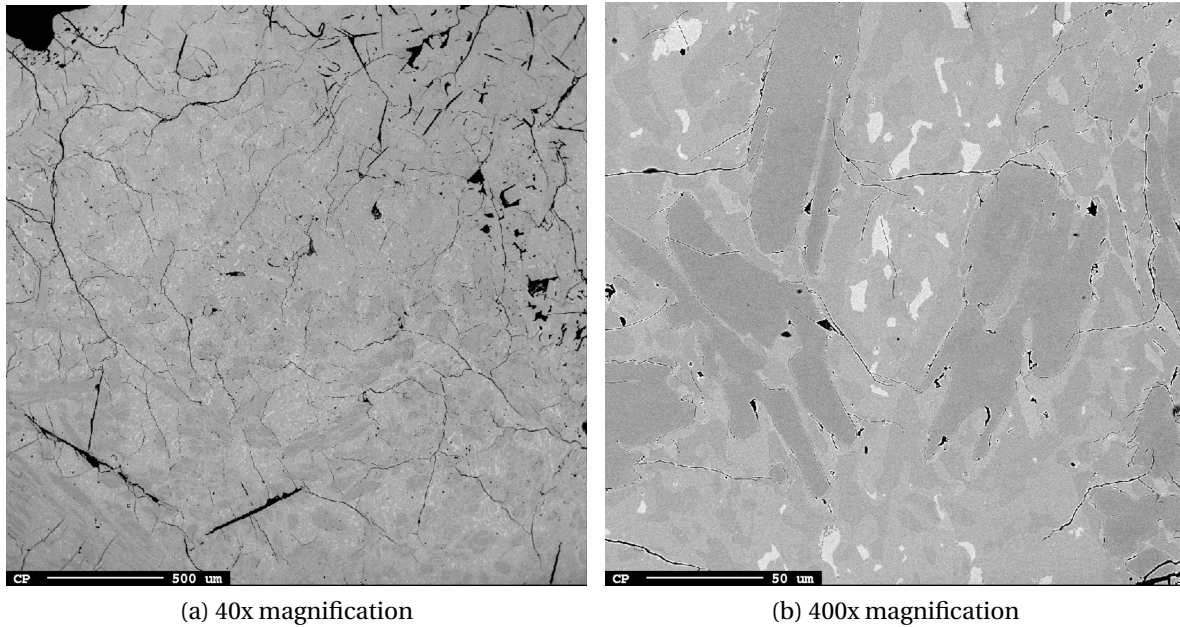


Figure 4.16: SEM Pictures from Sample L2. Pictures from the metal phase.

Figure 4.16 shows pictures from the metal phase in Sample L2. The pictures shows different phases, and the analysis of each phase is shown in Table 4.14. It is taken three spot analysis in each phase, and one out of three seems to be an out layer in both the grey and the dark phase. Thus, the more correct values for these phases seems to be about 9 % Si content and 10 % Fe content. The raw data for the experiments is in Appendix, Table C.1.

Table 4.14: Metal composition analyzed from L2 [wt%].

Phase	Si	Mn	Fe	Total
Brightest	8.40 ± 0.08	70.85 ± 0.58	13.01 ± 0.17	92.25 ± 0.42
Grey	7.87 ± 2.40	76.05 ± 1.90	10.39 ± 0.88	94.31 ± 1.39
Darkest	6.10 ± 5.24	78.32 ± 4.69	8.81 ± 2.65	93.24 ± 3.23

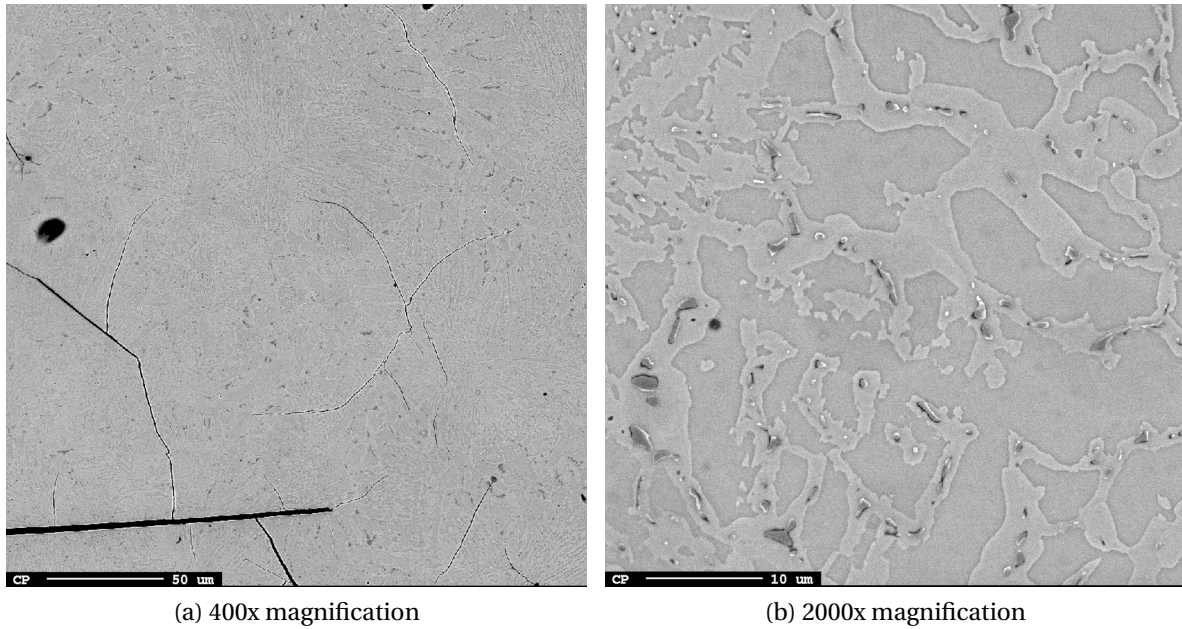


Figure 4.17: SEM Pictures from Sample L2. Pictures from the slag droplet which was located on the top of the lid after the experiment.

Figure 4.17 shows pictures from the metal found in the slag droplet on the top of the lid in Sample L2. This metal is analyzed and the result is presented in Table 4.15.

Table 4.15: Metal composition analyzed from the lid of L2 [wt%].

	Si	Mn	Fe	Total
Lid	9.84 ± 0.15	85.42 ± 0.03	0.35 ± 0.02	95.62 ± 0.13

Experiment L4

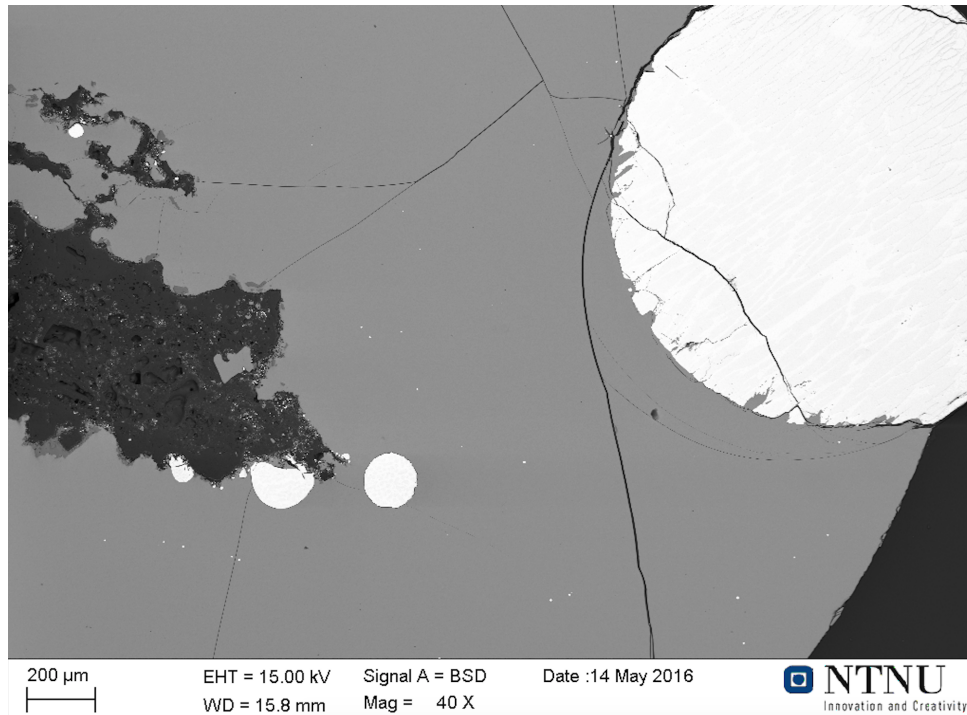


Figure 4.18: SEM Picture from Sample L4. Metal and slag, 40x magnification.

Table 4.16: Metal composition analyzed from L4 [wt%].

	Si	Mn	Fe	Total
L4	17.0 ± 5.5	80.6 ± 7.2	0.0 ± 0.0	97.6

Figure 4.18 shows a SEM picture from Sample L4 with both metal and slag. The slag phase is glassy. Table 4.16 shows the analysis of the metal in this sample. The data is normalized as described in Experimental Work, Chapter 6.2. The big standard deviation is due to one out of three spot analysis may be an out layer. The raw data from the analysis are attached in Appendix, Table D.1.

Table 4.17: Slag composition analyzed [wt%].

	SiO ₂	MnO	Al ₂ O ₃	CaO	FeO	MgO	Total
L4	47.3 ± 2.0	8.0 ± 1.0	11.4 ± 1.3	33.3 ± 1.9	0.0 ± 0.0	0.0 ± 0.0	100

Table 4.17 shows the analysis of the slag from Sample L4. The results are based on 12 spot analyses from EDS. The standard deviation given in this table are calculated from all these spot analyses. All the raw data are attached in Appendix, Table D.2 and Table D.3.

Experiment L5

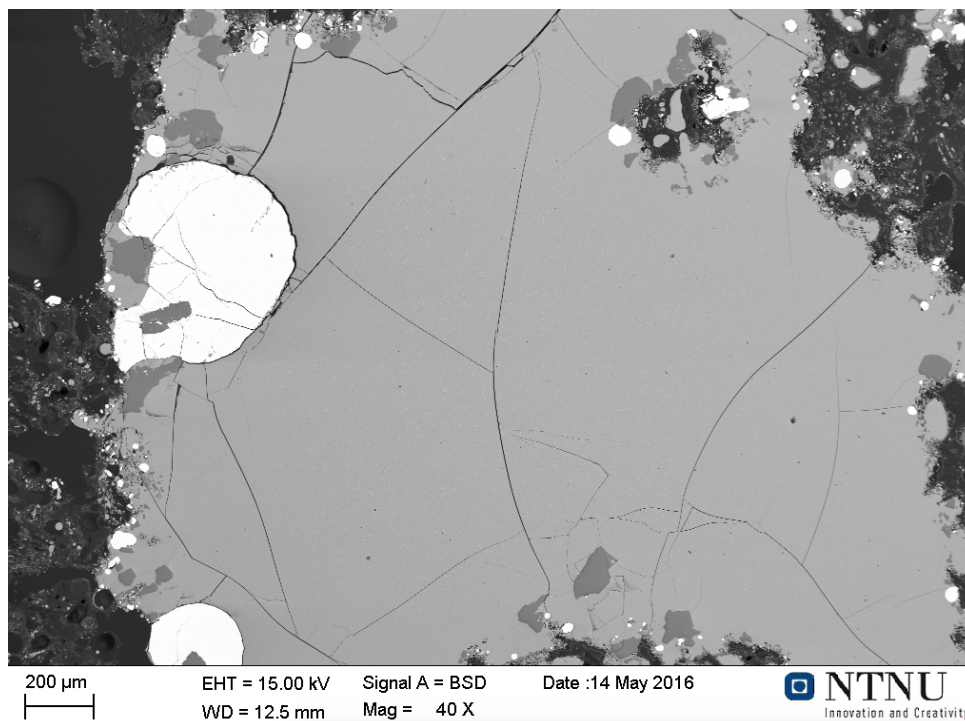


Figure 4.19: SEM Picture from Sample L5. Metal and slag, 40x magnification.

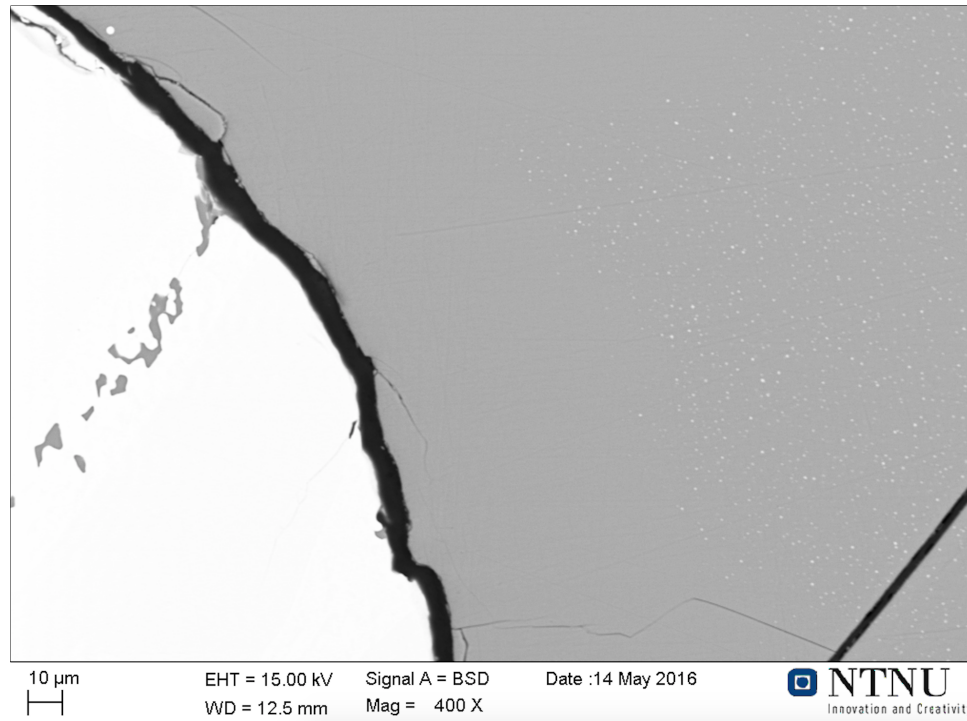


Figure 4.20: SEM Picture from Sample L5. Metal and slag, 400x magnification.

Table 4.18: Metal composition analyzed from L5 [wt%].

	Si	Mn	Fe	Total
L5	20.7 ± 1.6	78.0 ± 1.0	0.0 ± 0.0	98.7

Figure 4.19 shows a SEM picture with 40x magnification from Sample L5 with both metal and slag. An image of the same area with 400x magnification is presented in Figure 4.20. Table 4.18 shows the analysis of the metal in this sample. The data is normalized as described in Experimental Work, Chapter 6.2. The raw analysis data are attached in Appendix, Table D.1.

Table 4.19: Slag composition analyzed [wt%].

	SiO ₂	MnO	Al ₂ O ₃	CaO	FeO	MgO	Total
L5	40.7 ± 0.6	1.8 ± 0.1	17.5 ± 0.2	38.8 ± 0.7	0.0 ± 0.0	1.3 ± 0.1	100

Table 4.19 shows the analysis of the slag from Sample L5. The results are based on nine

spot analysis from EDS. The standard deviation given in this table are calculated from these spot analysis. All the raw data are attached in Appendix, Table D.2 and Table D.3.

Mass Losses and Slag Compositions



Figure 4.21: Weight loss graphs for experiments at high temperature with limestone as function of time.

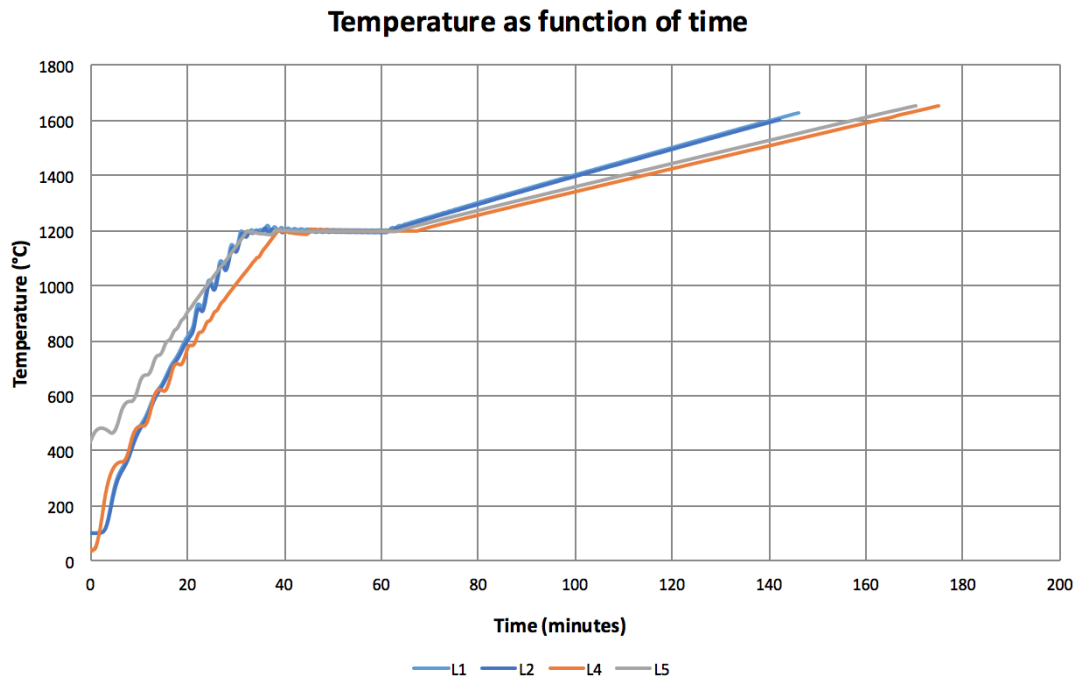


Figure 4.22: Temperature curves as function of time for the experiments stopped at high temperatures.

Figure 4.21 shows the weight loss curves for all experiments done with limestone at higher than 1600 °C. In this figure it can be seen that the weight loss of initial ore mass as function of time is plotted. Figure 4.23 shows the same weight loss curves, but as function of temperature instead of time. Experiment L4 and L5 are done in the SINTEF furnace. From Figure 4.23 it can be seen that the SINTEF furnace has much more stable temperature during heating from 900-1200 °C. This can also be seen from Figure 4.22. Experiments L1 and L2 does not have stable temperature time curves until higher than 1200 °C. The temperature time curves become stable at a much lower temperature in the SINTEF furnace.

Experiment L5 is done with a lot of extra coke added on the top of the charge. This may explain the difference in the weight loss between L4 and L5.

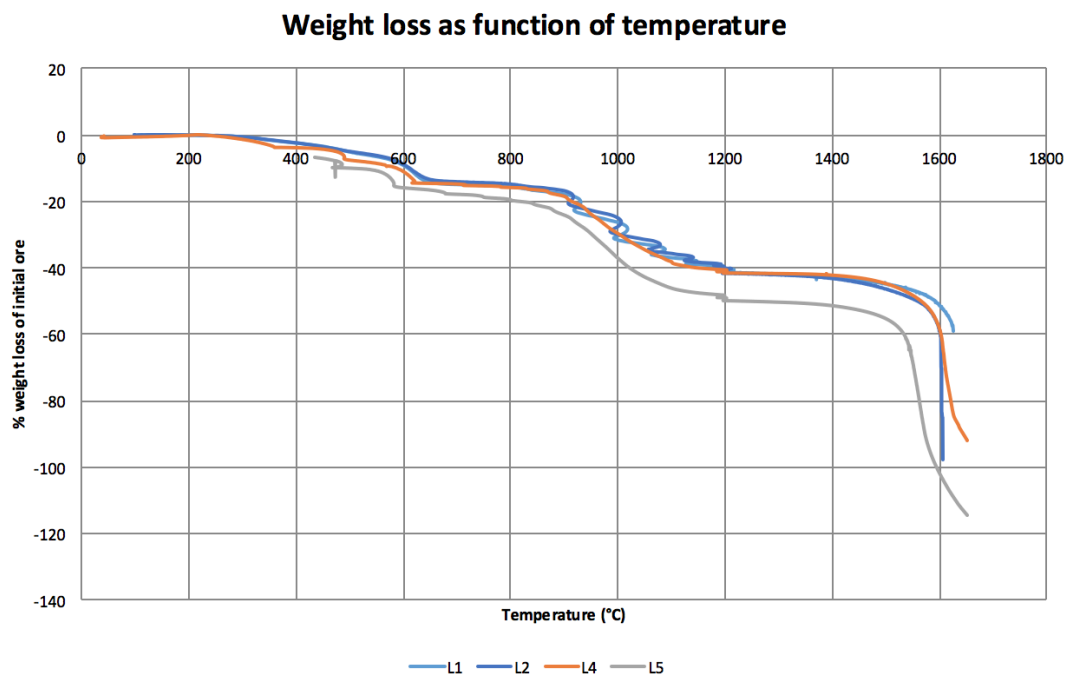


Figure 4.23: Weight loss graphs for experiments at high temperature with limestone as function of temperature.

Table 4.20: Slag composition analyzed [wt%].

Exp.	Max. Temp. [°C]	SiO ₂	MnO	Al ₂ O ₃	CaO	FeO	MgO	K ₂ O	Total
1.3	1250	35.0	40.0	8.0	12.0	0.4	0	0.6	96.0
1.2	1300	35.0	40.0	8.0	12.0	0.2	0	0.6	95.8
1.1	1400	25.5	43.5	14.2	12.0	0.1	0	0.1	95.4
9	<i>1600</i>	<i>40.0</i>	<i>3.8</i>	<i>13.8</i>	<i>38.0</i>	<i>0</i>	<i>0</i>	<i>0</i>	<i>95.6</i>
L2	1605	46.0	24.0	8.0	18.0	0	0.1	0.5	97.3
L1	1625	44.0	29.8	6.6	16.4	0	0.1	0.5	97.9
L5*	1650	40.7	1.8	17.5	38.8	0	0	0	100.1
L4*	1650	47.3	8.0	11.4	33.3	0	0	0	100

Table 4.20 shows an overview of the analysis of the slag from the experiments with Comilog ore, quartz and limestone. The experiments marked with * are analyzed with EDS, all others are analyzed by EPMA. Experiment 9 is in italic font because this experiment is held at 1600 °C for 30 minutes. The analyzed results from this sample is retrieved from Holtan (2015c).

Table 4.21 shows the calculated slag composition for all experiments with Comilog ore,

Table 4.21: Slag composition calculated based on measured wt% MnO and wt% SiO₂ and primary slag composition [wt%].

Experiment	Max. Temp. [°C]	SiO ₂	MnO	Al ₂ O ₃	CaO	MgO	Total
1.3	1250	35	40	8.72	15.76	0.51	100
1.2	1300	35	40	8.67	15.82	0.51	100
1.1	1400	25.5	43.5	10.74	19.62	0.64	100
9	1600	40	3.8	19.48	35.57	1.15	100
L2	1605	46	24	10.39	18.99	0.62	100
L1	1625	44	29.8	9.08	16.58	0.54	100
L5	1650	40.7	1.8	19.96	36.36	1.18	100
L4	1650	47.3	8.0	15.22	28.56	0.92	100

quartz and limestone. The values are calculated as described in Chapter 5. The R values for these experiments are 1.88.

Table 4.22: Metal composition analyzed [wt%].

Experiment	Max. Temperature [°C]	Si	Mn	Fe	Total
1.3	1250	2.6	73.0	25.0	100.6
1.2	1300		NA		
1.1	1400	0	32.4	67.6	100.0
9	1600	10.7	89.2	0.2	100.1
L2	1605	8.1	77.7	8.1	93.9
L1	1625	5.9	72.5	15.5	93.9
L5*	1650	17.0	80.6	0	97.6
L4*	1650	20.7	78.0	0	98.7

Experiments marked with * in Table 4.22 which are analyzed by EDS, are normalized the same way as EDS data in Table 4.7. This is described in Experimental Work, Chapter 6.2.

For Experiment 1.2 in Table 4.22 it was not observed any metal. Experiment 9 is in italic font because this experiment is held at 1600 °C for 30 minutes.

Table 4.23 shows an overview of the theoretical weight loss versus the measured weight loss during the experiments. Experiment L5 is done with 11.47 grams extra coke on the top of the charge. This is not corrected for in the calculation of the weight loss, and may explain the gap between the calculated and the measured weight loss for L5.

From the theoretical weight loss and the end slag composition, it is calculated a

Table 4.23: Calculated and measured weight loss from each experiment.

Experiment	Max. Temperature [°C]	Calculated [g]	Measured [g]
1.3	1250	10.44	7.25
1.2	1300	10.44	7.42
1.1	1400	13.89	7.75
9	1600	16.58	22.34
L2	1605	11.80	17.70
L1	1625	10.9	10.61
L5	1650	5.19	6.30
L4	1650	4.89	5.30

theoretical metal composition shown in Table 4.24.

Table 4.24: Metal composition calculated [wt%].

Experiment	Max. Temperature [°C]	Si	Mn	Fe	Total
1.3	1250	13.54	68.12	16.83	98.49
1.2	1300	13.54	68.12	16.83	98.49
1.1	1400	34.15	51.79	12.57	98.51
9	1600	21.75	69.28	7.47	98.5
L2	1605	11.34	75.36	11.78	98.51
L1	1625	10.24	74.30	13.95	98.49
L5	1650	17.93	72.81	7.75	98.49
L4	1650	17.15	73.07	8.28	98.5

Experiment L3 - Investigation of Melting Temperature

In this work, it also is investigated the melting temperature of this charge with large pieces of raw materials. The L3 experiment was done the same way as the other experiments, but with only one large piece of Comilog ore (18.47 g), one piece of quartz (7.11 g), one piece of limestone (6.00 g) and 5.81 grams of coke added to the crucible around the other pieces.

Figure 4.24 shows a picture taken of the raw materials after the heating up to 1350 °C. It is seen that the raw materials are not melted together during the experiment and have not created a liquid slag.



Figure 4.24: Picture of Sample L3. Quartz and Comilog ore piece after heating to 1350 °C.

Chapter 5

Discussion

In this chapter the results are discussed and compared with earlier research and investigations. The results from SiMn charge without flux added is discussed in the first part of the chapter, and then the second part discuss the SiMn charge with flux added. Last in this chapter the analysis methods are compared and discussed.

1 Comilog Ore and Quartz

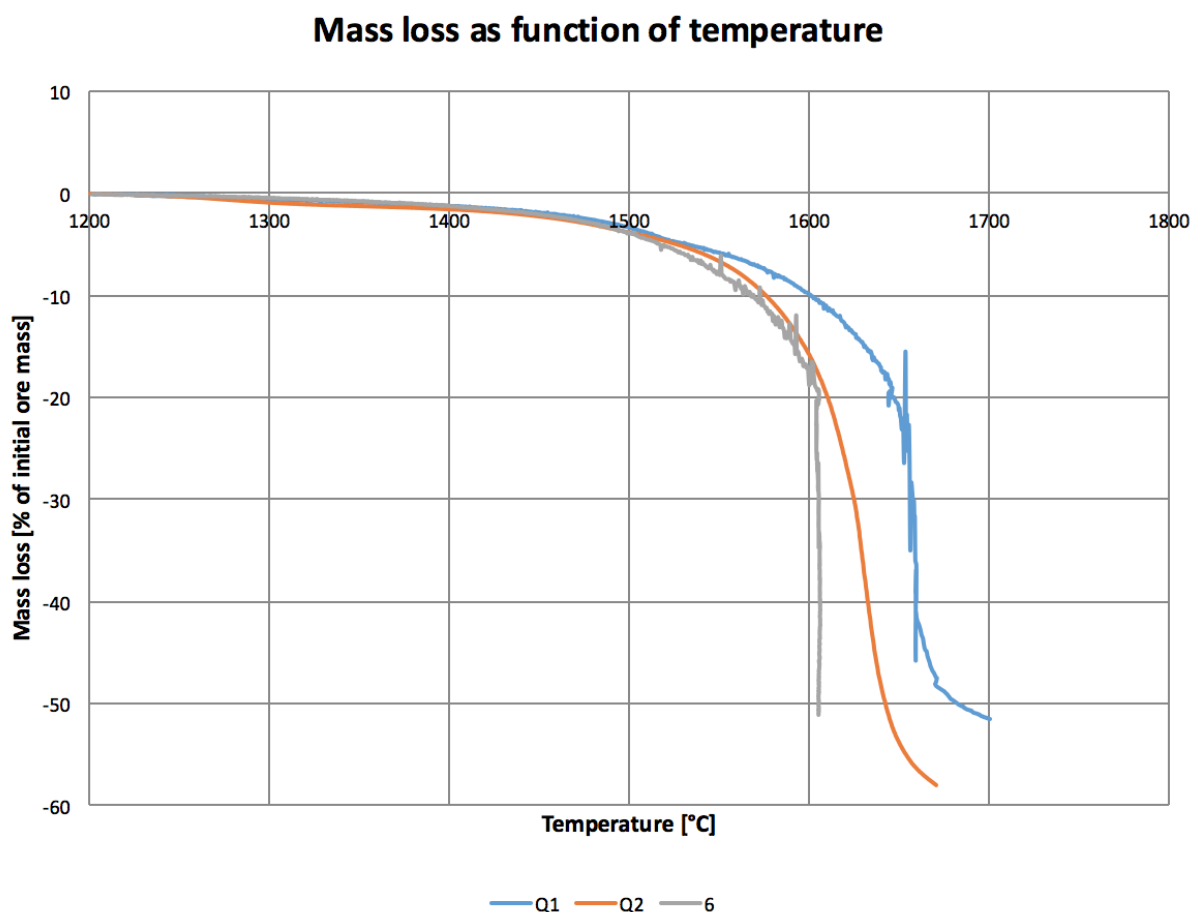


Figure 5.1: Mass loss in percentage of initial ore mass during reduction as function of temperature.

Figure 5.1 shows the weight loss curves from 1200 °C for experiments with Comilog ore and quartz stopped at higher temperature than 1600 °C. The calculated weight loss for Experiments 6 and Q2 fit very well with the measured weight loss, 17.08 vs 17.97 and 5.99 vs 6.49 respectively. Experiment 6 is held at 1600 °C for 30 minutes, and it can be seen from the figure that much of the reduction occur at that temperature during the holding time. The curve from Experiment Q2 is smooth which indicate no mass loss due to foaming for this experiment. Experiment Q1 had more measured weight loss than calculated weight loss, and this is due to foaming in the crucible mentioned in Experiments in Chapter 3. The

difference of the measured and the calculated weight loss is about 4 grams.

Experiment Q1 is modeled by Olsen (2016). He has worked with a mathematical model for reduction of SiMn charges. The data used in this model for Experiment Q1 is shown in Table 5.1.

Table 5.1: Values used in the model of Olsen (2016) for Experiment Q1.

E_a (Mn)	350 000 J/mol
E_a (Si)	800 000 J/mol
k (Mn)	0.0000053 mol/(s·cm ²)
k (Si)	0.000000143 mol/(s·cm ²)

Figure 5.2 shows the weight loss as function of time for Experiment Q1, both from the model and the experimental values. The foaming and loss of mass due to that is about 4 g from the model. The model stop at about 8 g loss and the curve from the experiment stop at about 12 g mass loss. The model for this experiment fit very well with the calculated mass loss from the mass balance described in Chapter 5.

From Figure 5.2 it can clearly be seen that the rapid mass loss due to foaming for this charge occur at 1650 °C. This is at a higher temperature than for charges with Assmang ore (Kim et al., 2016).

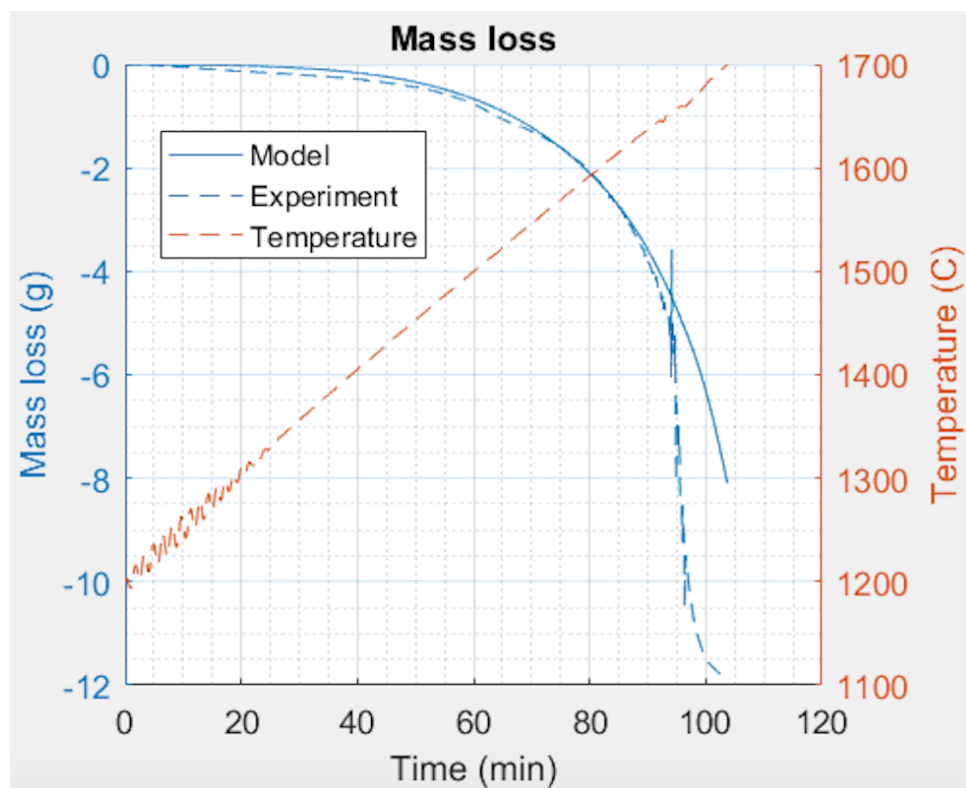


Figure 5.2: Mass loss as function of time, both from the model of Olsen (2016) and from Experiment Q1.

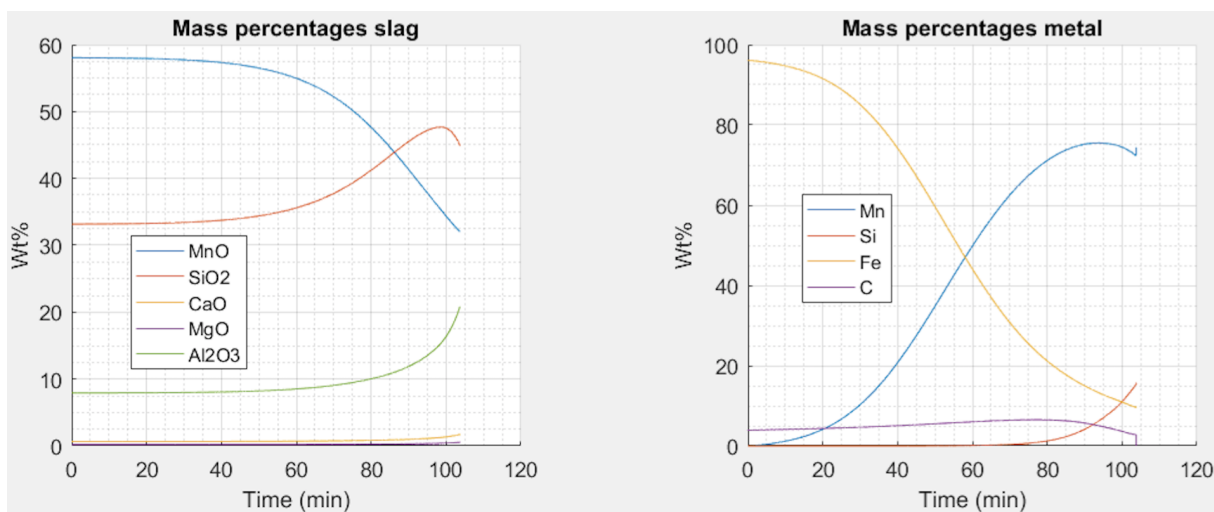


Figure 5.3: Weight percentages of slag and metal in Experiment Q1 calculated from the model of Olsen (2016).

Figure 5.3 show the mass percentages of the different species both in slag and metal

developing during experiment calculated from Olsen (2016) model. The temperature can be seen with comparing to Figure 5.2. From the analysis of the metal from Sample Q1 it is 14.9 % Si, 74.4 % Mn and 7.8 % Fe. This fit very well with Figure 5.3. The results from this figure is about 15 % Si, 73 % Mn and 10 % Fe. It can be seen from the metal curves in this figure that the silicon content start to increase at about 1550 °C, which indicate that the silica reduction start occur at this temperature.

It is almost no MgO and CaO in the Q1 Experiment due to very low MgO content in the ore and no lime added in the charge. The analysis of the slag show 44.8 % silica, 32 % MnO and 19.3 % alumina. These numbers fit very well with the results from Olsen (2016) model which show about 45 % SiO₂, 32 % MnO and 21 % Al₂O₃.

For the Q2 experiment it is not made any model due to the fact that it was not found any slag in this sample. This is further discussed later in this chapter.

From Figure 5.3 it can be seen that the MnO reduction start at 1400 °C. This is seen from the fact that MnO content in the slag starts to decrease at this temperature, and from the mass loss curves in Figure 5.1.

In Sample Q2 it is not found any slag. The weight loss measured is 6.49 g, and the calculated weight loss is 5.99 g. This is if 5 % MnO and 40 % SiO₂ are assumed. 2 grams of the weight loss is due to the prereduction with coke. Table 5.2 shows the calculated values for the slag composition before and after the reduction.

Table 5.2: Calculated slag phase [wt%].

	MnO	SiO ₂	CaO	Al ₂ O ₃	MgO
Primary slag	46.61	28.24	0.52	6.41	0.17
End slag	5	40	4.01	49.64	1.34

If this assumed slag composition is correct, the weight loss due to the reduction with CO is 3.89 grams. Then the total amount of slag after the reduction should be 1.29 g. From Persson (2007) a slag with Al₂O₃, CaO, MgO and SiO₂ should have a density about 2.67 g/cm³. Thus the volume of the slag is calculated as shown in Equation 5.1.

$$V = \frac{1.29 \text{ g}}{2.67 \text{ g/cm}^3} = 0.48 \text{ cm}^3 \quad (5.1)$$

If it is assumed that this slag will be one slag sphere, the size of this sphere will be as shown in Equation 5.2.

$$r = \sqrt[3]{\frac{3 \cdot 0.48 \text{ cm}^3}{4 \cdot \pi}} = 0.49 \text{ cm} \quad (5.2)$$

To compare the volume of the slag in Sample Q2 with other experiments, the theoretical volume of the slag phase in Sample Q1 is calculated to be 1.46 cm^3 . That is more than three times as much slag as Sample Q2. Hence, this could be the reason that it was not found any slag in Sample Q2.

2 Comilog Ore, Quartz and Limestone

In this chapter each of the experiments done with limestone added as a flux are discussed based on analysis, weight losses and calculations.

Olsen (2016) has worked with making a mathematical model to describe the reduction for SiMn charges such as the charge in these experiments. The values shown in Table 5.3 are the values used in the model for Experiment L1. E_a values for manganese and silicon are the same for all experiments modeled with this model, but k values are specific for each experiment.

Table 5.3: Values used in the model of Olsen (2016) for Experiment L1.

E_a (Mn)	350 000 J/mol
E_a (Si)	800 000 J/mol
k (Mn)	$0.0000046 \text{ mol}/(\text{s} \cdot \text{cm}^2)$
k (Si)	$0.00000023 \text{ mol}/(\text{s} \cdot \text{cm}^2)$

Results from Olsen (2016) are shown in Figure 5.4. This figure show the mass loss from

the model and from the experiment together, and the temperature during heating. The parameters in the model are adjusted to get the same slag from the model as from the experiment. Then the weight loss curves automatically fit well (Olsen, 2016).

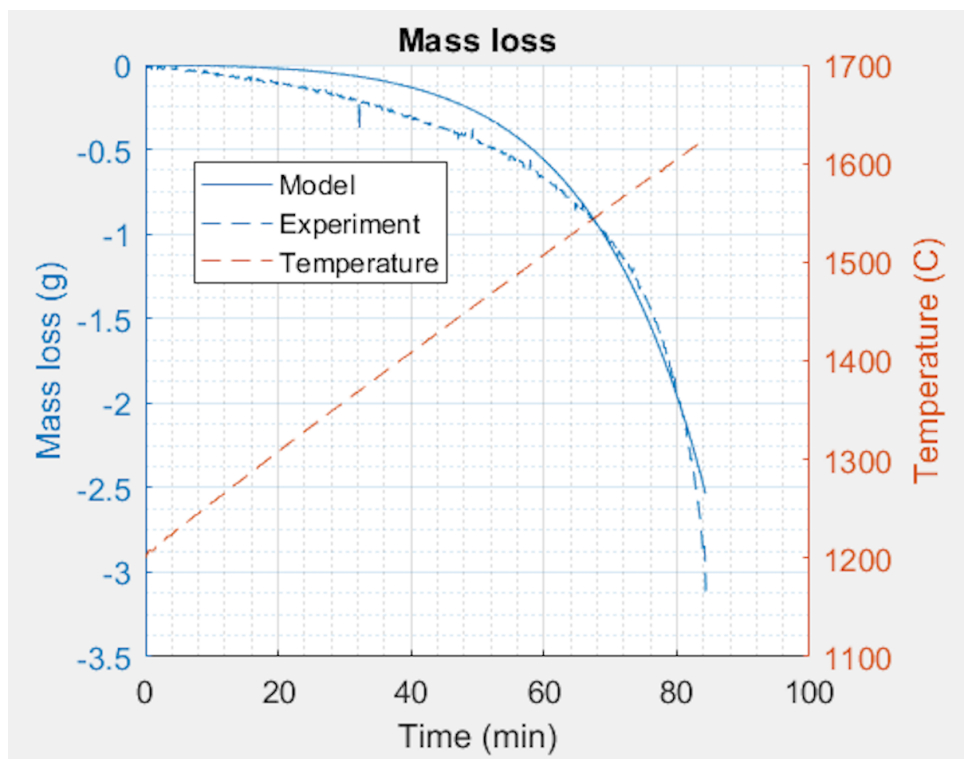


Figure 5.4: Mass loss as function of time, both from the model of Olsen (2016) and from the Experiment L1.

In Figure 5.5 the results from Olsen (2016) model are shown. The graph to the left in this figure show the composition in the slag as wt% during reduction, and the graph to the left shows the metal composition during reduction. The temperature can be found by comparing with the time from Figure 5.4.

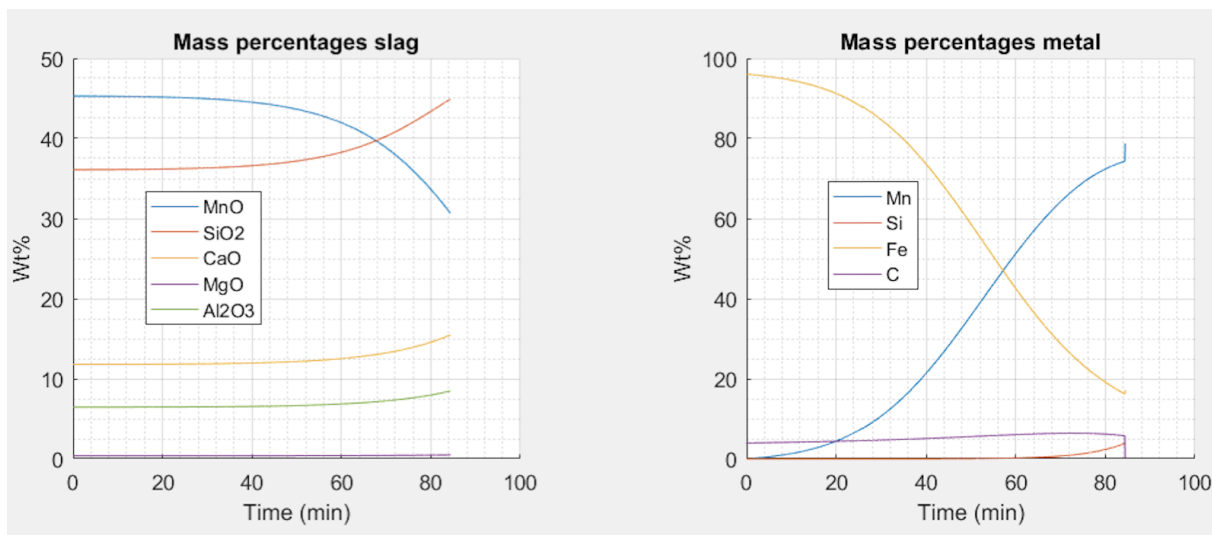


Figure 5.5: Weight percentages of slag and metal in Experiment L1 calculated from the model of Olsen (2016).

It can be seen from Figure 5.5 that the MgO content in the slag is about 0 during the entire experiment, which is not strange at all since it is used Comilog ore in the experiment. The Comilog ore used in this work has a MgO content of 0.13 wt% (Holtan, 2015c), and typically MgO content in Comilog ores are 0-0.3 wt% (Tangstad et al., 2004). The analyzed MgO content in the end slag from this sample was 0.1 wt%.

The MnO content in the end slag was 30 wt%, and it can be seen from Figure 5.5 this fit well. The graph in this figure stop at about 30 wt%.

From the model it can be seen that the silica content end at 45 wt%, and the analyzed slag composition is 44 wt% SiO_2 . The alumina content in the end slag is 7 wt% and the graph for Al_2O_3 from the model stop at 8-9 wt%. CaO content in the slag is 16 wt% and the graph stop at 15-16 wt%. All these results from the EPMA and the model of Olsen (2016) fit very well.

From the metal wt% curves in Figure 5.5 the same trend can be seen. Mn composition analyzed is 73 wt% and the model ends at about 75 %. Iron content in the metal is 16 wt% and the model ends at about this value. The amount of silicon in the metal is 6 wt% and the curve from the model ends at about 5 wt%.

This means that it is possible to make a good model for the reduction of this charge with

the thermodynamic constants presented earlier in this chapter.

From Figure 5.5 it can be seen that the silicon content in the metal start to increase at about 1550 °C. The temperature is found by compare with Figure 5.4. This means that the reduction of silica start at this temperature, and 1550 °C is the same temperature as for the experiment without limestone added. From this it can be concluded with that the silica reduction start to occur at 1550 °C.

The MnO content in the slag start to decrease at about 1400 °C seen from Figure 5.5.

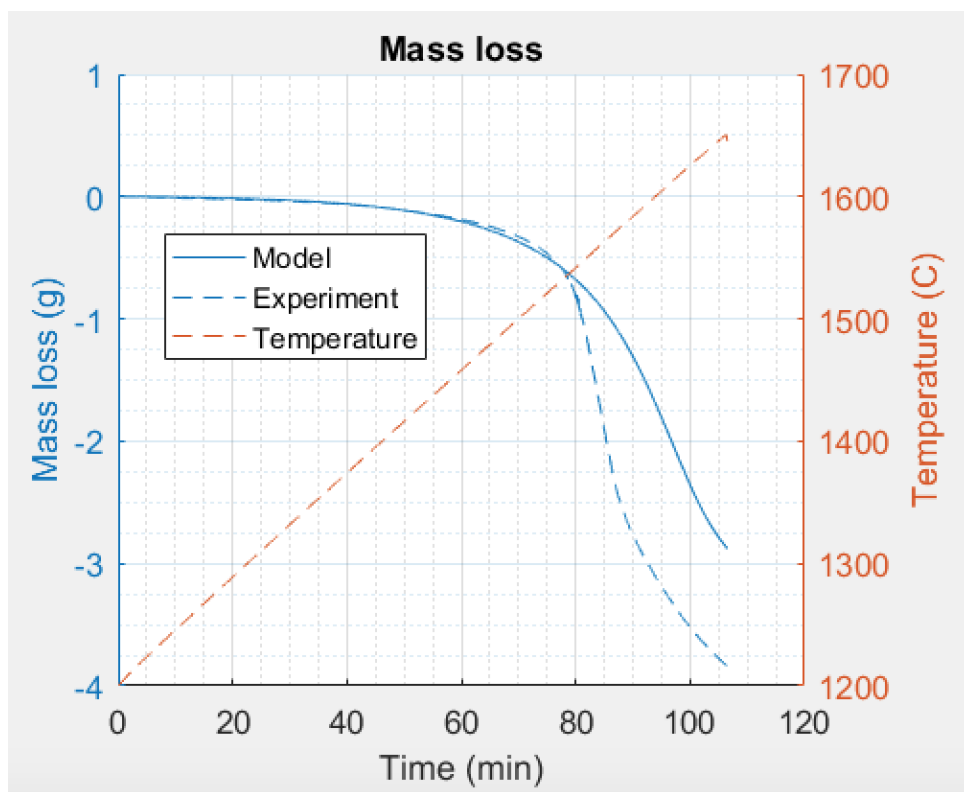


Figure 5.6: Mass loss as function of time, both from the model of Olsen (2016) and from the Experiment L5.

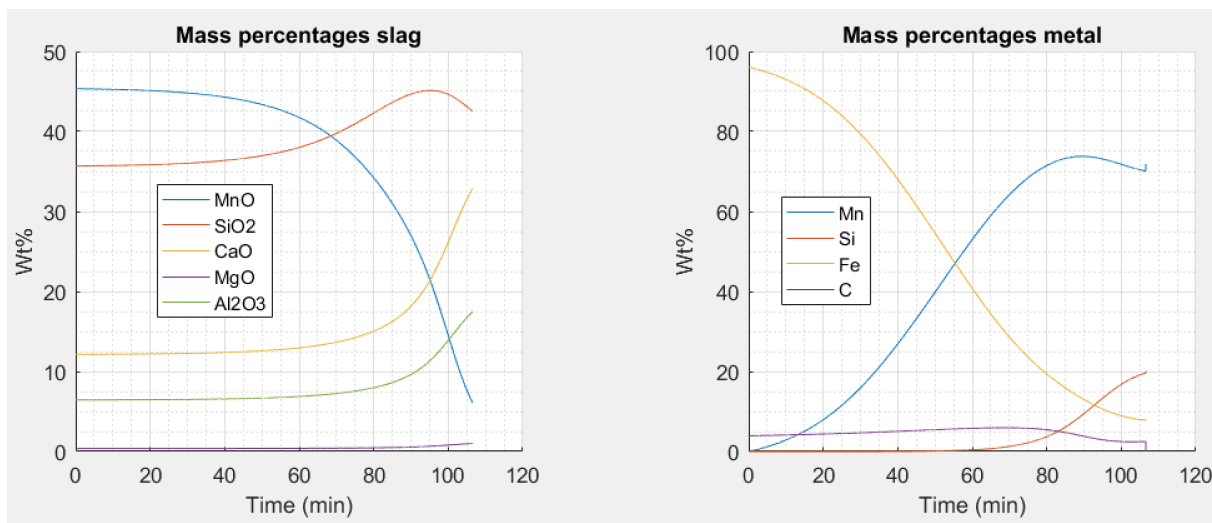


Figure 5.7: Weight percentages of slag and metal in Experiment L5 calculated from the model of Olsen (2016).

In Figure 5.7 the results from Olsen (2016) model are shown for Experiment L5. The graph to the left in this figure show the composition in the slag as wt% during reduction, and the graph to the left shows the metal composition during reduction. The temperature can be found by comparing with the time from Figure 5.6.

The silica content in the end slag is 41 wt%, and it is seen from Figure 5.7 that this fit well. The graph in this figure stop at 42.5 wt%. From the model it can be seen that the MnO content end at 6 wt%, and the analyzed slag composition is 2 wt%. The alumina content in the end slag is 17.5 wt% and the graph for Al_2O_3 from the model stop at exact that value. CaO content in the slag is 39 wt% and the graph stop at 34 wt%. All these results from the EDS and the model of Olsen (2016) fit well, except the MnO content which is very low in the end slag from the analyzed results.

From the metal wt% curves in Figure 5.7 the metal composition modeled by Olsen (2016) can be seen. Mn composition analyzed is 81 wt% and the model ends at about 70 %. Iron content in the metal is 0 wt% and the model ends at about 8 wt%. The amount of silicon in the metal is 17 wt% and the curve from the model ends at about 20 wt%.

The thermodynamic constants used for modeling this experiment is shown in Table 5.4. E_a values are the same as for the other experiments, but the k values are specific for this

experiment. This experiment was harder to fit to the model, so it ended with fitting the parameters to the end metal composition instead for the end slag composition (Olsen, 2016).

Table 5.4: Values used in the model of Olsen (2016) for Experiment L5.

E_a (Mn)	350 000 J/mol
E_a (Si)	800 000 J/mol
k (Mn)	0.000004 mol/(s·cm ²)
k (Si)	0.0000008 mol/(s·cm ²)

The L5 experiment is done with a lot of coke added on the top of the charge in the crucible. The reason for that was due to the foaming problem with the slag during experiments. Coke was added on the top of the charge to see if this could stop the slag to foam and leak from the crucible. It seems successful because it could not be observed any slag on the lid after this experiment, and the weight loss curves are smooth and continuous. The measured weight loss and the calculated weight loss also fit well, 5.19 g calculated and 6.30 g measured. 11.47 g extra coke with 3.5 % volatiles cause 0.4 g of the difference.

The addition of extra coke may also be the reason Olsen (2016) felt it harder to fit the L5 experiment to the model than the other experiments. The weight loss curves show more mass loss from this experiment than the others.

The MnO content in the slag start to decrease at about 1400 °C seen from Figure 5.5 and Figure 5.7 and compare time with temperature curves in Figure 5.4 and Figure 5.6 respectively. Compared with mass loss curves from Figure 5.8 it seems good, the weight loss start to occur at this temperature. The reduction from SiMn charges are independent of size fractions of the raw materials (Holtan, 2015c) and (Kim et al., 2016). This is due to a completely liquid slag phase at 1250 °C. From Kim et al. (2016) it seems like the reduction starts at 1300 °C for FeMn charges with 0.6-1.6 mm size fractions, and at 1350 °C for 4.0-6.3 mm size fractions. This is both for Comilog ore and Assmang ore charges. From this results it is possible to conclude with the MnO reduction start to occur at a higher temperature for SiMn charges. The MnO starts to reduce at 1400 °C in SiMn charges.

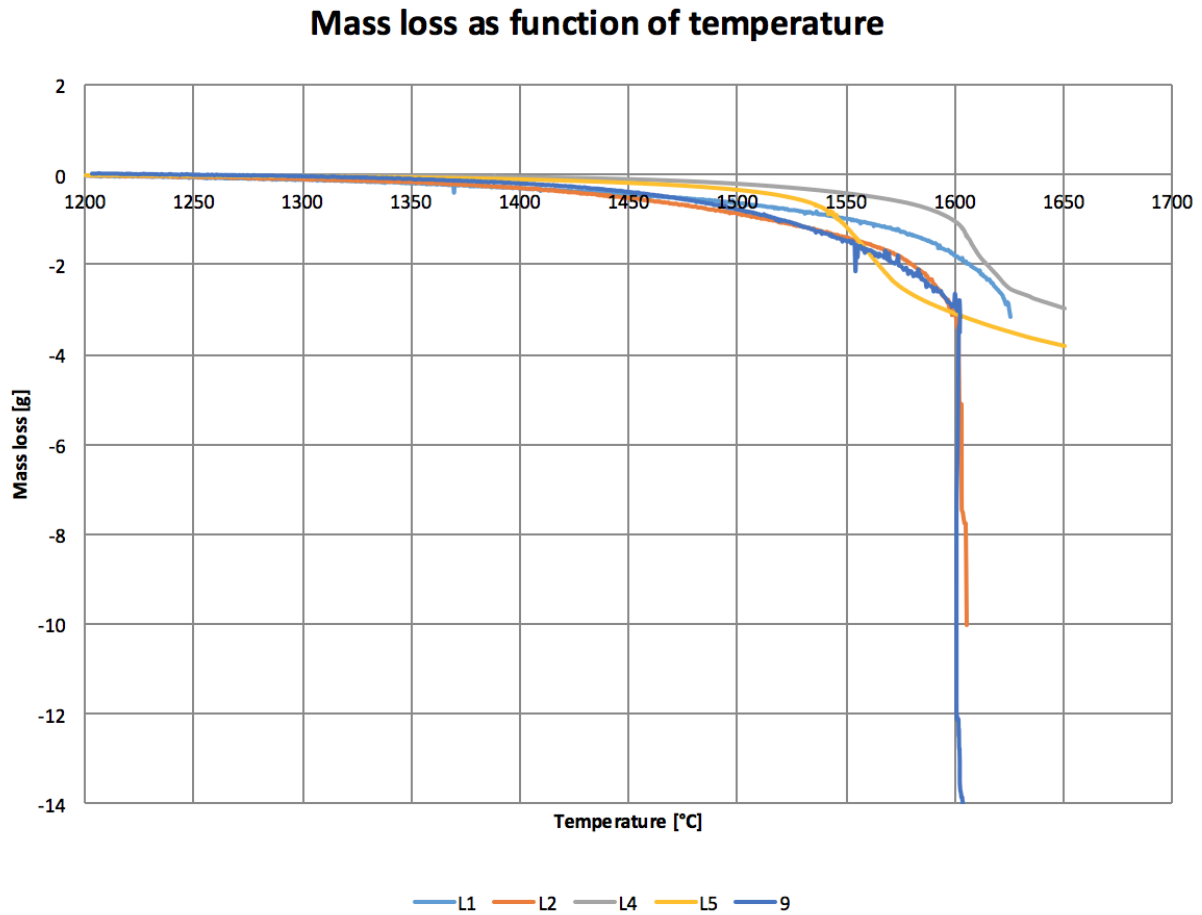


Figure 5.8: Mass loss during reduction as function of temperature.

The weight loss during reduction for the experiments are shown in Figure 5.8. Experiment 9 is from Holtan (2015c). Experiments L4 and L5 were done with 1/3 the amount of raw materials in order to reduce or get rid of the foaming problem. Hence the weight loss in percentage of initial ore mass are presented in Figure 5.9.

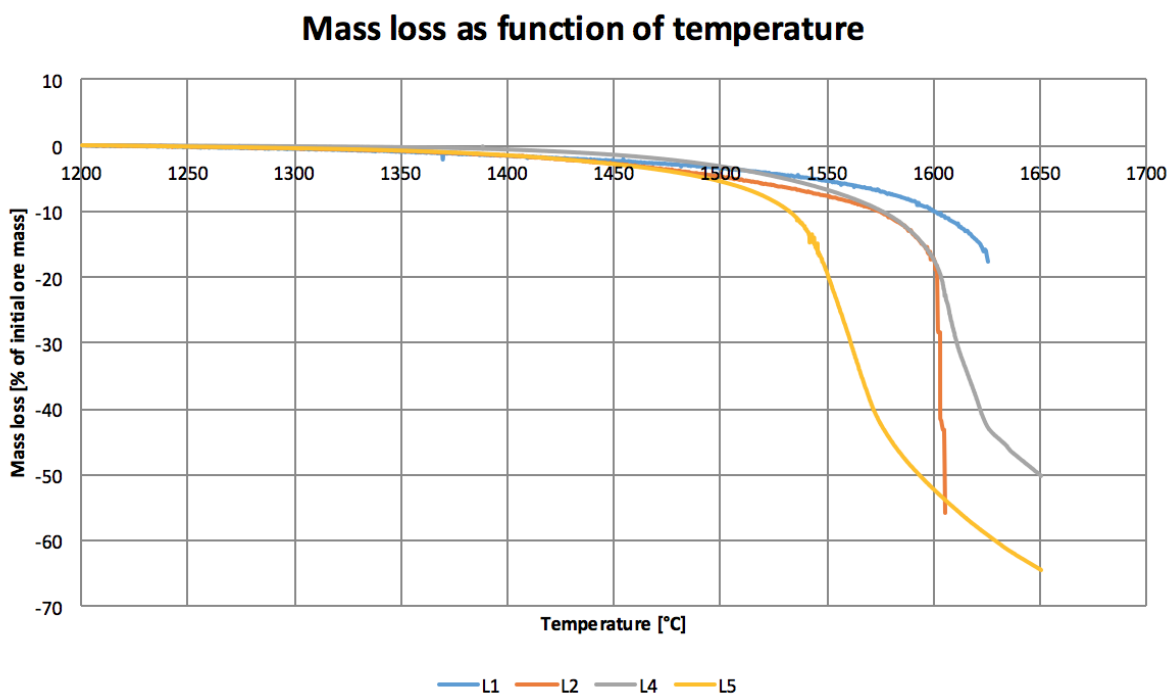


Figure 5.9: Mass loss in percentage of initial ore mass during reduction as function of temperature.

The reduction occur earlier and at a lower temperature in experiment L5, the one with coke added on the top. The larger reaction area between carbon and slag may be the reason for that. It was observed a bit slag on the top from experiment L4 as well, but it does not seem like it has been slag falling off the crucible from the mass loss curves.

For experiment L1, L4 and L5 the weight loss curves are trustable. The curves are smooth and the measured mass loss are about the same as the calculated weight loss from the mass balance described in Chapter 5. For experiments L2 and 9 (Holtan, 2015c) the slag analysis must be trusted, because it has been so much foaming and slag dropped down in the furnace from the crucible during reduction. The calculated weight loss for these experiments are much less than the measured weight loss and the mass loss curves are not continuous and smooth. From Figure 5.8 it could be seen that the rapid mass loss for L2 occur at 1600 °C, and it is about 7 grams loss. This is due to foaming.

In Table 5.5 the evolution of MnO and silica in the slag can be seen. Experiment 9 can not be compared directly because this experiment has been held at 1600 °C for 30 minutes

Table 5.5: Comparison of analyzed slag composition [wt%].

	Max. Temp. [°C]	SiO ₂	MnO
1.3	1250	35	40
1.2	1300	35	40
1.1	1400	25.5	43.5
9	1600	35	3.8
L2	1605	46	24
L1	1625	44	30
L5	1650	40.7	1.8
L4	1650	47.3	8.0

(Holtan, 2015c). The amount of silica in the slag is about 35 wt% from 1200 °C up to about 1450-1500 °C out from this analysis and from the model shown in Figure 5.5 and 5.7 (Olsen, 2016). Then the silica amount in the slag increase up to about 45 wt%, and it may decrease some percentage again after about 1600 °C. The graph from the model shown in Figure 5.7 show decreasing amount of silica over 1600 °C, the same as Experiment L5. This is because of reduction of silica, and this shape of the silica curve was also seen in Nadir (2015) calculations based on equilibrium data shown in Chapter 2.

The weight loss curve show more reduction at a lower temperature for L5 than for L4. L4 and L5 are stopped at the same temperature and the metal analysis are about the same for both samples. If it is assumed that the extra weight loss for Experiment L5 compared with L4 come from the extra coke added, this make sense. Both experiments end up with a silicon content in the metal about 18 wt% and 5 % MnO and 40 % SiO₂ in the slag which the charge composition was calculated for. This is close to equilibrium at 1600 °C for both experiments. The equilibrium values are 18 % Si in the metal and 42 % SiO₂ in the slag for slags with CaO/Al₂O₃ = 4 (Olsen, 2001). In Figure 5.10 it is shown with a red cross where the samples L4 and L5 are in Si-SiO₂ diagram for distribution between slag and metal. The cross is put in at the average point for these two samples. This is at equilibrium at about 1640 °C for slag with R ratio equal 4. In these slags this value is close to 3 in the end slag, and from Olsen and Tangstad (2004) lower R ratio will increase the silicon content in the metal hence move the lines in Figure 5.10 in the direction shown by the blue arrows. Which means this is at equilibrium for lower temperature than 1640 °C, maybe at about 1600 °C. Figure 2.6 in

Chapter 2 shows the Si distribution between slag and metal as function of R ratio.

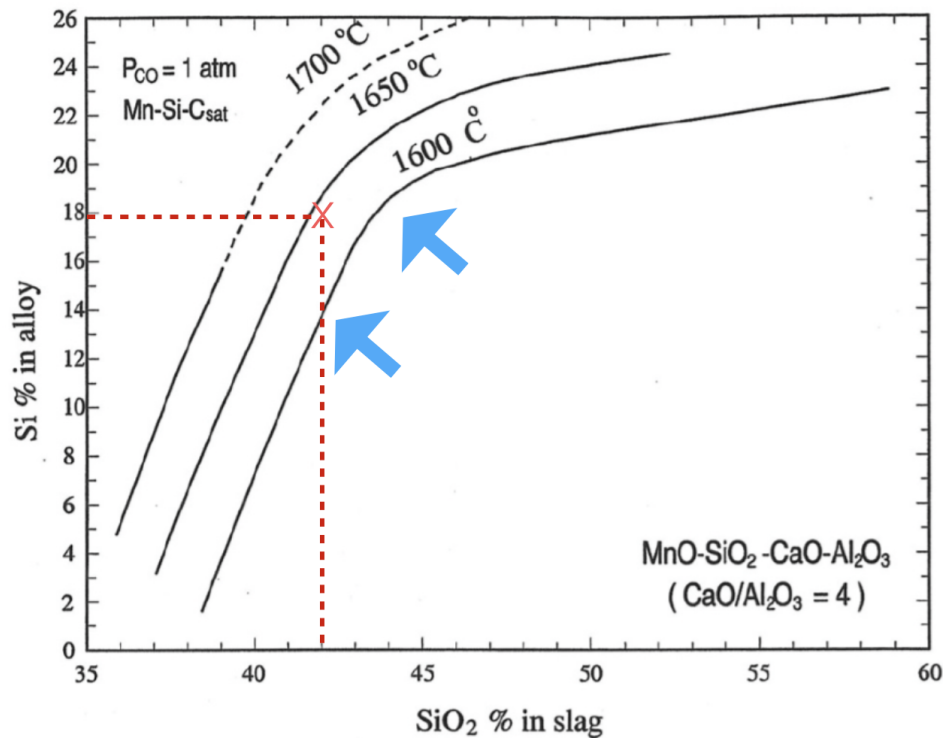


Figure 5.10: The red cross represent about the distribution of Si between the metal and the slag in Sample L4 and L5. Modified from Olsen (2001).

The kinetics are faster for L5 due to larger reaction area of carbon. A larger carbon/slag interface will increase the reduction rate, specially when the carbon is from a naturally carbon source such as coke (Dijks and Smith, 1980).

3 Degree of Reduction and Si Distribution

For comparing all the experiments it is valuable to investigate the degree of reduction. This can be done by looking at mass manganese and silicon produced in each experiment or by calculate mass of manganese and silicon produced per mass ore added in the charge. In this chapter the last one is choice because of different amount of ore in the experiments.

Table 5.6 shows the degree of reduction for the experiments. Experiments over the line are without limestone added, and under the line are experiments with limestone.

Table 5.6: Comparison of degree of reduction for the experiments.

	Max. Temp. [°C]	g Mn/g ore	g Si/g ore
Q1	1700	0.38	0.08
Q2	1670	0.47	0.14
6	1600	0.46	0.12
2.1	1400	0.10	0.00
L4	1650	0.44	0.11
L5	1650	0.47	0.14
L1	1625	0.25	0.03
L2	1605	0.32	0.05
9	1600	0.46	0.14

The slag compositions are used as basis for calculating the degree of reduction for Experiments Q1, Q2 and 6. For Q1 the extra measured mass loss of 4 g is assumed to be due to foaming in the slag, and for Q2 and 6 the mass losses fit well both measured and calculated which indicate that the slag compositions are trustable. In Sample Q2 it was not found any slag, so the calculations are based on the weight loss and the assumptions of 5 % MnO and 40 % SiO₂ in the slag.

For Experiment 2.1 it is quite big difference between the calculated mass loss based on the analysis of the slag (10.93 g) and the measured mass loss (6.66 g). The measured mass loss is the most trustable for this experiment, because no reduction can occur without mass loss. The slag had several phases (Holtan, 2015a) so the real slag composition deviate from the analysis of the slag. For calculating the degree of reduction, the mass balance was adjusted to get 0 g Si reduced and to get total mass loss for the experiment to become close to the measured value. The slag composition is adjusted to 52.1 % MnO and 38 % silica, then the values given in Table 5.6 are achieved.

Under the rule in Table 5.6 the experiments done with limestone added are presented. The slag compositions are the basis for the calculations of degree of reduction for Experiments L4, L5, L1 and L2. The weight loss calculated based on the slag composition and the measured weight loss fit well for Experiments L4, L5 and L1. For Experiment L2 the measured weight loss is about 6 g more than the calculated mass loss. From Figure 5.8 it can be seen that it is 6-7 grams rapid mass loss due to foaming and slag falling out of the

crucible. Hence the analysis of the slag is more trustable than the measured weight loss for this experiment. Also for Experiment 9 the slag composition is used for calculating the degree of reduction, due to the assumption that the extra measured mass loss came from foaming of slag.

Experiments 6 and 9 are retrieved from Holtan (2015c) and are held at 1600 °C for 30 minutes. Because of the holding time these experiments are not directly comparable with the other experiments. Nevertheless, these experiments can be compared with one another. The difference in degree of reduction for manganese for these two experiments are 0.007 and the difference for silicon is 0.020. This is just 1.5 % difference for manganese, but it is 16 % difference for silicon. From these results it seems like it is biggest degree of reduction for experiments with limestone added.

Experiment Q2 has about the same degree of reduction as Experiment L5. No slag from Q2 was analyzed, so this is based on 5 % MnO and 40 % silica assumptions. Q2 also was stopped at a higher temperature than L5 which should have resulted in higher degree of reduction.

By comparing Experiment Q1 which has a good analysis of the slag with Experiments L4 and L5 which are the experiments with limestone stopped at the closest temperature. The difference between Q1 and L5 is 25 % in degree of manganese reduction and 76 % for silicon reduction. This is big differences. L5 has more degree of reduction even L5 is stopped at 50 °C lower temperature than Q1. Both Q1 and L5 have trustable mass loss curves, slag compositions and models from Olsen (2016). From this data it could be concluded with a SiMn charge with added limestone has more degree of reduction than a SiMn charge without limestone. The limestone has biggest impact on the degree of reduction of silicon. The silicon degree of reduction is much higher in experiments with added limestone.

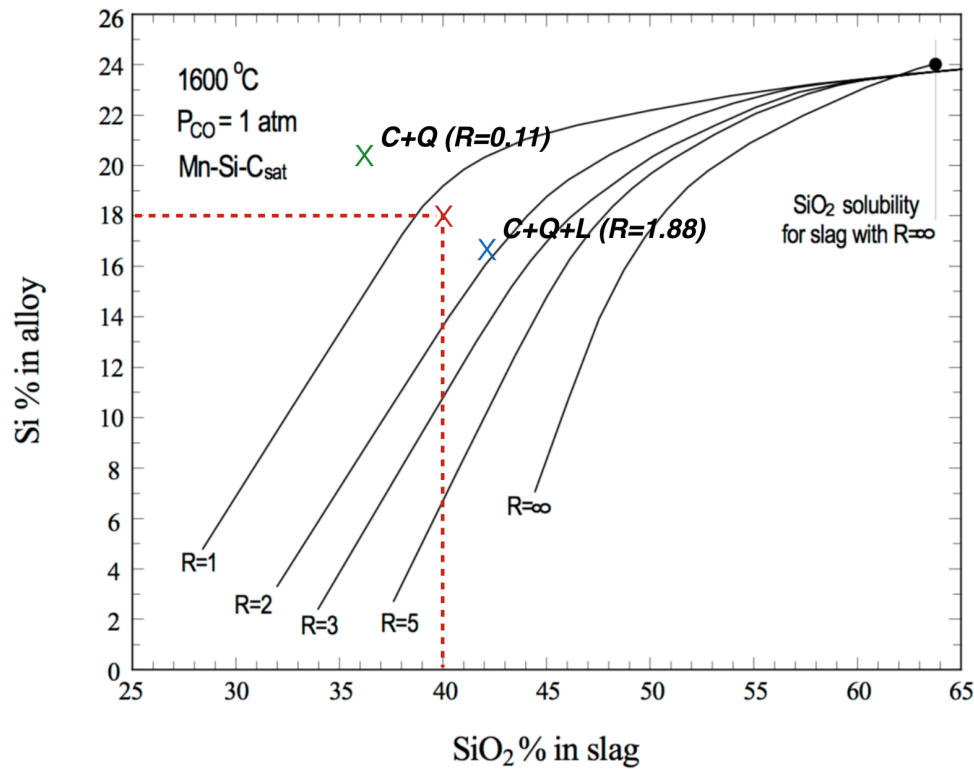


Figure 5.11: The equilibrium silicon distribution between the slag and the metal for both charges. Modified from Olsen and Tangstad (2004).

Figure 5.11 shows the Si distribution between slag and metal for both charges used in this work. The red cross indicate the aim distribution of Si from the amount of quartz added in the charge. The green cross is the equilibrium silicon distribution at 1600 °C for the charge with Comilog ore and quartz, and the blue cross is for the charge with limestone added. Limestone increase the R ratio and from the equilibrium calculation of silicon distribution between slag and metal by Olsen and Tangstad (2004) this should decrease the silicon content in the metal with constant amount of quartz in the charge. This can be show from the equilibrium expression shown in Equation 5.3.

$$K = \frac{\%Si \cdot \gamma_{Si}}{\%SiO_2 \cdot \gamma_{SiO_2}} \quad (5.3)$$

If lime is added, the γ_{SiO_2} will decrease and hence the % Si also have to decrease to maintain K constant.

The results from this work show the opposite, it is higher degree of reduction of Si for

charge with lime added. Hence the kinetics are more important for this system than the thermodynamics. With lime added the reduction rate has to be higher due to the calculations of degree of reduction. This may be due to physical properties of the slag, viscosity as an example. Lime will increase the CaO content in the slag, which decreases the viscosity as shown in Figure 2.2 from Kvande (2014) in Chapter 2.3. Lower viscosity may affect the slag/coke interface, which is important for the kinetics. Eissa et al. (2004) found that the initial R ratio of 1.8 gives maximum recovery for manganese and silicon. The initial R ratio for the SiMn charge used in this work was 1.88. So that it is a high degree of reduction for both Si and Mn for the charge with limestone fit well with the results from Eissa et al. (2004).

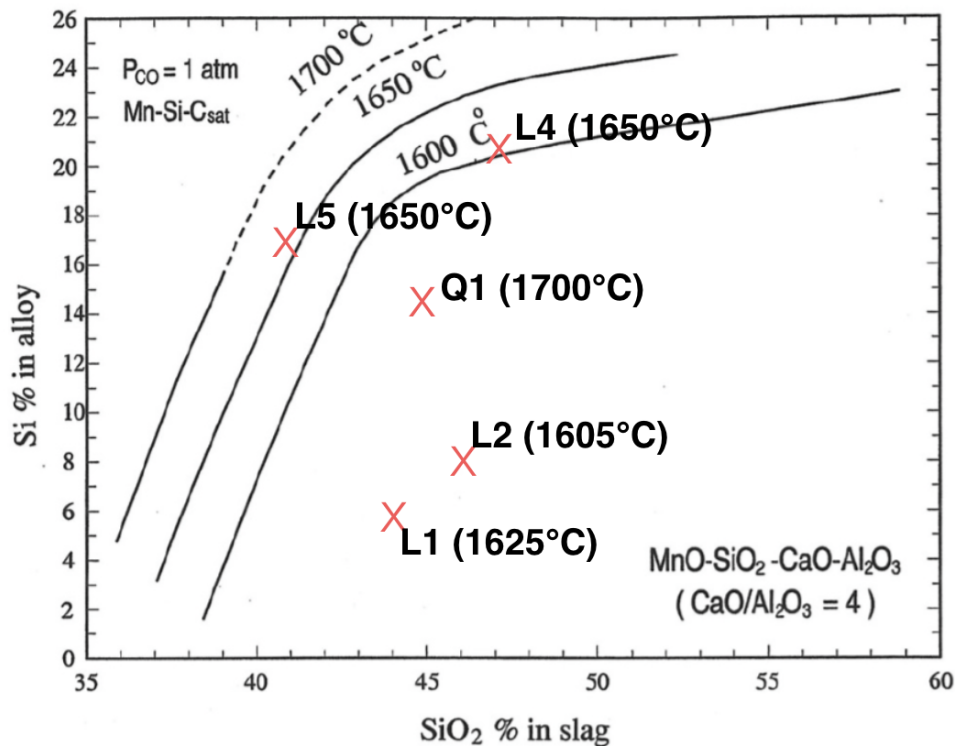


Figure 5.12: The silicon distribution between the slag and the metal for the samples. The lines show equilibrium distribution for some temperatures. Modified from Olsen (2001).

In Figure 5.12 the silicon distribution between slag and metal is shown for some samples. This shows that the L4 and L5 samples are close to equilibrium as discussed earlier, and it also shows that Sample Q1 is far from equilibrium. This supports that the reduction rate is slower

for SiMn charge without limestone added.

4 Melting Temperature of the Charge

The L3 experiment is done for comparing raw materials melting behavior with the results found by Holtan (2015a), who found that liquid slag is created at as low as 1250 °C for raw materials with size 0.6-1.6 mm and for 4.0-6.3 mm size. This result shows that this composition follow the binary phase diagram in Figure 5.13 and melts at 1250 °C. From the ternary MnO-SiO₂-Al₂O₃ phase diagram it also can be seen that this composition should be liquid at equilibrium at 1250 °C. So the results from Holtan (2015a) fit well with different phase diagrams for the composition investigated in this work.

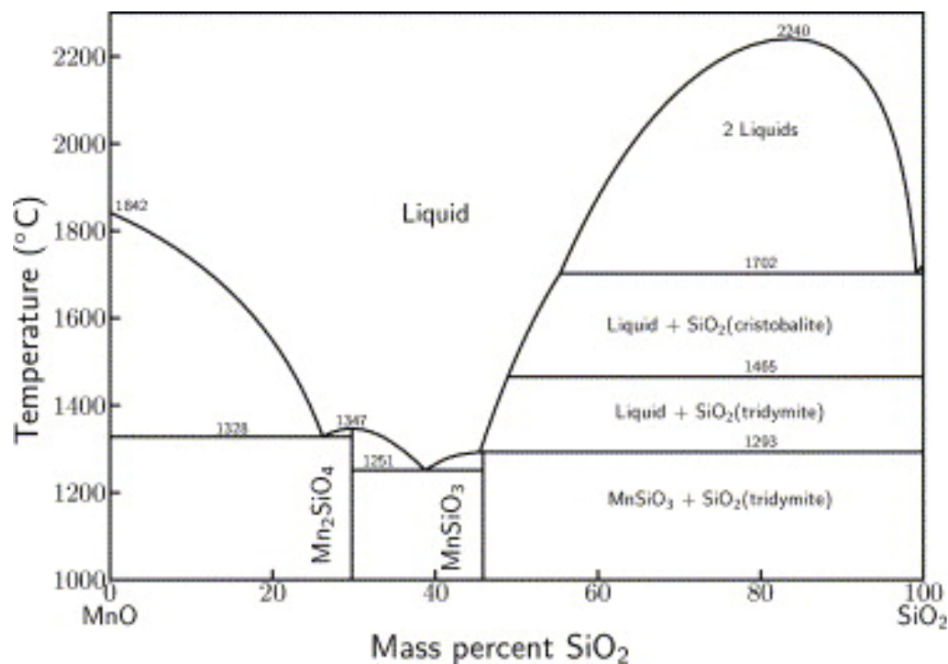


Figure 5.13: Binary phase diagram for MnO and SiO₂ (Eriksson et al., 1994).

The L3 experiment from this work was stopped at 1350 °C, and the raw materials have not created a liquid slag during heating. This may be due to several reasons. One reason is that the contact area between the raw materials was very small. If that was the case, it is not surprising that the raw materials do not melt. The melting temperature for only MnO is

1842 °C and at least 1700 °C for just SiO₂ as well (Eriksson et al., 1994). If the contact area is very small, the diffusion may just occur on small spots, and the sample will be very far from equilibrium. And all phase diagrams are only valid at equilibrium.

One other reason may be that the large pieces conduct heat slower than the small pieces investigated by Holtan (2015a). The heat conductivity is the same for a material independent of size, but the heat transfer depend on the size. It is a quadratic relationship between the radius on a particle and the time it take to obtain the maximum temperature in the senter. This can be shown from Fourier's law (Rosenqvist, 2004).

5 EDS

In this part of the chapter it is discussed how the SEM and EDS analysis affect the results compared with the EPMA.

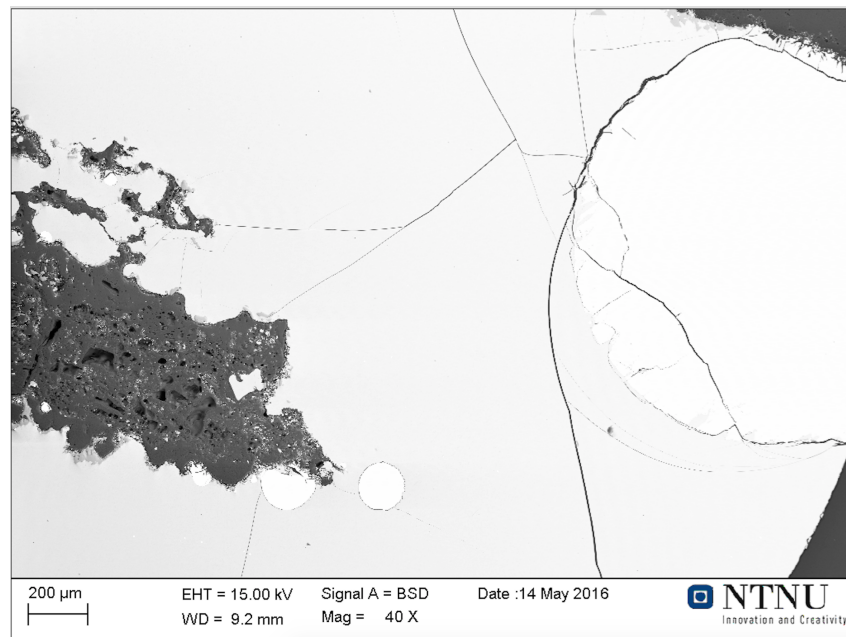


Figure 5.14: SEM Picture from Sample L4. 9.2 mm working distance.

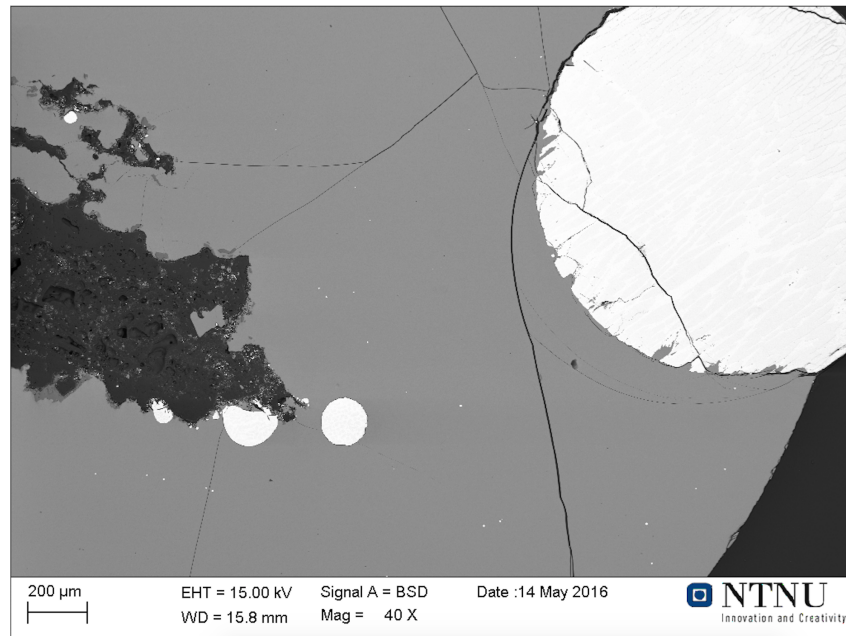


Figure 5.15: SEM Picture from Sample L4. 15.8 mm working distance.

Figure 5.14 and Figure 5.15 show images of the same part of Sample L4. The circular phase to the right is metal and the phase around is a glassy slag phase. It also is some coke and small metal droplets in the images. These two pictures are taken with few minutes apart, and with the same settings on the SEM. The only difference is the working distance. It is easy to see the slag phase and the metal phase in Figure 5.15 with longest working distance, and not so easy to see the difference between the two phases in Figure 5.14 with short working distance.

For using the SEM to analyze samples with EDS, a working distance about 10 mm is required (Yu, 2015). That is because the EDS detector got more X-rays with shorter working distance and hence more data to process. If the working distance is too short, the lens block most of the X-rays. Thus 10 mm is suitable.

From Figure 5.14 it seems like 10 mm is too short to get good images with Back Scattering Detector. With increased working distance, the image of slag and metal phase together is better. Thus the working distance should be increased from the EDS distance for taking SEM pictures.

Table 5.7 shows the analysis of the same slag phase both with EDS and EPMA. The

Table 5.7: Comparison of EPMA and EDS analysis [wt%] (Li, 2016).

	SiO ₂	MnO	Al ₂ O ₃	CaO	FeO	MgO	Total
EDS	32.12	40.26	12.36	9.19	2.24	3.84	100
EPMA	32.55	37.13	13.83	9.26	3.34	3.88	100
Variance	0.43	3.13	1.48	0.07	1.10	0.05	0
% deviation	1.32	8.43	10.70	0.76	32.93	1.29	0

absolute values of the EDS data subtracted from the EPMA data are presented in the variance row. % deviation means the variance divided on the EPMA value and describe better how much the difference between the EDS data and the EPMA data are. That is because 1 wt% off is very much if the total is 2 wt%, but it is very little off if the total amount of this compound is 40 wt%.

It is shown a comparison of one slag phase in Table 5.7. The spot analysis data this table is based on is attached in Appendix E, Table E.1. In Appendix E it could be found results from total seven different slag phases from different samples that are analyzed with both EDS and EPMA.

The results from Appendix E are normalized. This is due to the high carbon content from the analysis because of the carbon coating. All samples are coated with carbon for the necessary conductivity in the SEM. This carbon coating also need to be applied for EPMA. From Appendix D it seems like the EDS results give 8-9 % carbon. The emission depth of the electrons is much bigger than the thickness of the carbon coating, but the coating still affect the results. How deep the backscattered electrons can give information about is given in Equation 5.4 (Hjelen, 1986). E_0 is the acceleration voltage (keV), A in g/mol, ρ in g/cm³ and Z is the average atom number.

$$R_{BS} = \frac{8.3 \cdot 10^{-3} \cdot A \cdot E_0^{1.67}}{Z^{0.889} \cdot \rho} \quad (\mu m) \quad (5.4)$$

It is possible to replace the carbon coating with gold coating. That is an opportunity if the carbon content is required, but it will increase the costs of sample preparations.

Table 5.8 shows the difference between the EPMA and the EDS results. Results from

Table 5.8: Differences between EPMA and EDS analysis [% off].

Sample	SiO ₂	MnO	Al ₂ O ₃	CaO	FeO	MgO
1	1.32	8.43	10.70	0.76	32.93	1.29
2	2.95	0.80	9.44	0.92	100	9.82
3	0.11	1.81	4.74	1.17	100	9.46
4	0.56	1.93	4.97	0.92	100	7.73
5	5.99	1.17	2.58	4.99	0	3.08
6	7.48	9.33	2.15	0.39	133.33	1.17
7	1.72	0	14.11	18.20	500	19.01

both EPMA and EDS are attached in Appendix E. The analysis results are not that much off for most of the oxides, but for FeO the results are very different for EDS compared with EPMA. In most of the samples the FeO content is very low, lower than 1 wt%. The only slag with more FeO is the slag presented in Table 5.7. For most of the slags the EDS results show 0 % Fe. This is also the case for the EDS results presented in Appendix D. Very low or 0 % iron may due to low acceleration voltage, but 15 keV should be more than enough for Fe. Fe need at least 7.11 keV to give K_{α} data (Hjelen, 1986). A rule of thumb is to use twice as high acceleration voltage as the value for the heaviest element. Nevertheless it is advisable to use as low acceleration voltage as possible due to the emission depth shown in Equation 5.4. Advantages with low acceleration voltage are also low fluorescence and minimum absorption correction (Hjelen, 1986).

The EDS and the EPMA results are similar for MnO and SiO₂ in most of the samples, even if the content of these oxides are very low. For example the MnO content in Sample 7 is 0.5 wt% both from the EPMA and the EDS results, shown in Table E.7. Also results from Sample 5 is very good for MnO, even though the total amount of MnO in this sample is 2.5 %.

Hence it looks like the EDS is not so suitable for detecting iron, if it is assumed that the EPMA is most trustable (Tangstad, 2016). Nevertheless EDS is quite suitable for these slags, cause it is so small amounts of FeO and cause it is often assumed that iron oxides reduces in the prereduction.

Chapter 6

Conclusion

The main conclusions based on the examinations done in this work can be summarized as follows:

- A charge with Comilog ore and quartz start foaming of the slag at a bit lower temperature than 1650 °C, and at about 1650 °C it is so much foaming that the slag will come out of the crucible. This was observed for a heating rate of 4.5 °C/minute which is close to the heating rate in industrial furnaces.
- For charges with Comilog ore, quartz and limestone the foaming of the slag occur at about 1600 °C, about 50 °C lower than for charge without limestone.
- The reduction of SiO_2 starts at 1550 °C. This was observed for charges with Comilog ore and quartz, both with and without limestone added.
- The reduction of MnO starts at 1400 °C in SiMn charge. This was observed for charges with Comilog ore and quartz, both with and without limestone added. This is at a higher temperature than for FeMn charge.
- SiMn charges with limestone added as a flux have higher degree of reduction of both Mn and Si than SiMn charges without added limestone. This is based on calculated gram Mn produced in experiments done at 1600-1700 °C per gram ore added in the

charge, and equally for Si. The limestone has biggest impact on the degree of silicon reduced.

- A mix of Comilog ore and quartz create a liquid slag phase at 1250 °C. This was observed for both 0.6-1.6 mm particle size and for 4.0-6.3 mm size. Liquid slag was also observed for charges with limestone added. One single experiment with lumps larger than 12 mm, one lump of ore, one of quartz and one of limestone, show no liquid slag phase at 1350 °C. In this experiment the interface between the lumps was very small or zero.
- For slags with low iron content, EDS is a good substitution for EPMA.

Chapter 7

Further Work

In this chapter it is presented some suggestions to further work and research in this field.

To obtain more knowledge of the SiMn production process, it is needed more investigations. More experiments done with the charges used in this work is required. Use of a TGA furnace is suggested to get mass loss curves. The experiments should be stopped at different temperatures for investigating the chemical compositions of the slag and metal and compare this with weight loss. This is necessary to get better information at which temperatures the manganese and silicon reduces.

It is interesting to further investigate the melting temperature of the charges with large lumps. Experiment L3 in this work should been melted due to equilibrium, but something made that this not happen. Thus it is interesting to do that experiment again, maybe with larger contact area and at different temperatures.

Bibliography

- Allibert, M., Gaye, H., Geiseler, J., Janke, D., Keene, B. J., Kirner, D., Kowalski, M., Lehmann, J., Mills, K. C., Neuschütz, D., Parra, R., Saint-Jours, C., Spencer, P. J., Susa, M., Tmar, M., and Woermann, E. (1995). *Slag Atlas*. Stahleisen, 2nd edition.
- Aylward, G. and Findlay, T. (2008). *SI Chemical Data 6th edition*. John Wiley and Sons Australia, Ltd.
- Brynjulfson, T. (2013). *Reduction of manganese ore agglomerates*. PhD thesis, NTNU.
- Dijs, H. M. and Smith, D. J. (1980). Factors effecting the resistivity and reactivity of carbonaceous reducing agents for the electric-smelting industry. *J. South African Inst. Min. Metallurgy*, pages 286–296.
- Eissa, M., Fathy, A., Ahmed, A., El-Mohammady, A., and El-Fawakhry, K., editors (2004). *Factors Affecting Silicomanganese Production Using Manganese Rich Slag in the Charge*, Cape Town, South Africa. Proceedings of the Tenth International Ferroalloys Congress (INFACON X).
- Eriksson, G., Wu, P., Blander, M., and Pelton, A. D. (1994). Critical evaluation and optimalization of the thermodynamic properties and phase diagrams of the mno-sio₂ and cao-sio₂ systems. *Canadian Metallurgical Quarterly*, 33:13–21.
- Hjelen, J. (1986). Scanning elektron-mikroskopi. Compendium. SINTEF, Avdeling for metallurgi and Metallurgisk institutt, NTH.

- Holtan, J. (2015a). Phase composition in comilog charges during heating and reduction. NTNU internal report.
- Holtan, J. (2015b). Reduction of manganese ore with quartz and limestone. *20th International Seminar on Materials Processes, Aalto University, Finland, speaker.*
- Holtan, J. (2015c). Reduksjon av comilog-malm med koks, kvarts og kalkstein. NTNU internal report.
- Kim, P. P., Holtan, J., and Tangstad, M., editors (2016). *Reduction Behavior of Assmang and Comilog Ore in the SiMn Process*, Seattle, Washington, USA. Proceedings of the 10th International Conference on Molten Slags, Fluxes and Salts.
- Kvande, H. (2014). NTNU, TMT4155. Lecture notes.
- Li, X. (2016). Postdoctoral Fellow, Department of Materials Science and Engineering, NTNU. Personal communication.
- Nadir, B. (2015). Kinetics of manganese oxide reduction. Master's thesis, NTNU.
- Olsen, H. A. H. (2016). Master's thesis. Department of Material Science and Engineering, NTNU. To be published.
- Olsen, S. E. (2001). Fundamental principles of silicomanganese production, Technical report, SINTEF.
- Olsen, S. E. and Tangstad, M., editors (2004). *Silicomanganese Production - Process Understanding*, Cape Town, South Africa. Proceedings of the Tenth International Ferroalloys Congress (INFACON X).
- Olsen, S. E., Tangstad, M., and Lindstad, T. (2007). *Production of Manganese Ferroalloys*. tapir academic press.
- Ostrovski, O., Olsen, S. E., Tangstad, M., and Yastreboff, M. (2002). Kinetic modelling of mno reduction from manganese ore. *Canadian Metallurgical Quarterly*, pages 309–318.

- Persson, M. (2007). *Investigation of Slag Properties and Reactions*. PhD thesis, Royal Institute of Technology, Stockholm, Sweden.
- Ringdalen, E., Gaal, S., Tangstad, M., and Ostrovski, O. (2010). Ore melting and reduction in silicomanganese production. *Metallurgical and materials transactions B*, 41:1220–1229.
- Rosenqvist, T. (2004). *Principles of Extractive Metallurgy*. Tapir Academic Press, second edition.
- Skjervheim, T. A. (1994). *Kinetics and Mechanisms for transfer of manganese and silicon from molten oxide to liquid manganese metal*. PhD thesis, Department of Metallurgy, NTH.
- Tangstad, M. (1996). *The high carbon ferromanganese process - Coke bed relations*. PhD thesis, NTH.
- Tangstad, M. (2013). Chapter 7 - manganese ferroalloys technology. In Gasik, M., editor, *Handbook of Ferroalloys*, pages 221 – 266. Butterworth-Heinemann, Oxford.
- Tangstad, M. (2016). Professor, Department of Materials Science and Engineering, NTNU. Personal communication.
- Tangstad, M., Calvert, P., Brun, H., and Lindseth, A., editors (2004). *Use of Comilog ore in ferromanganese production*, Cape Town. Proceedings of the tenth international congress on ferroalloys (INFACON 10).
- Tangstad, M. and Olsen, S. E., editors (1995). *The Ferromanganese Process - Material and Energy Balance*. Proceedings of the Seventh International Ferroalloys Congress (INFACON 7), Trondheim, Norway.
- Yu, Y. (2015). Senior Engineer, Department of Materials Science and Engineering, NTNU. Personal communication.

Appendix A

Mass Balance

Table A.1: Shows the excel sheet used for mass balances. These numbers are valid for Sample Q1.

Charge	Comilog	Coke	Quartz	Limestone	tot											
Mass	23,08	6,86	6,02	0	35,96											
In	MnO	MnO2	SiO2	Fe2O3	CaO	MgO	Al2O3	CO2	Fix C	Etc	Tot	R				
mass	0,96	16,23	8,12	1,64	0,16	0,05	1,94	0,02	5,42	1,41	35,96	0,11				
mol	0,01	0,19	0,14	0,01	0,00	0,00	0,02	0,00	0,45		0,82					
After prereduction																
	MnO	MnO2	SiO2	Fe2O3	CaO	MgO	Al2O3	CO2	Fix C	Etc	Tot	R	Fe	Weightloss		
mass	14,21		8,12		0,16	0,05	1,94		5,42		29,90	0,11	1,15	with C	6,11	
mol	0,20		0,14		0,00	0,00	0,02		0,45		0,81		0,02			
Primary slag																
	MnO	SiO2	CaO	Al2O3	MgO	tot	R									
mass%	47,52	27,16	0,52	6,50	0,18	81,88247	0,11									
mol%	24,72	16,70	0,35	2,35	0,16	44,2836										
End slag																
	MnO% target	SiO2% target	MnO	SiO2	CaO	Al2O3	MgO	total	R							
mass	5	40	0,20	1,57	0,16	1,94	0,05	3,92	0,11							
mol			0,00	0,03	0,00	0,02	0,00	0,05								
wt%			5	40	4,00	49,66	1,34	100,00								
Metal																
	Fe	Mn	Si	Weightloss g with CO	% C	% Fe	%Mn	% Si	total							
mass	1,15	10,85	3,07	11,65	1,5	7,49	70,95	20,06	100							
mol	0,02	0,20	0,11													

Appendix B

Calculations of charge mixture

Here is an example of how the needed amount of quartz in the experiments are calculated.

Table B.1: 100 g Comilog MMA ore [Olsen et al. (2007)]

	Mass [g]	mol	Molar mass [g/mol]
Mn	50.5	0.9192	54.94
Fe ₂ O ₃	3.9	0.02442	159.70
SiO ₂	4.0	0.06657	60.09
Al ₂ O ₃	5.5	0.05394	101.96
MgO	0.3	0.00744	40.31
CaO	0.2	0.00357	56.08
MnO			70.94

Table B.2: Slag

MnO	15%
SiO ₂	40%
Al ₂ O ₃	
MgO	45%
CaO	

$$\text{Mass (Al}_2\text{O}_3\text{+CaO+MgO)} = 6.0\text{g}$$

$$\frac{6.0\text{g}}{0.45} = 13.3\text{gslag}$$

$$13.3g \cdot 0.15 = 2.0g MnO$$

Table B.3: Slag

MnO	15%	2.0g
SiO ₂	40%	5.3g
Al ₂ O ₃		
MgO	45%	6.0g
CaO		

$$0.9192mol \cdot 70.94 \frac{g}{mol} = 65.21g MnO$$

MnO which will be reduced: $65.21g - 2.0g(slag) = 63.21g$

$$\frac{63.21g}{54.94 \frac{g}{mol}} = 0.891mol \text{ Mn in the metal}$$

$$\text{Mn in the metal: } 0.891 \cdot 54.94 \frac{g}{mol} = 48.95g$$

Table B.4: Metal

Si	18%	
C	1.5%	
Fe		2.73g
Mn		48.95g

$$Fe+Mn = 51.68g = 80.5\%$$

$$\text{Total mass metal: } \frac{51.68}{0.805} = 64.2g$$

$$18\% \text{ Si: } 0.18 \cdot 64.2g = 11.56g = 0.4114mol$$

$$\text{Mass quartz: } 0.4114mol \cdot 60.09 \frac{g}{mol} = 24.72g$$

Table B.5: Total quartz

Metal	24.72 g
+Slag	5.3 g
-Ore	4.0 g
Total	26 g

Appendix C

Raw Data from EPMA

Table C.1: Raw data from the EPMA, metal analyzes from Sample L1 and L2 [wt%].

Analyze no	Si	Fe	Mn	Total	Comment		Si	Fe	Mn	Total	Phase
1	3,591	29,901	60,427	93,919	L1,1						
2	3,488	29,575	60,881	93,944	L1,2	Average:	3,57	30,03	60,83	94,43	bright
3	3,644	30,599	61,191	95,434	L1,3	Standard deviation:	0,08	0,52	0,38	0,87	
4	6,176	28,728	59,15	94,054	L1,4						
5	6,965	28,634	59,012	94,611	L1,5	Average:	6,68	28,63	58,85	94,16	grey
6	6,889	28,534	58,381	93,804	L1,6	Standard deviation:	0,44	0,10	0,41	0,41	
7	0	18,344	70,937	89,281	L1,7						
8	0,015	18,068	71,589	89,672	L1,8	Average:	0,01	18,08	71,39	89,47	dark
9	0	17,825	71,634	89,459	L1,9	Standard deviation:	0,01	0,26	0,39	0,20	
10	9,707	0,383	85,507	95,597	L1,10						
11	9,821	0,378	85,542	95,741	L1,11	Average:	9,77	0,39	85,43	95,58	bright lid
12	9,767	0,403	85,239	95,409	L1,12	Standard deviation:	0,06	0,01	0,17	0,17	
13	9,068	0,338	85,505	94,911	L1,13						
14	9,092	0,371	86,582	96,045	L1,14	Average:	9,31	0,36	85,91	95,59	dark lid
15	9,784	0,364	85,656	95,804	L1,15	Standard deviation:	0,41	0,02	0,58	0,60	
16	8,48	12,919	70,605	92,004	L2,1						
17	8,373	13,206	70,427	92,006	L2,2	Average:	8,40	13,01	70,85	92,25	bright
18	8,334	12,896	71,506	92,736	L2,3	Standard deviation:	0,08	0,17	0,58	0,42	
19	9,272	10,994	75,036	95,302	L2,4						
20	9,228	10,799	74,863	94,89	L2,5	Average:	7,87	10,39	76,05	94,31	grey
21	5,099	9,388	78,236	92,723	L2,6	Standard deviation:	2,40	0,88	1,90	1,39	
22	0,056	5,75	83,725	89,531	L2,7						
23	9,102	10,271	75,356	94,729	L2,8	Average:	6,10	8,81	78,32	93,24	dark
24	9,148	10,416	75,882	95,446	L2,9	Standard deviation:	5,24	2,65	4,69	3,23	
25	10,011	0,343	85,409	95,763	L2,10						
26	9,755	0,376	85,395	95,526	L2,11	Average:	9,84	0,35	85,42	95,62	lid
27	9,765	0,343	85,458	95,566	L2,12	Standard deviation:	0,15	0,02	0,03	0,13	

Table C.2: Raw data from the EPMA, slag analyzes from Sample L1 and L2 [wt%].

No.	SiO2	MgO	K2O	MnO	Al2O3	CaO	FeO	BaO	Total	Comment	SiO2	MgO	K2O	MnO	Al2O3	CaO	FeO	BaO	Total
1	46.028	0.191	0.494	28.433	6.584	16.638	0.078	0.202	98.648	L1.1									
2	43.864	0.223	0.5	28.622	6.763	16.46	0.086	0.348	96.866	L1.2									
3	44.895	0.199	0.553	28.551	6.693	16.476	0.072	0.23	97.669	L1.3									
4	44.348	0.179	0.511	29.56	6.597	16.238	0.074	0.222	97.729	L1.4	Average:	44	0.2	0.5	29.4	6.6	16.4	0.1	0.2
5	44.216	0.191	0.507	29.714	6.618	16.29	0.091	0.273	97.9	L1.5	Standard deviation:	1	0	0	0.8	0.1	0.3	0	0.7
6	44.209	0.22	0.504	29.918	6.553	16.217	0.078	0.304	98.003	L1.6									
7	42.882	0.213	0.519	30.491	6.36	16.16	0.073	0.169	96.867	L1.7									
8	42.725	0.206	0.499	30.363	6.445	16.217	0.099	0.213	96.767	L1.8									
9	43.175	0.177	0.444	29.181	6.697	17.047	0.045	0.158	96.924	L1.9									
10	43.338	0.186	0.479	29.879	6.521	16.362	0.059	0.222	97.046	L1.10									
11	43.342	0.208	0.433	29.944	6.524	16.069	0.1	0.22	96.84	L1.11	Average:	43.4	0.2	0.5	30	6.5	16.1	0.1	0.2
12	43.512	0.201	0.457	30.055	6.478	15.872	0.119	0.289	96.983	L1.12	Standard deviation:	0.1	0	0	0.1	0	0.2	0	0.1
13	47.169	0.263	0.566	20.062	8.413	19.581	0.035	0.411	96.5	L2.1									
14	47.607	0.252	0.477	20.21	8.634	19.377	0.075	0.468	97.1	L2.2	Average:	47.5	0.3	0.5	20.3	8.5	19.4	0.1	0.5
15	47.715	0.254	0.558	20.606	8.562	19.386	0.054	0.505	97.64	L2.3	Standard deviation:	0.3	0	0	0.3	0.1	0.1	0	0.6
16	45.046	0.224	0.46	26.361	7.384	17.145	0.043	0.532	97.195	L2.4									
17	45.339	0.212	0.531	26.232	7.393	17.178	0.069	0.294	97.248	L2.5	Average:	45.2	0.2	0.5	26.4	7.4	17.2	0.1	0.4
18	45.307	0.227	0.465	26.571	7.293	17.162	0.057	0.427	97.509	L2.6	Standard deviation:	0.2	0	0	0.2	0.1	0	0.1	0.2

Appendix D

Raw Data from EDS

Table D.1: Raw data from EDS, metal analyzes from Sample Q1 and Q2, L4 and L5 [wt%].

	Mn	Si	Fe	C	Total		Mn	Si	Fe	C	Total
Q1	73,42	8,39	7,25	8,46	97,52	Standard deviation:	6,5	5,8	0,7	0,4	
	69,35	7,97	8,04	8,8	94,16						
	67,49	8,26	5,9	8,2	89,85	Average:	66,1	13,2	6,9	8,4	86,2
	61,61	19,75	7,03	8,39	96,78						
	58,4	19	7,02	8,16	92,58	Normalized:	74,4	14,9	7,8	3	97
	58,16	19,17	6,81	8,03	92,17						97
	60,37	19,3	7,53	8,21	95,41						
	72,96	8,4	6,47	8,86	96,69						
	72,82	8,52	6,06	8,63	96,03						
	68,48	18,62	0	8,4	95,5						
	68,2	13,64	0	7,75	89,59						
	76,63	8,92	0	9,51	95,06						
	76,27	11,29	0	8,21	95,77						
	73,78	13,31	0	8,59	95,68						
Q2	60,82	17,92	8,26	8,57	95,57	Standard deviation:	5,9	5,4	2,1	0,6	
	72,68	7,91	8,24	8,03	96,86						
	60,5	19,2	9,62	9	98,32	Average:	63,4	14,2	9,8	8,6	87,4
	59,4	19,61	9,78	8,54	97,33						
	58,26	8,73	13,91	8,04	88,94	Normalized:	70,6	15,8	10,9	2,7	97,3
	68,73	11,71	9,21	9,54	99,19						
L4	80,28	8,84	0	8,07	97,19	Standard deviation:	7,2	5,5	0,0	0,2	
	66,34	18,21	0	7,72	92,27	Normalized:	80,6	17,0	0,0	2,4	100,0
	69,89	18,47	0	8,02	96,38	Average:	72,2	15,2	0,0	7,9	87,3
L5	68,7	20,18	0	8,65	97,53	Standard deviation:	1,0	1,6	0,0	0,1	
	70,72	17,01	0	8,52	96,25	Normalized:	78,0	20,7	0,0	1,3	100,0
	69,98	18,36	0	8,36	96,7	Average:	69,8	18,5	0,0	8,5	98,7

Table D.2: Raw data from EDS, slag analyzes from Sample Q1, L4 and L5 [at%].

	O	Si	Al	Mn	C	Ca	K	S	Mg
Q1	51,43	17,08	12,91	10,29	5,63	1,48	0,75	0,44	0
	52,22	19,6	11,09	10,29	4,29	1,26	0,85	0,29	0
	52,03	18,93	11,3	10,45	4,79	1,32	0,77	0,41	0
	51,43	17,08	12,91	10,29	5,63	1,48	0,75	0,44	0
	52,22	19,6	11,09	10,29	4,29	1,26	0,85	0,39	0
	52,03	18,93	11,3	10,45	4,79	1,32	0,77	0,41	0
	52,26	20,96	5,65	14,92	4,8	0,67	0,72	0	0
	51,75	21,18	5,72	14,49	5,47	0,7	0,69	0	0
	52,15	21,31	5,83	14,48	4,39	0,73	0,71	0,4	0
L4	46,86	17,71	4,75	2,65	13,1	14,94	0	0	0
	46,61	19,62	4,76	3,05	12,8	13,15	0	0	0
	46,32	19,09	4,84	3,17	13,36	13,23	0	0	0
	46,68	17,7	5,45	2,22	13,12	14,82	0	0	0
	47,3	17,18	5,96	1,98	12,85	14,74	0	0	0
	46,61	18,88	5,28	2,48	13,26	13,49	0	0	0
	45,04	18,51	5,1	2,58	14,18	14,41	0	0	0
	44,49	17,58	6,71	2,55	14,01	14,66	0	0	0
	45,15	19,03	5,37	2,69	13,54	14,22	0	0	0
	46,21	19,61	4,57	2,85	13,92	12,84	0	0	0
	45,25	18,73	5,54	2,77	13,83	13,88	0	0	0
	45,71	19,23	4,71	3,12	13,76	13,47	0	0	0
L5	47,26	15,38	7,62	0,53	12,68	15,37	0	0,47	0,68
	47,68	14,93	7,75	0,59	12,15	15,62	0	0,56	0,74
	47,33	15,39	7,75	0,59	12,7	15,1	0	0,49	0,65
	47,57	15,26	7,81	0,57	12,18	15,33	0	0,59	0,69
	46,89	15,27	7,69	0,57	13,07	15,27	0	0,51	0,73
	47,01	15,28	7,67	0,54	12,21	16,11	0	0,49	0,7
	46,75	14,58	7,58	0,6	13,65	15,61	0	0,57	0,66
	47,21	14,94	7,72	0,49	12,68	15,73	0	0,54	0,69
	46,43	15,51	7,81	0,64	12,94	15,33	0	0,59	0,75

D. Raw Data from EDS

Table D.3: Slag analyze data from EDS, calculated to mass % and oxides. Analyzes from Sample Q1, L4 and L5 [wt%].

	SiO2	Al2O3	MnO	CaO	K2O	MgO	tot		SiO2	Al2O3	MnO	CaO	K2O	MgO
Q1	40,5	26,0	28,8	3,3	1,4	0,0	100	Std. Derivation:	2,4	2,0	0,3	0,3	0,1	0,0
	45,6	21,9	28,3	2,7	1,5	0,0	100							
	44,3	22,5	28,9	2,9	1,4	0,0	100	Average:	43,5	23,4	28,7	3,0	1,5	0,0
	40,5	26,0	28,8	3,3	1,4	0,0	100							
	45,6	21,9	28,3	2,7	1,5	0,0	100							
	44,3	22,5	28,9	2,9	1,4	0,0	100							
	47,0	10,8	39,5	1,4	1,3	0,0	100	Average:	47,5	10,9	38,8	1,5	1,2	0,0
	47,8	10,9	38,6	1,5	1,2	0,0	100	Std. Derivation:	0,4	0,2	0,6	0,1	0,0	0,0
	47,8	11,1	38,3	1,5	1,2	0,0	100							
L4	45,6	10,4	8,1	35,9	0,0	0,0	100	Std. Derivation:	2,0	1,3	1,0	1,9	0,0	0,0
	49,6	10,2	9,1	31,0	0,0	0,0	100							
	48,6	10,5	9,5	31,4	0,0	0,0	100	Average:	47,3	11,4	8,0	33,3	0,0	0,0
	45,6	11,9	6,8	35,7	0,0	0,0	100							
	44,8	13,2	6,1	35,9	0,0	0,0	100							
	48,6	11,5	7,5	32,4	0,0	0,0	100							
	47,1	11,0	7,7	34,2	0,0	0,0	100							
	44,0	14,2	7,5	34,2	0,0	0,0	100							
	47,5	11,4	7,9	33,2	0,0	0,0	100							
	50,5	10,0	8,7	30,9	0,0	0,0	100							
	47,2	11,9	8,2	32,7	0,0	0,0	100							
	48,7	10,1	9,3	31,8	0,0	0,0	100							
L5	41,3	17,3	1,7	38,5	0,0	1,2	100	Std. Derivation:	0,6	0,2	0,1	0,7	0,0	0,1
	40,1	17,6	1,9	39,1	0,0	1,3	100							
	41,4	17,7	1,9	37,9	0,0	1,2	100	Average:	40,7	17,5	1,8	38,8	0,0	1,3
	40,9	17,8	1,8	38,3	0,0	1,2	100							
	41,0	17,5	1,8	38,3	0,0	1,3	100							
	40,3	17,2	1,7	39,6	0,0	1,2	100							
	39,7	17,5	1,9	39,7	0,0	1,2	100							
	40,1	17,6	1,6	39,5	0,0	1,2	100							
	41,1	17,6	2,0	37,9	0,0	1,3	100							

Appendix E

Data for Comparing EDS and EPMA

Table E.1: Data from EDS and EPMA. From sample RX-3-1700 (Li, 2016).

	Spot	<u>MnO</u> wt%	<u>SiO₂</u> wt%	<u>CaO</u> wt%	<u>MgO</u> wt%	<u>Al₂O₃</u> wt%	<u>FeO</u> wt%	Total
EDS	1	40.39	32.04	9.20	3.79	12.24	2.34	100.00
	2	40.23	32.07	9.15	3.85	12.44	2.27	100.00
	3	40.16	32.25	9.22	3.87	12.39	2.11	100.00
	Average	40.26	32.12	9.19	3.84	12.36	2.24	100.00
EPMA	1	37.21	32.50	9.26	3.80	13.87	3.37	100.00
	2	37.22	32.50	9.32	3.89	13.70	3.37	100.00
	3	37.03	32.49	9.29	3.97	13.90	3.31	100.00
	4	37.27	32.48	9.27	3.92	13.76	3.30	100.00
	5	36.93	32.77	9.18	3.85	13.94	3.35	100.00
	Average	37.13	32.55	9.26	3.88	13.83	3.34	100.00
Data gap		3.13	-0.43	-0.07	-0.05	-1.48	-1.10	0.00

Table E.2: Data from EDS and EPMA. From sample RX-4-1600 (Li, 2016).

	Spot	MnO wt%	SiO ₂ wt%	CaO wt%	MgO wt%	Al ₂ O ₃ wt%	FeO wt%	Total
EDS	1	36.70	34.97	9.71	4.40	14.22	0.00	100.00
	2	36.23	35.39	9.64	4.29	14.44	0.00	100.00
	3	36.15	35.24	9.71	4.38	14.52	0.00	100.00
	Average	36.36	35.20	9.69	4.36	14.39	0.00	100.00
EPMA	1	36.02	34.29	9.74	3.97	15.90	0.09	100.00
	2	36.27	34.26	9.76	3.93	15.67	0.11	100.00
	3	36.15	33.89	9.80	3.99	16.09	0.08	100.00
	4	35.84	34.35	9.94	3.98	15.76	0.14	100.00
	5	36.07	34.15	9.66	3.99	16.04	0.11	100.00
	Average	36.07	34.19	9.78	3.97	15.89	0.10	100.00
Data gap		0.29	1.01	-0.09	0.39	-1.50	-0.10	0.00

Table E.3: Data from EDS and EPMA. From sample RX-6-60 min (Li, 2016).

	Spot	MnO wt%	SiO ₂ wt%	CaO wt%	MgO wt%	Al ₂ O ₃ wt%	FeO wt%	Total
EDS	1	36.82	34.87	9.65	4.24	14.43	0.00	100.00
	2	36.90	34.92	9.45	4.28	14.46	0.00	
	3	37.12	34.85	9.45	4.30	14.28	0.00	
	4	36.80	35.14	9.53	4.28	14.25	0.00	100.00
	5	36.75	34.92	9.60	4.31	14.42	0.00	100.00
	Average	36.88	34.94	9.54	4.28	14.37	0.00	100.00
EPMA	1	37.58	35.07	9.39	3.95	13.67	0.35	100.00
	2	37.59	34.88	9.44	3.93	13.78	0.37	100.00
	3	37.69	34.84	9.43	3.86	13.75	0.43	100.00
	4	37.45	35.02	9.54	3.89	13.71	0.39	100.00
	5	37.52	35.07	9.31	3.89	13.79	0.44	100.00
	6	37.53	34.98	9.47	3.96	13.61	0.45	100.00
	Average	37.56	34.98	9.43	3.91	13.72	0.41	100.00
Data gap		-0.68	-0.04	0.11	0.37	0.65	-0.41	0.00

Table E.4: Data from EDS and EPMA. From sample RX-8-60 min (Li, 2016).

	Spot	<u>MnO</u> <u>wt%</u>	<u>SiO2</u> <u>wt%</u>	<u>CaO</u> <u>wt%</u>	<u>MgO</u> <u>wt%</u>	<u>Al2O3</u> <u>wt%</u>	<u>FeO</u> <u>wt%</u>	Total
EDS	1	35.74	35.38	9.88	4.28	14.72	0.00	100.00
	2	35.48	35.38	9.92	4.38	14.84	0.00	100.00
	3	35.41	35.53	9.96	4.32	14.79	0.00	100.00
	Average	35.54	35.43	9.92	4.33	14.78	0.00	100.00
EPMA	1	36.46	35.38	9.85	3.99	14.06	0.25	100.00
	2	36.02	35.69	9.88	3.99	14.19	0.23	100.00
	3	36.27	35.62	9.87	3.98	14.10	0.16	100.00
	4	36.04	35.86	9.77	4.09	14.06	0.19	100.00
	5	36.41	35.66	9.78	4.01	13.94	0.19	100.00
	6	36.26	35.54	9.82	4.01	14.18	0.19	100.00
	Average	36.24	35.63	9.83	4.01	14.09	0.20	100.00
Data gap		-0.70	-0.20	0.09	0.31	0.70	-0.20	0.00

Table E.5: Data from EDS and EPMA. From sample RX-10-80 min (Li, 2016).

	Spot	<u>MnO</u> <u>wt%</u>	<u>SiO2</u> <u>wt%</u>	<u>CaO</u> <u>wt%</u>	<u>MgO</u> <u>wt%</u>	<u>Al2O3</u> <u>wt%</u>	<u>FeO</u> <u>wt%</u>	Total
EDS	1	2.77	33.97	22.73	9.31	31.22	0.00	100.00
	2	2.83	34.09	22.66	9.32	31.11	0.00	100.00
	3	2.36	33.68	22.73	9.45	31.79	0.00	100.00
	4	2.39	33.78	22.76	9.42	31.66	0.00	100.00
	Average	2.59	33.88	22.72	9.38	31.45	0.00	100.00
EPMA	1	2.59	35.96	21.70	9.07	30.66	0.02	100.00
	2	2.55	35.99	21.56	9.09	30.80	0.00	100.00
	3	2.56	36.07	21.73	9.02	30.61	0.00	100.00
	4	2.57	36.13	21.49	9.14	30.67	0.00	100.00
	5	2.53	36.06	21.73	9.13	30.55	0.00	100.00
	Average	2.56	36.04	21.64	9.09	30.66	0.00	100.00
Data gap		0.03	-2.16	1.08	0.28	0.79	0.00	0.00

Table E.6: Data from EDS and EPMA. From sample RX-18 min (Li, 2016).

	Spot	<u>MnO</u> <u>wt%</u>	<u>SiO2</u> <u>wt%</u>	<u>CaO</u> <u>wt%</u>	<u>MgO</u> <u>wt%</u>	<u>Al2O3</u> <u>wt%</u>	<u>FeO</u> <u>wt%</u>	Total
EDS	1	36.09	34.70	10.21	4.27	14.48	0.25	100.00
	2	36.23	34.50	10.28	4.19	14.64	0.17	100.00
	3	35.99	34.75	10.27	4.24	14.53	0.21	100.00
	Average	36.10	34.65	10.25	4.23	14.55	0.21	100.00
EPMA	1	33.02	37.58	10.19	4.27	14.89	0.05	100.00
	2	32.97	37.66	10.17	4.22	14.84	0.13	100.00
	3	33.12	37.13	10.50	4.29	14.87	0.09	100.00
	4	32.85	37.51	10.29	4.32	14.95	0.08	100.00
	5	33.13	37.35	10.31	4.31	14.82	0.08	100.00
	Average	33.02	37.45	10.29	4.28	14.87	0.09	100.00
Data gap		3.08	-2.80	-0.04	-0.05	-0.32	0.12	0.00

Table E.7: Data from EDS and EPMA. From sample RX-19 (Li, 2016).

	Spot	<u>MnO</u> <u>wt%</u>	<u>SiO2</u> <u>wt%</u>	<u>CaO</u> <u>wt%</u>	<u>MgO</u> <u>wt%</u>	<u>Al2O3</u> <u>wt%</u>	<u>FeO</u> <u>wt%</u>	Total
EDS	1	0.47	28.47	34.91	4.54	31.58	0.04	100.00
	2	0.42	30.84	35.51	4.65	28.46	0.12	100.00
	3	0.47	29.70	33.02	4.76	32.04	0.00	100.00
	4	0.75	31.96	36.55	4.43	26.24	0.07	100.00
	Average	0.53	30.24	35.00	4.60	29.58	0.06	100.00
EPMA	1	0.55	29.09	29.39	5.93	35.01	0.03	100.00
	2	0.57	29.26	29.25	5.62	35.30	0.00	100.00
	3	0.47	31.08	30.32	5.25	32.85	0.02	100.00
	4	0.51	29.28	30.08	5.26	34.86	0.00	100.00
	5	0.53	29.95	29.00	6.34	34.18	0.00	100.00
	Average	0.52	29.73	29.61	5.68	34.44	0.01	100.00
Data gap		0.00	0.51	5.39	-1.08	-4.86	0.05	0.00

Appendix F

Risk Assessment and Safe Job Analysis

NTNU		Kartlegging av risikofylt aktivitet		Utarbeidet av		Nummer		Dato	
				HMS-avd.		HMSRV2601		22.03.11	
HMS				Godkjent av		Side		Erstatter	
				Rektor				01.12.06	

Enhet: IMT **Dato:** 26.08.15

Linjeleder: Jostein Mårdalen

Deltakere ved kartleggingen (m/ funksjon): Merete Tangstad, Joakim Holtan

Kort beskrivelse av hovedaktivitet/hovedprosess: Masteroppgave student Joakim Holtan. Reduksjon av Mn-malm.

Er oppgaven er rent teoretisk? (JA/NEI) nei

Er det trygt å utføre arbeidet utenfor normal arbeidstid (8-17)? (JA/NEI) nei



Signaturer: *Herle Tangstad* *Joakim Holtan*

Ansvarlig veileder: *Herle Tangstad* **Student:** *Joakim Holtan*

ID nr.	Aktivitet/prosess	Ansvarlig	Eksisterende dokumentasjon	Eksisterende sikringstiltak	Lov, forskrift o.l.	Kommentar
1	Sette inn prøve	Joakim	HMS-håndbok	Vernebriller, gassdetektorer	Lab-forskrifter	
2	Gjennomføre forsøk	Joakim	HMS-håndbok	Vernebriller, gassdetektorer	Lab-forskrifter	
3	Ta ut prøve	Joakim	HMS-håndbok	Vernebriller, gassdetektorer	Lab-forskrifter	
4						
5						
6						

/Users/joakimholtan/Library/Containers/com.apple.mail/Data/Library/Mail Downloads/09DE2AC7-0BDD-486E-9683-1E5205ED568/Kartlegging_risikovurdering_v2.xlsx

26.08.15 Side 3 av 6

NTNU	Risikovurdering					
						
HMS /KS						
Utarbeidet av		Nummer		Dato		
HMS-avd.		HMSRV2603		04.02.11		
Godkjent av		Side		Erstatter		
Rektor				09.02.10		

Enhet: IMT Dato: 26.08.15

Linjeleder: Jostein Mårdalen

Deltakere ved risikovurderingen (m/ funksjon):

(Ansv. veileder, student, evt. medveiledere, evt. andre m. kompetanse)

Merete Tangstad, Joakim Holtan

Risikovurderingen gjelder hovedaktivitet:

Masteroppgave student Joakim Holtan. Reduksjon av Mn-malm.

Signaturer:

Ansvarlig veileder:

Merete Tangstad

Student:

Joakim Holtan

ID nr.	Aktivitet/prosess fra kartleggingsskjemaet	Mulig uønsket hendelse	Vurdering av sannsynlighet (1-5)	Vurdering av konsekvens			Risiko-verdi (menneske)	Kommentarer/status Forslag til tiltak
				Menneske (A-E)	Ytre miljø (A-E)	Øk./materiell (A-E)		
1	Sette prøve inn i ovn	klemfare	1	A			A1	Vernebriller
2	Sette på CO(g)	gasslekasje	1	E			E1	Vernebriller, CO-detektor
3	Oppvarming av prøve og ovn	Vannlekasje	2	A			A2	Vernebriller
4	Ta ut prøve etter forsøk	klemfare, brannskade	1	B			B1	Vernebriller, vente til det blir kaldt
5								
6								

**SINTEF**

Safe Job Analysis (SJA) Joint Form

**NTNU****SJA title:** SJA for forsøk i termogravimetrisk grafittovn**Date:** 27.5.15**Place:**

Enter cross on completion of checklist:

x

Bergbygget E-214

Participants:

Joakim Holtan

Jonas Gjøvik

Person responsible for completing SJA: Joakim Holtan

Description of work:

Forsøk i ovn. Sette inn prøver i ovnen og skru på varme og CO-atmosfære.

Risks associated with the work:

CO(g)-lekasje, klemfare i forbindelse med lukking av ovn, brannskade fra varme deler/gjenstander

Protection/safeguards:

CO-detektor, vernebriller

Waste handling:**Conclusion/remarks:**

CO er absolutt største faremomentet

Recommendation/approval:	Date/Signature:	Recommendation/approval:	Date/Signature:
Person responsible for completing SJA:	28.5.15 Joakim Holtan	Area Officer/Apparatus resp.:	28.5.15 Jonas Gjøvik
Person responsible for carrying out the work	Joakim Holtan	Project leader:	Herck Tangstad

HSE factor

Yes No Not

Remarks / actions**Pers. resp.**



SINTEF

Safe Job Analysis (SJA) Joint Form



NTNU

			Clear		
Documentation, experience, skills/expertise					
Familiar task/operation?		x			
Knowledge of experience/unwanted incidents in connection with similar tasks/operations? -ask supervisor		x			
Have you received training from apparatus/instrument responsible? Note date	x			Får opplæring snart / for forsende	
Routine for handling of a possible incident (alarm, evacuation)?	x				
Requirement for additional supervision/ Lone-worker-alarm?	x				
Is the workplace clean and orderly?	x				
Protective equipment in addition to HSE-handbook?	x				
Illumination, ventilation?	x				
Use of lifts/harnesses/slides?		x			
Ionising radiation?		x			
Evacuation routes OK?	x				
Use of harmful/toxic/corrosive chemicals?	x			CO(g)	
If toxic, substitute?		x			
Use of potentially inflammable or explosive chemicals?		x			
HSE-datasheet in folder in lab?		x			
Chemical registered in EcoOnline?	x				
Dust/asbestos?		x			
Stability/strength/tension?		x			
Risk from clamping/cutting/striking?		x			
Noise/pressure/temperature?	x				
Need for special tools?	x				
Current/voltage/in excess of 1000V?		x			
Shock/stray current?		x			
Problem with power failure?		x			
Other					

**SINTEF**

Safe Job Analysis (SJA) Joint Form

**NTNU**

SJA title: SJA for prøvepreparering			
Date: 28.5.15		Place:	
Enter cross on completion of checklist:	x	Bergbygget M-115	

Participants:		
Joakim Holtan		
Person responsible for completing SJA: Joakim Holtan		

Description of work:
 Prøvepreparering.
 Knuse og sikte materialer, vaske og rense prøvene.

Risks associated with the work:
 Hørselsskade, steinsprut, væskesprut
 Støv ved knusing

Protection/safeguards:
 Vernebriller, hørselsvern, hansker, støvmaske

Waste handling:
 Vann og etanol tømmes i vasken

Conclusion/remarks:
 Bruk sikkerhetsutstyr tilpasset arbeidet

Recommendation/approval:	Date/Signature:	Recommendation/approval:	Date/Signature:
Person responsible for completing SJA:	28.5.15 Joakim Holtan	Area Officer/Apparatus resp.:	Stieversen, Duvén
Person responsible for carrying out the work	Joakim Holtan	Project leader:	Perle Tangstad

HSE factor	Yes	No	Not	Remarks / actions	Pers. resp.
------------	-----	----	-----	-------------------	-------------



SINTEF

Safe Job Analysis (SJA) Joint Form



NTNU

			Clear	
Documentation, experience, skills/expertise				
Familiar task/operation?		x		
Knowledge of experience/unwanted incidents in connection with similar tasks/operations? -ask supervisor		x		
Have you received training from apparatus/instrument responsible? Note date	x			Vil få snart
Routine for handling of a possible incident (alarm, evacuation)?	x			
Requirement for additional supervision/ Lone-worker-alarm?		x		
Is the workplace clean and orderly?	x			
Protective equipment in addition to HSE-handbook?	x			
Illumination, ventilation?	x			
Use of lifts/harnesses/slides?		x		
Ionising radiation?		x		
Evacuation routes OK?	x			
Use of harmful/toxic/corrosive chemicals?		x		
If toxic, substitute?		x		
Use of potentially inflammable or explosive chemicals?		x		
HSE-datasheet in folder in lab?		x		
Chemical registered in EcoOnline?	x			
Dust/asbestos?	x			
Stability/strength/tension?		x		
Risk from clamping/cutting/striking?		x		
Noise/pressure/temperature?	x			Kan bli høy lyd
Need for special tools?	x			
Current/voltage/in excess of 1000V?		x		
Shock/stray current?		x		
Problem with power failure?		x		
Other				

